University of Kentucky
UKnowledge

Theses and Dissertations--Mechanical Engineering

Mechanical Engineering

2013

ASSESSING AND MITIGATING AIRBORNE NOISE FROM POWER GENERATION EQUIPMENT

Limin Zhou
University of Kentucky, lzh222@uky.edu

Right click to open a feedback form in a new tab to let us know how this document benefits you.

Recommended Citation

Zhou, Limin, "ASSESSING AND MITIGATING AIRBORNE NOISE FROM POWER GENERATION EQUIPMENT" (2013). *Theses and Dissertations--Mechanical Engineering*. 22.
https://uknowledge.uky.edu/me_etds/22

This Doctoral Dissertation is brought to you for free and open access by the Mechanical Engineering at UKnowledge. It has been accepted for inclusion in Theses and Dissertations--Mechanical Engineering by an authorized administrator of UKnowledge. For more information, please contact UKnowledge@lsv.uky.edu.

STUDENT AGREEMENT:

I represent that my thesis or dissertation and abstract are my original work. Proper attribution has been given to all outside sources. I understand that I am solely responsible for obtaining any needed copyright permissions. I have obtained and attached hereto needed written permission statements(s) from the owner(s) of each third-party copyrighted matter to be included in my work, allowing electronic distribution (if such use is not permitted by the fair use doctrine).

I hereby grant to The University of Kentucky and its agents the non-exclusive license to archive and make accessible my work in whole or in part in all forms of media, now or hereafter known. I agree that the document mentioned above may be made available immediately for worldwide access unless a preapproved embargo applies.

I retain all other ownership rights to the copyright of my work. I also retain the right to use in future works (such as articles or books) all or part of my work. I understand that I am free to register the copyright to my work.

REVIEW, APPROVAL AND ACCEPTANCE

The document mentioned above has been reviewed and accepted by the student's advisor, on behalf of the advisory committee, and by the Director of Graduate Studies (DGS), on behalf of the program; we verify that this is the final, approved version of the student's dissertation including all changes required by the advisory committee. The undersigned agree to abide by the statements above.

Limin Zhou, Student

Dr. David W. Herrin, Major Professor

Dr. James M. McDonough, Director of Graduate Studies

ASSESSING AND MITIGATING AIRBORNE NOISE FROM POWER GENERATION EQUIPMENT

DISSERTATION

A dissertation submitted in partial fulfillment of the
requirements for the degree of Doctor of Philosophy in the
College of Engineering
at the University of Kentucky

By

Limin Zhou

Lexington, Kentucky

Co-Directors: Dr. David W. Herrin, Professor of Mechanical Engineering
and Dr. Tingwen Wu, Professor of Mechanical Engineering

Lexington, Kentucky

2013

Copyright © Limin Zhou 2013

ABSTRACT OF DISSERTATION

ASSESSING AND MITIGATING AIRBORNE NOISE FROM POWER GENERATION EQUIPMENT

This dissertation examines the assessment and mitigation of airborne noise from power generation equipment.

The first half of the dissertation investigates the diagnosis and treatment of combustion oscillations in boilers. Sound is produced by the flame and is reflected downstream from the combustion chamber. The reflected sound waves perturb the mixture flow or equivalence ratio increasing the heat release pulsations and the accompanying sound produced by the flame. A feedback loop model for determining the likelihood of and diagnosing combustion oscillations was reviewed, enhanced, and then validated. The current work applies the feedback loop stability model to two boilers, which exhibited combustion oscillations. Additionally, a feedback loop model was developed for equivalence ratio fluctuations and validated. For the first boiler, the combustion oscillation problem is primarily related to the geometry of the burner and the intake system. For the second boiler, the model indicated that the combustion oscillations were due to equivalence ratio fluctuations. Principles for both measuring and simulating the acoustic impedance are summarized. An approach for including the effect of structural-acoustic coupling was developed. Additionally, a method for determining the impedance above the plane wave cut-off frequency, using the acoustic FEM, of the boiler was proposed.

The second half of the dissertation examines the modeling of bar silencers. Bar silencers are used to mitigate the airborne noise from large power generation equipment (especially gas turbines). Due to the large dimensions of the full cross section, a small representative cell is isolated from the entire array for analysis purposes. To predict the acoustical performance of the isolated cell for different geometric configurations, a numerical method based on the direct mixed-body boundary element method (BEM) was used. An analytical solution for a simplified circular geometry was also derived to serve as a comparison tool for the BEM. Additionally, a parametric study focusing on the effects of flow

resistivity, perforate porosity, length of bars, and cross-sectional area ratio was performed. A new approach was proposed to evaluate the transmission loss based on a reciprocal work identity. Moreover, extension of the transmission loss computation above the plane wave cut-off frequency was demonstrated.

KEYWORDS: Combustion-Driven Oscillations, Feedback Loop Stability Models, Acoustic Load Impedance, Bar Silencers, Reciprocal Work Identity

Limin Zhou

Student's Signature

04/29/2013

Date

ASSESSING AND MITIGATING AIRBORNE NOISE FROM POWER GENERATION EQUIPMENT

By

Limin Zhou

David W. Herrin
Co-Director of Dissertation

Tingwen Wu
Co-Director of Dissertation

James M. McDonough
Director of Graduate Studies

04/29/2013
Date

DEDICATION

To my parents, Shengzhao Zhou and Lanying Jing,

my beloved wife, Ke Wei,

and my lovely daughter, Emily Y. Zhou.

ACKNOWLEDGEMENTS

First of all, I would like to express my deepest gratitude to, my co-supervisors, Dr. David W. Herrin and Dr. Tingwen Wu, without whom this dissertation will not be possible. During the course of my graduate studies at University of Kentucky, they provided wonderful opportunities for me to work on several intriguing and challenging projects from which I was tremendously benefited. Their guidance, patience, expertise, encouragement and friendship helped me confront the periods of difficulty and frustration, maintain my energy on the exploration of noise and vibration control engineering problems, and facilitate my assimilation of knowledge and experience on acoustics and growth as an acoustician.

I would also like to thank my other committee members: Dr. Kozo Saito, Dr. T. Michael Seigler and Dr. Qiang Ye, for their invaluable and helpful suggestions which helped me improve the research work. Thanks also go to Dr. Kwok-Wai Ng, who served as the Outside Examiner for my final doctoral examination. I would also like to thank Dr. Andrew F. Seybert for the useful discussions.

I am grateful to Jinghao Liu, Xin Hua, Zhe Cui, Jiawei Liu, Srinivasan Ramalingam, Quentin Hunsucker, Wentao Zhuo, Yitian Zhang, Rui He, Kangping Ruan, Wanlu Li, Gong Cheng, Jiazhu Li, Huangxing Chen, and Shishuo Sun, who all have made my stay enjoyable.

Most importantly, I would like to express love and appreciation to my parents, for fostering, supporting and educating me, to my wife, for her love, support, patience and encouragement, and to my lovely daughter, for giving me tremendous happiness.

TABLE OF CONTENTS

LIST OF TABLES

LIST OF FIGURES

CHAPTER 1 INTRODUCTION

1.1 Background

As the population grows, demand for energy will increase. In order to meet these needs, various types of power equipment have been designed and manufactured since the first industrial revolution. Though wind, solar, and nuclear are viable alternatives, fossil fuel usage will continue to be the primary source of our growing energy needs. However, in all fossil fuel combustion processes, noise will be produced and will need to be reduced or minimized. This is certainly the case in the heating, ventilation and air-conditioning systems (HVAC) and gas turbine industries.

1.1.1 Power Equipment

Among the popular power equipment, two types, namely boilers and gas turbines, are extensively used in heating systems and power generation industries.

Boilers

Boilers are pressure vessels designed to transfer released heat (produced by combustion) to a fluid which is usually water in the form of liquid or steam [1]. They consist of a combustion chamber made of cast-iron, stainless steel, aluminum or copper, and a jacket in which cold fluid is heated. A piping system is then used to convey heated fluid to the use point and then return the cooled fluid to the boiler. Boilers are typically categorized into various groups depending on their working pressure and temperature, fuel used, material of construction, type of draft (natural or mechanical), whether they use condensing or non-condensing fuel gas, their shape and size, the application (such as heating or process), and the state of the output medium (steam or water) [1].

Gas Turbines

Gas turbines, also called combustion turbines, are similar to internal combustion engines and essentially large compressors. However, in contrast to internal combustion engines which rely on serial piston strokes to maintain air and fuel flow, gas turbines maintain a continuous air and fuel flow [2]. In addition to high

operating efficiency and lower pollutant emission, gas turbines require low capital investment, and can be built and installed quickly. Moreover, there are fewer regulations for operation when compared to other power generation equipment [3]. These advantages are why gas turbines are commonly used for power generation.

There are three main components in gas turbines, a) upstream compressor, b) downstream turbine and c) the combustion chamber in between. Air is sucked into the compressor and then forced through the compressor at an elevated pressure and flow velocity. Mixed with the fuel injected by the fuel injector, the pressurized air goes through the combustor and is ignited. The gas leaving the combustor at a higher temperature and flow velocity is directed towards the downstream turbine. The turbine provides the energy to generate power. Gas turbines can be categorized into five broad groups: frame type heavy-duty gas turbines, aircraft-derivative gas turbines, industrial type gas turbines, small gas turbines and micro-turbines [4].

1.1.2 Combustion Noise

As the requirements for reducing the pollutant emissions such as oxides of nitrogen (NO_x) and carbon monoxide (CO) are becoming increasingly stringently, as a result, efforts are being made to increase combustion efficiency and lower the level of pollutant emissions in both the boiler and gas turbine industries [3]. Consequently, lean premixed gas combustion is becoming more widely adopted. It produces excess air, which helps in maintaining the temperature of the products of combustion below the threshold value that is required for production of thermal NO_x [5].

Although lean premixed design minimizes the emission level of pollutants and performs at high efficiency, it is more likely to lead to combustion oscillation problems or thermo-acoustic instabilities [6, 7]. Putnam [8] pointed out that combustion systems often generate acoustical oscillations and it is difficult to design a combustion system exhibiting no oscillations. Instabilities in the combustion produce a sound source due to the fluctuating (or acoustic) volume

velocity at the flame. Sound is then reflected back from the combustion chamber and disturbs the gas flow rate or mixture composition. Ali et. al. [9] investigated the effect of acoustic-combustion interaction. They pointed out that the acoustic effect can reduce NOx formation from combustion in some cases. However, the sound is usually abnormal and objectionable.

There are several noise sources in a typical combustion system including periodic combustion-driven oscillations, panel vibrations, fan noise, and transient start-up and shut-down noise [10]. The noise radiated due to the combustion can be grouped into two classes: tonal and broadband noise. The former phenomenon usually happens in the boiler industry while the latter one is often the case in the gas turbine industry. These two different types of noise are treated using different approaches. Noise caused by the combustion process can be further categorized into two types: turbulent combustion noise (combustion roar and hiss) and combustion-driven oscillations [8]. These two types of combustion noise are caused by different mechanisms [6].

Turbulent Combustion Noise

Turbulent combustion noise, which is also called combustion roar and hiss, is a random phenomenon and therefore has a broadband spectrum [6]. The acoustic energy might be concentrated in a certain frequency range but it is not usually at a single frequency. It is caused by turbulent fluctuations in heat release, which results from turbulent velocity fluctuations in the flow supply [10]. The turbulence induced noise radiates from the source (the turbulent motion of the flame front) and there is no significant feedback from the radiated acoustic field back to the flame front. Levels of turbulent combustion noise are heavily dependent on the levels of turbulence in the flame [11].

Combustion-driven Oscillations

In contrast to turbulent combustion noise, combustion-driven oscillations are self-excited and characterized by a feedback cycle that converts chemical energy to acoustic energy [12]. Taking the flame as the sound source, the sound is radiated from the flame and reflected back to the source due to the confinement

of the combustion chamber. The reflected sound pressure fluctuation perturbs the flame via the mixture supply system which normally amplifies the heat release rate and therefore forms what Baade called "a vicious cycle" [6] as shown in Figure 1.1. The amplitude of the pressure grows exponentially in time following the onset of oscillations, until non-linear effects limit this growth [10].

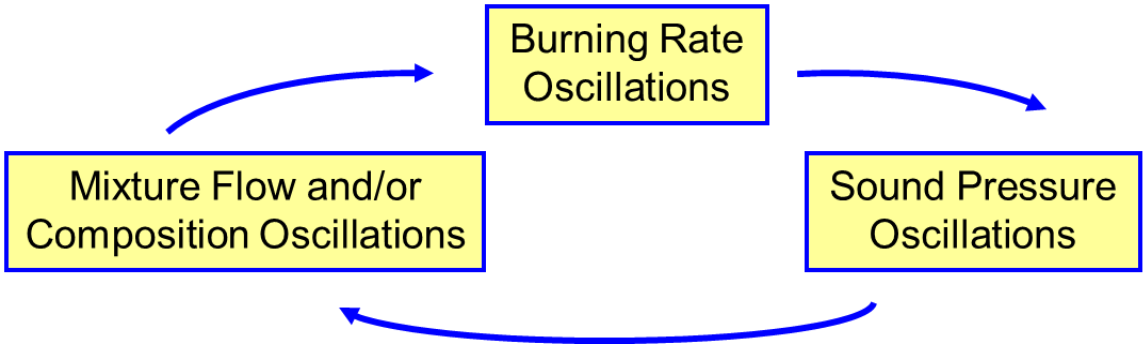

Figure 1.1 Schematic showing the vicious cycle.

It is also pointed out that combustion-driven oscillations often produce tonal noise and are dominated by a single frequency associated with side-bands and/or higher harmonics of that frequency [6]. This tonal sound is abnormal and objectionable.

The other important characteristic of combustion-driven oscillations only occur at certain operating conditions of firing rate, equivalence ratio, flow speed, vent length, and intake length [6]. Though the instabilities only occur at specific operating conditions, it is likely that a combination of conditions will lead to a problem at few particular frequencies. In that case, measures must be taken to diagnose and alleviate the problem.

Combustion instabilities not only may be annoying, but at times may become so violent as to damage or destroy the equipment [8]. They also deteriorate combustion efficiency and increase pollutant emission. In extreme cases, severe structural damage may occur [13].

Though combustion instabilities are a common phenomenon in both the gas turbine and HVAC industries, the focus in this work is on HVAC components like

boilers, furnaces, and water heaters. This problem is especially prevalent when using lean premixed combustion. During the development of higher efficiency, lower emission boilers, unacceptable noise is produced which must be treated.

1.1.3 Noise Diagnosis

Most combustion instability problems are solved in a "trial-and-error" fashion. In boiler, furnace, and water heater industry, this consumes an inordinate amount of time and effort. Putnam noted: "*Because of the uniqueness of almost every individual combustor installation, if only in regard to the associated ducting and surroundings, the acoustic acceptability of a given installation is often unpredictable on the basis of past performance of similar units. Furthermore, specific information on the acoustic behavior of components is ordinarily not available to the extent that unqualified predictions of pulsation-free performance can be made, even if the mechanism by which the pulsations could occur is known.*" [8] However, researches are now capable of modeling most of the components upstream or downstream of the flame.

Numerous researchers have tried to predict combustion instabilities. However, much of the research has focused exclusively on the combustion process with little effort on examining the acoustic dynamics. Elsari and Cummings [14] proposed a simple one-dimensional model based on standard acoustic transmission line theory, and used it to predict the instability frequencies of a system. Nevertheless, the flame dynamics were not included in the model, so it could not predict the instability regimes. They also pointed out that no universal model for predicting combustion instabilities exists.

Baade proposed a feedback loop stability model for diagnosing the combustion-driven oscillations 30 years ago [6, 15, 16]. The model assumed that the oscillations are caused by the volume flow fluctuations in the mixture supply system (not equivalence ratio fluctuations). Three transfer functions are identified either experimentally or by simulation, and are used to construct the positive feedback loop of the combustion system. One is the transfer function describing the dependence of the volume flow rate on the pressure fluctuation in the combustion chamber. The second transfer function represents the acoustic

driving point impedance of the combustion chamber at the flame front. The third one is the flame transfer function which was experimentally determined by Goldschmidt et al. [17] There is also an empirical model available [18]. The criterion for diagnosing the occurrence of combustion-driven oscillations has been established and is detailed in Section 2.2.1.

Apart from the consideration of volume flow fluctuations, Lieuwen et al. [7, 19] found that combustors operating in a lean premixed mode of combustion are highly sensitive to variations in the equivalence ratio of the mixture that enters the combustor. They also found that equivalence ratio fluctuations can be induced by interactions of the pressure and flow oscillations along with the reactant supply rates. The convective time from the point of formation of the reactive mixture at the fuel injector to the flame front controls whether or not instabilities will occur. Moreover, Lieuwen [19] summarized how premixed combustion-acoustic wave interactions can be modeled.

Similarly, Sattelmayer [20, 21, 22] investigated the influence of the combustor aerodynamics on combustion instabilities from equivalence ratio fluctuations. The fluctuations of equivalence ratio are convected into the flame which leads to heat release fluctuations. Spatial dispersion of equivalence ratio convected from the gas injector downstream to the flame front was also included. Sattlelmayer concluded that equivalence ratio fluctuations are often the cause of instabilities.

1.1.4 Noise Suppression

There is no universal approach or equipment which mitigates combustion instabilities for all applications. A vast amount of abatement research has been conducted in the past, passive, active and hybrid control have been used to solve issues. Passive control generally refers to the static modification of the engine combustion systems to damp combustion instabilities, while active control refers to the class of control techniques that use actuators to reduce the gain of the combustion system [23]. Passive and active control techniques are combined in the hybrid control.

Active noise control uses externally powered actuators to generate sound to reduce the unwanted disturbances in a system [24]. The source and system responses are monitored by a set of reference sensors. A simple example is to use a loudspeaker as a source to generate a feedback sound wave that is opposite in phase and cancels the source wave. Sound pressure is measured by sensors in the vicinity of the flame and is used to cancel sound pressure oscillations in the vicinity of the flame [25]. See References [26, 27] for more information.

In contrast to active control, passive control utilizes static devices and sound absorbing material to alleviate the noise problem. There are a variety of strategies for implementing passive control techniques including absorption material, damping, and changing the intake and exhaust lengths.

1.1.5 Bar Silencers

Silencers are devices used to abate noise. There are two types: reactive and dissipative. Reactive silencers mitigate the sources through successive reflections of sound by means of impedance mismatching [28]. Dissipative silencers convert the incident sound energy into heat [28].

A bar silencer is primarily type of dissipative silencers and uses sound absorbing materials, such as foams, fiberglass and perforates. Nilsson and Söderqvist proposed the idea of bar silencers in 1983 [29]. Bar silencers, usually with large dimensions, consist of an array of rectangular or round bars made of sound absorbing materials packed in a rectangular lattice arrangement. Each bar is covered by a perforated facing sheet to protect the material from being blown away by the exhaust gas. Sound absorbing materials have excellent broadband frequency absorption capabilities, especially at high frequencies. Bar silencers are commonly used to attenuate the turbulent combustion noise in the gas turbine and HVAC industries.

1.2 Objectives

This dissertation has two different sets of objectives. The first set focuses on combustion instabilities and the second on simulation of bar silencers. The objectives are as follows:

I. The low-order feedback loop stability models for the combustion-driven oscillations were validated.
   i. The combustion-driven oscillations were identified under certain operating conditions via experimental investigation.
   ii. The driving impedance of combustion chambers as well as impedance of the mixture supply systems was measured and modeled.
   iii. The burners were characterized by the transfer impedance.
   iv. The flame transfer functions were measured using the built test rig and also simulated using existing models.
   v. The low-order feedback loop model for mixture flow oscillations was validated based on the measured and simulated data.
   vi. A low-order feedback loop model for equivalence ratio oscillations was proposed and used for diagnosing the combustion-driven oscillations.
   vii. Panel vibrations were incorporated into the low-order acoustic models.
   viii. A design approach was proposed for preventing and solving combustion oscillation problems.

II. The acoustic performance of bar silencers was analyzed via analytical and numerical solutions.
   i. The direct mixed-body boundary element method was used to model the bar silencers.
   ii. An analytical model based on pressure and velocity matching, was investigated and used for assessing the sound attenuation in bar silencers.

iii. A parametric study was performed to evaluate the effects of different parameters, such as flow resistivity of material, perforate porosity of the facing sheet, length of bars and cross-sectional area ratio, on the acoustic performance of bar silencers.

iv. A new approach based on the reciprocal work identity was proposed and extended to calculate the *TL* above plane wave cut-off frequency.

1.3 Organization

This dissertation is arranged in the following fashion:

CHAPTER 1 introduces the background knowledge for power equipment and combustion noise due to roar or instabilities.

CHAPTER 2 to CHAPTER 4 discuss low-order models for diagnosing and alleviating the combustion-driven oscillations. CHAPTER 2 describes the feedback loop stability model for mixture flow oscillations and the newly developed model for equivalence ratio oscillations. Both models are then applied to two commercial boilers which exhibited mixture flow or equivalence ratio fluctuations respectively. In addition, the measurement and simulation of the flame transfer function, which is one of the three significant components in low-order models, is detailed. CHAPTER 3 proceeds to investigate the other two acoustic transfer functions, namely the driving impedance of the combustion chambers and impedance of the mixture supply. Transfer matrix theory, which is the basis for the low-order model, is reviewed. For complicated boilers, the procedure using acoustic FEM to predict the impedance is described. Additionally, a transfer matrix element for including structural vibrations for a flat plate is developed and validated. CHAPTER 4 introduces a design approach for preventing and solving combustion oscillation problems.

The broadband noise mitigation using dissipative bar silencers is emphasized in CHAPTER 5 to CHAPTER 6. In CHAPTER 5, the direct mixed-body boundary element method is employed to evaluate the acoustic performance of bar silencers. Serving as a comparison tool, the analytical approach based on the

pressure and velocity matching technique is elaborated and applied to determine the transmission loss of a hypothetical bar silencer. Due to the large dimension of bar silencers, it is not practical to evaluate the acoustic performance above the plane wave cut-off frequency using the conventional definition of *TL*. *TL* is then defined above plane wave cut-off frequency. A parametric study is carried out to detect the effects of four important parameters: flow resistivity, perforate porosity, length of bars and cross-sectional area ratio. To calculate the *TL* above the plane wave cut-off frequency numerically, a new approach is proposed which is detailed in CHAPTER 6. First, CHAPTER 6 reviews the current techniques for obtaining the *TL* of silencers and details a new approach which is based on the reciprocal work identity. Further, the extension including higher order modes is discussed and a test case is studied.

Summary, conclusions and suggestions for future work are presented in CHAPTER 7.

CHAPTER 2 ASSESSING THE CAUSES OF COMBUSTION-DRIVEN OSCILLATIONS IN BOILERS USING A FEEDBACK LOOP STABILITY MODEL

2.1 Introduction

When a new boiler is developed, it is probable that a tonal noise will develop that is both abnormal and objectionable. This tonal noise results from a thermo-acoustic instability known as a combustion-driven oscillation. Combustion-driven oscillations occur when sound is reflected from the combustion chamber into the mixture supply chamber or even further upstream to the gas valve. The sound, which is a fluctuating pressure, leads to either mixture flow or composition (i.e., equivalence ratio) fluctuations. This results in a fluctuating heat release or volume velocity, which is an acoustic disturbance in the combustion chamber. Baade [6] noted that this phenomenon is a positive feedback loop that will lead to higher amplitude combustion oscillations until the behavior is no longer linear.

At the present time, boiler, water heater, and furnace manufacturers solve these problems in a trial-and-error fashion and in a variety of different ways. Typical solutions include modifying the geometry of the combustion chamber, adding acoustic absorption, switching burners and gas valves, and setting the boiler controls to avoid certain operating conditions. However, problems are not generally solved by the industry in a systematic manner.

The aim of this work documented herein is to assist the boiler industry in moving towards a more systematic approach. Specifically, a low-order model for the combustion oscillation phenomenon is documented and then demonstrated on two boilers that exhibited oscillations. The model, proposed by Baade [6, 15] over 30 years ago, was targeted towards combustion oscillations that arise from a fluctuating mixture flow. Since oscillations can also result from a fluctuating mixture composition, a complementary model has been developed based on work by Sattelmayer [20, 21].

It appears that Higgins [30] was the first to document the existence of combustion oscillations. In his classic work, Lord Rayleigh later explained the phenomenon stating: "*If heat be periodically communicated to, and abstracted from, a mass of air vibrating (for example) in a cylinder bounded by a piston, the effect produced will depend upon the phase of the vibration at which the transfer takes place. If heat be given to the air at the moment of greatest condensation, or taken from it at the moment of greatest rarefaction, the vibration is encouraged.*" [31] Lord Rayleigh noted that a primary requirement for amplification of the instability via the feedback process is the phase relationship between the acoustic pressure and the heat transfer.

In the 1950's, Putnam [8] mathematically described the Rayleigh criterion and suggested that thermo-acoustic instabilities may occur if

$$\int_0^T p(t)q(t)dt > 0 \tag{2.1}$$

where $p(t)$ is the acoustic pressure and $q(t)$ the pulsating portion of the heat release rate. It was assumed that the acoustic particle velocity ($v(t)$) is proportional to the pulsating portion of the heat release of the flame ($q(t)$). It follows that the left hand side of Equation (2.1) is also proportional to the acoustic energy generated for a cycle (i.e. the sound power). For thermo-acoustic instabilities to occur, the left hand side must be positive and greater than the amount of acoustic energy dissipated.

Perturbations in the burn rate are unavoidable. However, these perturbations will not necessarily lead to thermo-acoustic instabilities unless a self-exciting mechanism is present. Instabilities occur when small modulations of the flow rate or composition of the mixture lead to heat release oscillations. Heat release oscillations result in a fluctuating volume velocity (i.e. an acoustic disturbance) leading to acoustic oscillations that feed back into the mixture.

2.2 Low-Order Model for Mixture Flow Oscillations

2.2.1 Feedback Loop Stability Model

Baade [6, 15] contributed significantly by 1) restating Putnam's equation in the form of a feedback loop and 2) defining this relationship in the frequency domain. In doing so, Baade identified three transfer functions that need to be determined. Two of the transfer functions (Z and H) are acoustic and can be determined experimentally or by simulation. The other transfer function (G_f) is related to the flame and is best determined experimentally though a few models are available.

Figure 2.1 shows a schematic of Baade's feedback loop stability model (Baade [6, 15]) for the prediction of combustion oscillations. Perturbations to the volume velocity of the flame, which are external to the feedback loop, are indicated by $\tilde{q}_{ext}$. The driving point impedance (Z) of the combustion chamber is the ratio of the oscillating pressure ($\tilde{p}$) to the volume velocity in the combustion chamber ($\tilde{q}_{tot}$ or $\tilde{Q}$). H is the transfer function relating the perturbation of the mixture flow ($\tilde{q}_i$) to the acoustic pressure in the combustion chamber ($\tilde{p}$).

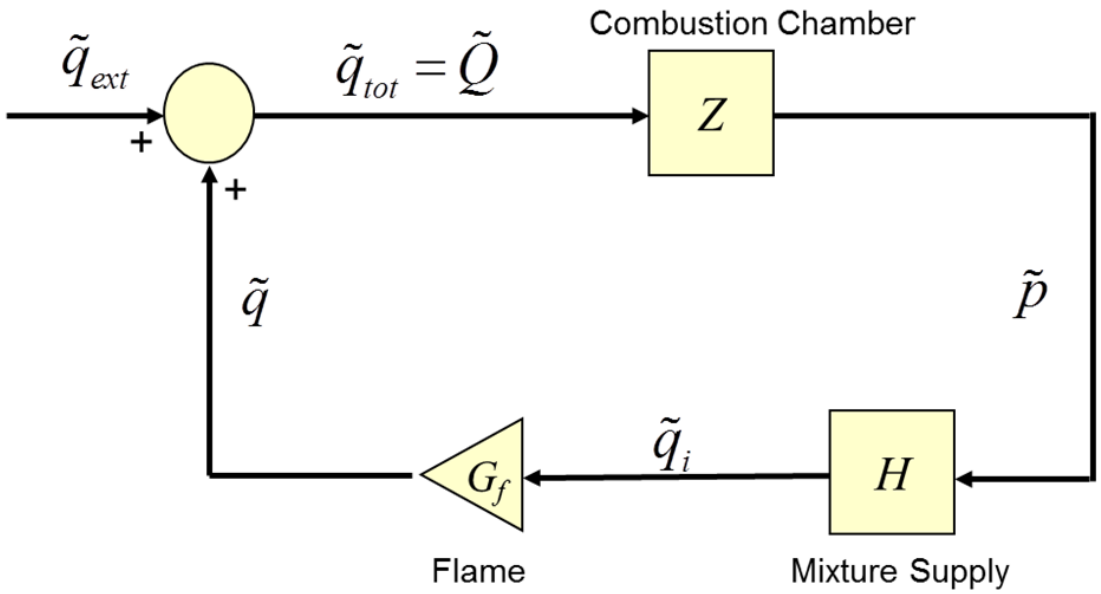

Figure 2.1 Feedback loop stability model defined by Baade [6, 15].

In order to close the loop, a transfer function describing the flame is required which Baade [6] terms the flame transfer function (G_f). In a companion paper to Baade's work, Goldschmidt et al. [17] defined G_f as the ratio of the volume flow oscillations ($\tilde{q}$) to the volume velocity of the mixture flow ($\tilde{q}_i$). Thus,

$$G_f = \frac{\tilde{q}}{\tilde{q}_i} \tag{2.2}$$

The flame transfer function can alternatively be defined as the ratio of the fluctuating part of the burned mass flow rate to the injected mass flow rate (Goldschmidt et al. [17]). This transfer function is typically measured and will be described in greater detail later.

After defining the three transfer functions (Z, H, and G_f), it is straightforward to derive an expression for the stability criterion based on the feedback loop (Baade [6]). If all three transfer functions are multiplied together, one obtains

$$H \times G_f \times Z = \frac{\tilde{q}_i}{\tilde{p}} \times \frac{\tilde{q}}{\tilde{q}_i} \times \frac{\tilde{p}}{\tilde{q} + \tilde{q}_{ext}} = \frac{\tilde{q}}{\tilde{q} + \tilde{q}_{ext}} \tag{2.3}$$

If $\tilde{q}_{ext}$ is assumed to be zero, the ratio on the right hand side of the equation is unity. Thus,

$$H \times G_f \times Z = 1 \tag{2.4}$$

There is an alternative to obtain Equation (2.4). Z relates the fluctuating pressure to the volume velocity in the combustion chamber and can be defined as

$$Z = \frac{\tilde{p}}{\tilde{Q}} \tag{2.5}$$

In addition, the volume velocity consists of two parts: 1) fluctuating flame and 2) external fluctuating volume input and can be defined as

$$\tilde{Q} = \tilde{q}_{ext} + G_f H \tilde{p} \tag{2.6}$$

Rearranging the Equation (2.5) and Equation (2.6), the fluctuating pressure and the external fluctuating volume velocity can be related and expressed as

$$\frac{\tilde{p}}{\tilde{q}_{ext}} = \frac{Z}{1 - ZHG_f} \tag{2.7}$$

If $\tilde{q}_{ext} = 0$ is assumed, then the above equation becomes infinite and hence Equation (2.4) is obtained.

Equation (2.4) defines a threshold for when self-excited oscillations maintain themselves but do not grow (Baade [6]). Note that Z, H, and G_f are each complex functions of frequency. However, the right hand side of Equation (2.4) is real. This implies that instabilities can only occur at frequencies where the summation of the phase angles of Z, H, and G_f is equal to 0° or a multiple of 360°. Accordingly, conditions for thermo-acoustic instabilities are favorable at frequencies where the left hand side of Equation (2.4) exceeds 1 and is real. For simplicity, Baade [15] and Baade and Tomarchio [16] recast Equation (2.4) as the inequality

$$|Z \times H| > \frac{1}{|G_f|} \tag{2.8}$$

Combustion oscillations are more likely to occur at frequencies where the left hand side of Equation (2.8) exceeds the right hand side.

2.2.2 Acoustic Model of the System

In the following discussion, we have chosen to follow the line of reasoning in Elsari and Cummings [14] to describe the acoustic model. The model assumes

- Plane wave propagation inside the duct.
- Low Mach number flow.
- The length of the flame is small compared to an acoustic wavelength.

The validation of plane wave propagation in burner is detailed in APPENDIX A.

Figure 2.2 shows a diagram of a duct with heat release. The flame can be assumed to be a volume velocity source having volumetric source strength (Q). Conservation of mass requires that

$$Q = S_1\tilde{u}_1 + S_2\tilde{u}_2 \tag{2.9}$$

where $\tilde{u}_1$ and $\tilde{u}_2$ are the acoustic particle velocities in the upstream and downstream duct respectively and S_1 and S_2 are the corresponding cross-sectional areas.

Assuming that Δ is small compared to an acoustic wavelength, the acoustic pressures $\tilde{p}_1$ and $\tilde{p}_2$ (indicated in Figure 2.2) should be equal to each other due to continuity of acoustic pressure. Z_u and Z_d are the upstream and downstream acoustic impedance (ratio of sound pressure to volume velocity) respectively.

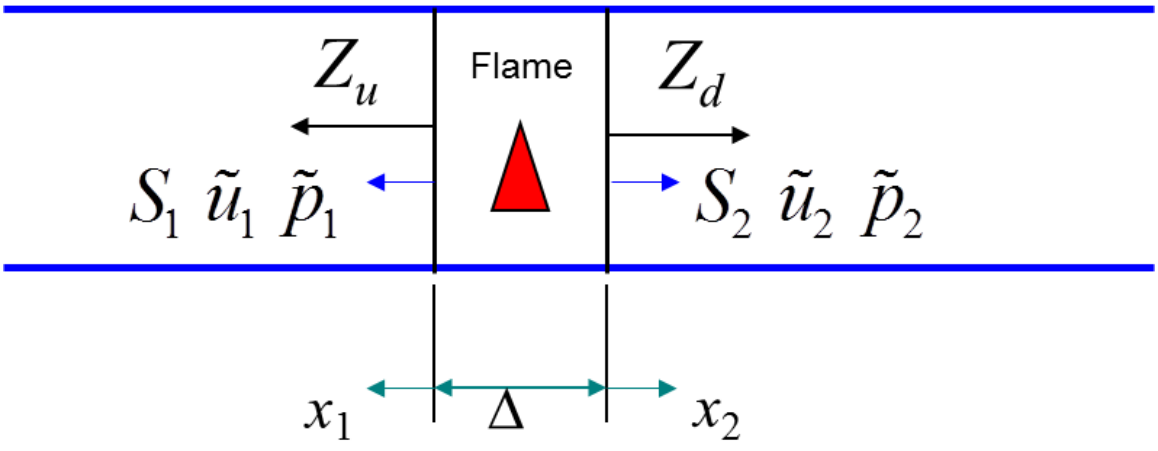

Figure 2.2 Schematic of flame showing upstream and downstream impedances.

An acoustic circuit can be constructed as shown in Figure 2.3. The constructed circuit is analogous to an electrical circuit in which the sound pressure and volume velocity correspond to voltage and current respectively. Note that the upstream and downstream impedances (Z_u and Z_d) are in parallel to one another. It follows that Z is the equivalent acoustic impedance of the acoustic circuit shown in Figure 2.3 and can be written as

$$Z = \frac{\tilde{p}}{\tilde{q}_{tot}} = \frac{Z_u Z_d}{Z_u + Z_d} \tag{2.10}$$

Baade [6] noted that $\tilde{q}_{tot}$ and $\tilde{p}$ are not the input and output to the combustion chamber but are instead the respective inputs and outputs to the dynamic process taking place within the combustion chamber.

Perturbation of the volume velocity of the mixture flow is indicated by $\tilde{q}_i$ and is equal to the negative of $S_1\tilde{u}_1$ in Figure 2.2. Therefore, H is the negative admittance (admittance is the reciprocal of acoustic impedance) of the burner ports looking into the mixture supply (Baade [6]) and can be expressed as

$$H = \frac{\tilde{q}_i}{\tilde{p}} = \frac{-S_1\tilde{u}_1}{\tilde{p}} = -\frac{1}{Z_u} \tag{2.11}$$

Again, $\tilde{q}_i$ and $\tilde{p}$ are not the input and output to the mixture supply but instead describe the dynamic process taking place at the mixture supply.

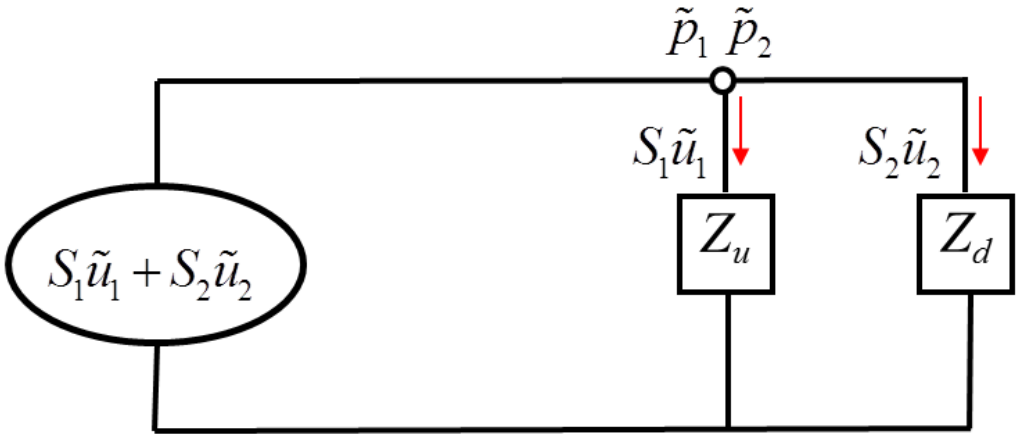

Figure 2.3 Schematic showing equivalent acoustic circuit illustrating that the upstream and downstream impedances at then flame are in parallel.

2.2.3 Measurement of Flame Transfer Function

The flame transfer function is the ratio of the fluctuating burned mass flow rate to injected mass flow rate [17]. Goldschmidt et al. [17] used an acoustic approach

to measure the flame transfer function. A loudspeaker was used as an excitation below the burner to fluctuate the burner inlet flow and sound pressure was measured with and without the flame.

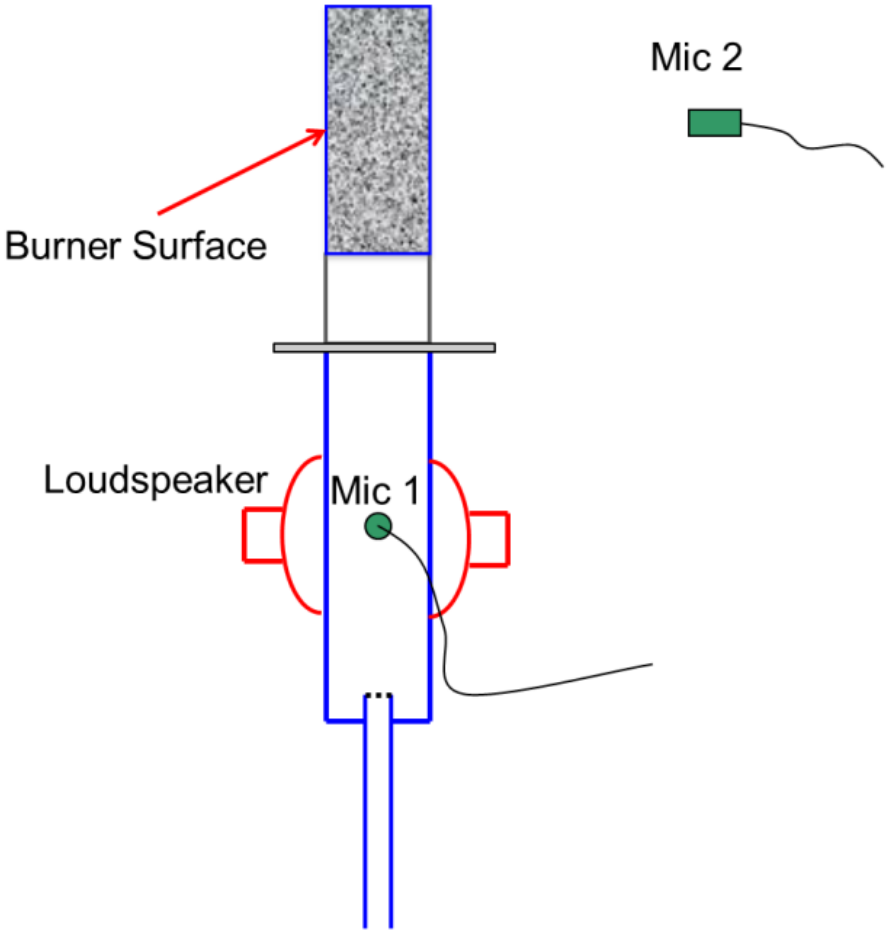

Figure 2.4 Schematic illustrating the approach to measure flame transfer function from Goldschmidt et al. [17]

Figure 2.4 shows a schematic of the approach suggested by Goldschmidt et al. [17] to oscillate the inlet flow and measure the flame oscillation. Notice that the loudspeaker is placed in the fuel-air mixing chamber. Sound pressure is measured in both the mixing chamber (Microphone 1) and after the combustion (Microphone 2). The sound pressure (measured at Microphone 2) with the flame off (p_{off}) is proportional to the fluctuating volume flow in the burner inlet (q_i). Similarly, the sound pressure with the flame on (p_{on}) is proportional to the volume

flow oscillations (q) in the combustion chamber. Microphone 1 is used to monitor the input to insure that it is consistent between both tests. The flame transfer function G_f is then defined as

$$G_f = \frac{\tilde{q}}{\tilde{q}_i} = \frac{\tilde{p}_{on} - \tilde{p}_{off}}{\tilde{p}_{off}} \tag{2.12}$$

Alternatively, Kornilov [18] and Kornilov et al. [32] and Khanna [5] used chemi-luminescence to detect OH^+ as a heat release rate indicator which can be directly related to $\tilde{q}$. In the case of Kornilov, a hot wire anemometer was used to measure the flow velocity oscillations ($\tilde{q}_i$) with the flame off. The gain of the flame transfer function was found by taking the ratio of the amplitude of the Fourier transform of the I_{OH+} signal to the amplitude of the acoustic velocity signal measured by the hot wire anemometer. Like Goldschmidt et al. [17], the flow rate was perturbed by a loudspeaker excitation.

2.2.4 Prediction of Flame Transfer Function

Kornilov [18] developed an empirical formula, which was modified by Baade and Tomarchio [16], for the flame transfer function for a Bunsen burner. The flame transfer function is expressed as

$$G_f = \frac{1}{1 + A_0}\left(\frac{e^{-j\tau_0\omega}}{(j\tau_1\omega + 1)^2} + A_0\right)\left(\frac{\rho_u}{\rho_d} - 1\right) \tag{2.13}$$

where A_0 denotes the offset term of flame transfer function, τ_0 time delay parameter, τ_1 attenuation parameter, ω the angular frequency, ρ_u density of the unburned mixture and ρ_d density of the combustion products.

τ_0 is defined as

$$\tau_0 = \frac{2\pi V_0}{T_0 H} \tag{2.14}$$

where V_0 represents the mean gas velocity, H flame height and T_0 an empirical constant.

τ_1 is defined as

$$\tau_1 = \frac{T_1}{\sqrt{H} S_L} \tag{2.15}$$

where S_L is the flame propagation velocity and T_1 an empirical constant.

Kornilov's model should be useful as an estimate. The model was developed for Bunsen burners and most commercial burners can be thought of an array of Bunsen burners. However, the model does not take into account the actual burner geometry, the presence of diffusers to control flow, or the effect of metal or ceramic meshes on the burner surface.

2.3 Boiler 1 – Mixture Flow Fluctuations

Boiler 1 was a 58 kW (200,000 BTU/hour) capacity propane gas boiler representative of relatively massive and rigid fire tube boilers. The heat exchanger is cast aluminum with numerous fingers in the lower chamber to facilitate heat transfer. The combustion oscillation problem occurred when the boiler was running lean at approximately 2100 Hz. If the equivalence ratio was increased, the instability did not occur. A simplified schematic of the heat exchanger for Boiler 1 is shown in Figure 2.5.

Table 2.1 and Table 2.2 list the operating conditions and whether or not combustion oscillations occurred. Additionally, temperature measurements were also made inside of the combustion chamber using thermocouples. There were three ports in the chamber (upper, middle, and lower) where temperature measurements could be made.

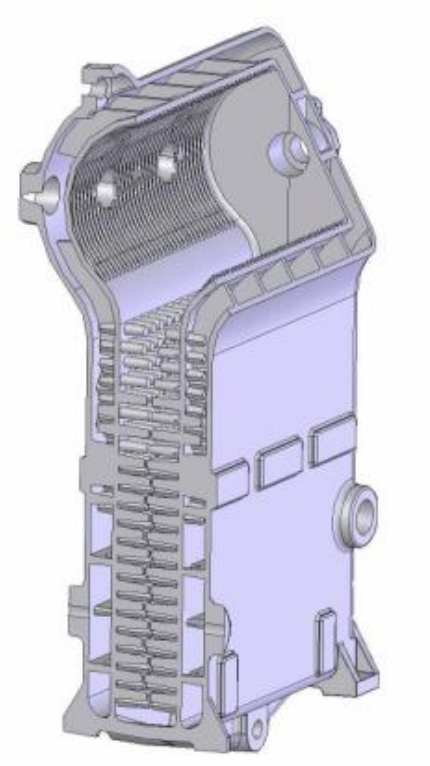

Figure 2.5 Schematic showing the heat exchanger for Boiler 1.

The sound pressure level at the combustion oscillation frequency exceeded 80 dB at some positions. Background noise had been checked as a first step, and noise levels were below 50 dB.

Table 2.1 Operating conditions for Boiler 1

No.	Combustion Driven Oscillation	Frequency (Hz)	Intake Duct Length (in)	Exhaust Duct Length (in)	CO2	Gas Rate (Watts)	Equivalency Ratio
1	NO		30	40	12.46%	2.27E+05	1.15
2	NO				11.40%	2.07E+05	
3	NO		30	40	13.25%	1.71E+05	1.13
4	YES	2132	30	40	13.34%	2.20E+05	
5	YES	2125	30	40	13.21%	2.07E+05	1.16
6	YES	2132	288	40	13.22%	2.11E+05	
7	YES	2031	528	40	13.25%	1.98E+05	
8	YES	2125	30	288		2.10E+05	1.14
9	YES	2031	30	528		1.94E+05	1.10
10	YES		288	288			

Table 2.2 Operating conditions for Boiler 1 Continued.

No.	Air Fuel Ratio	Inducer RPM (Strobe)	Intake Flow Rate (ft/s)	Exhaust Flow Rate (ft/s)	Notes
1	13.6	4577	24	39.4	Baseline
2					Increase AFR and vary lengths
3	13.8	4602	18.4	29.9	Change burner and vary lengths
4		4591		38.1	Partially block intake
5	13.4	4581	21.7		Partially block exhaust
6		4598		37.7	
7		4605		36.4	Weaker instability
8	13.7	4622	22.3		
9	14.2	4584	21.3		Weaker instability
10					

Table 2.3 Temperature measurements for Boiler 1.

No.	Temperatures (°F)						
	Upper Combustion Chamber (0.125 in from Burner)	Upper Combustion Chamber (1 in from Burner)	Middle Combustion Chamber	Lower Combustion Chamber	Lower Flue Outlet	Upper Flue Outlet	Inlet Air
1	1689	720	912	128	130	128	57
2		655	880	121	122	120	56
3		898	709	117	116	118	56
4	1684	770	882	131	126	132	56
5	1680	813	842	130	126	131	55
6	1640	863	867	133	128	133	57
7	1670	930	825	136	130	136	56
8	1660	830	856	139	143	139	55
9	1644	819	805	137	141	138	56

Temperature measurements were made in the positions shown in Figure 2.6. Three thermocouples were inserted into the top, middle and lower combustion chamber respectively. The temperature measurements were conducted twice in the top position: one was $1/8$ inch from burner and the other was 1 inch from burner. In addition, the temperature at the lower and upper flue outlet as well as inlet air were monitored. Temperature measurements are tabulated in Table 2.3. The number indicates the operating condition number in Table 2.1 and Table 2.2.

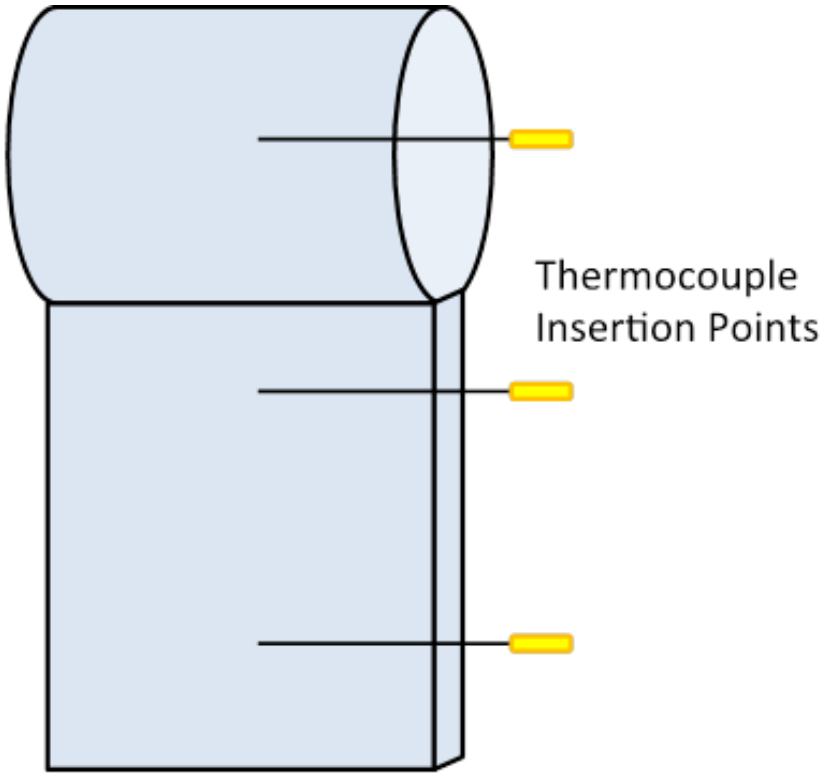

Figure 2.6 Schematic showing thermocouple insertion points for Boiler 1.

2.4 Results for Boiler 1

2.4.1 Boiler 1 Measurement of Flame Function

The flame transfer function was measured using the method of Goldschmidt et al. [17] described in Section 2.2.3. Figure 2.7 shows the flame transfer function measurement test rig that was created by the team. The burner was mounted horizontally in order to better represent the manner in which the burner was installed. Two microphones were utilized in the experiment. One was placed in the mixture tube and used as a phase reference. The other microphone is positioned away from the test rig and used to measure the sound pressure with flame on and flame off.

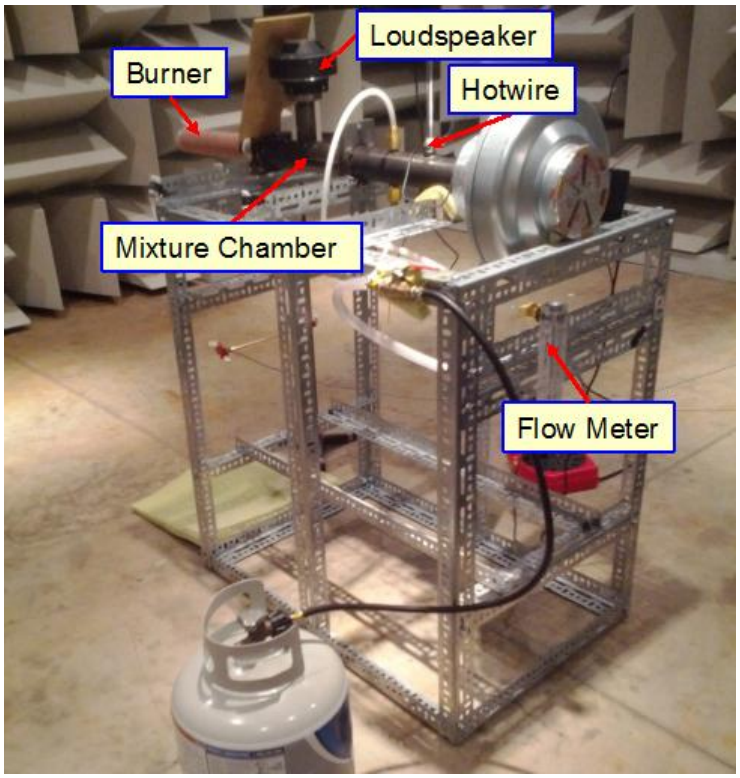

Figure 2.7 Flame transfer function measurement rig.

A loudspeaker was placed inside the mixture tube and was excited using sinusoidal excitation. White noise excitation was also attempted but there was not enough sound energy produced for accurate measurement of the flame transfer function. The phase, in particular, was difficult to measure.

At each frequency examined, measurements were performed with the flame on and off. The sound pressure level inside the mixture tube was monitored and adjusted to be at the same level for each test. The fan controller was unchanged for both tests to insure the same flow rate.

Switching burners eliminated the combustion oscillation for Boiler 1. Accordingly the flame transfer function was measured for the original burner and for the burner that eliminated the instability. Before measuring, the equivalence ratio was fixed by adjusting the air and fuel flow. The flow rates were adjusted to match the operating cases for both burners. The flow velocity of the air was measured using a hot wire and the gas flow with a flow meter (Figure 2.7).

Figure 2.8 and Figure 2.9 compare the flame transfer function magnitude and phase for both burners. With Burner 1 installed, the boiler exhibited combustion oscillations. Notice that the flame transfer function is similar in each case, which suggests that the effect of switching burners on the flame transfer function is minimal. The fact that the phase is stable and relatively smooth lends confidence to the measurement.

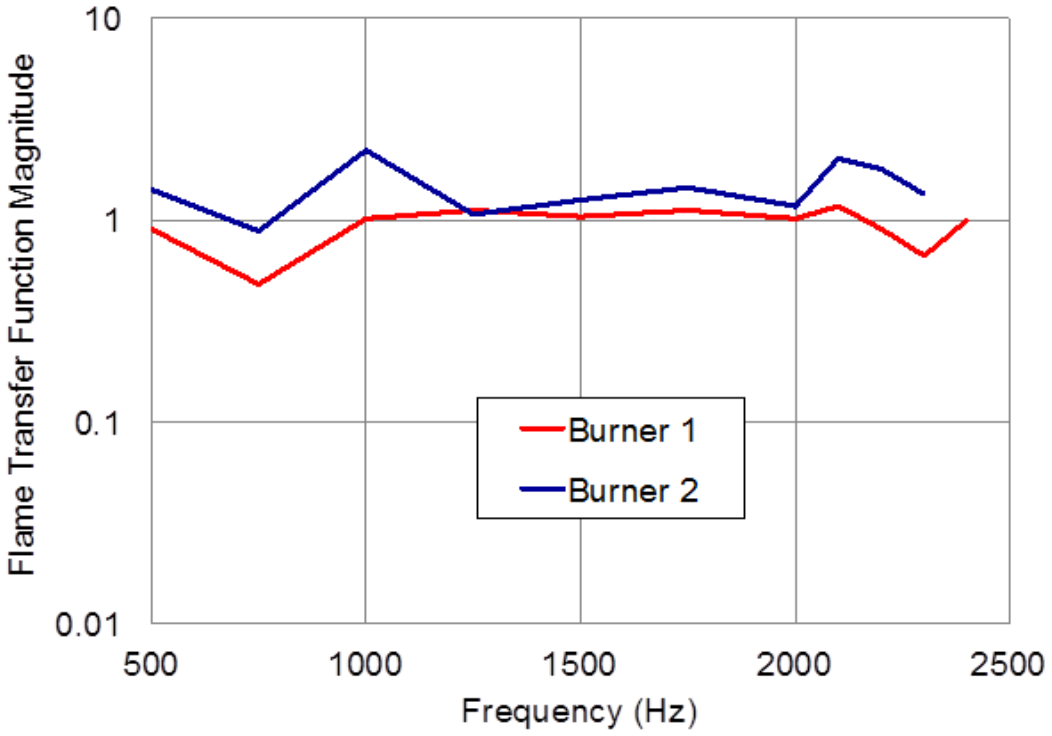

Figure 2.8 Comparison of flame transfer function magnitude with different burners.

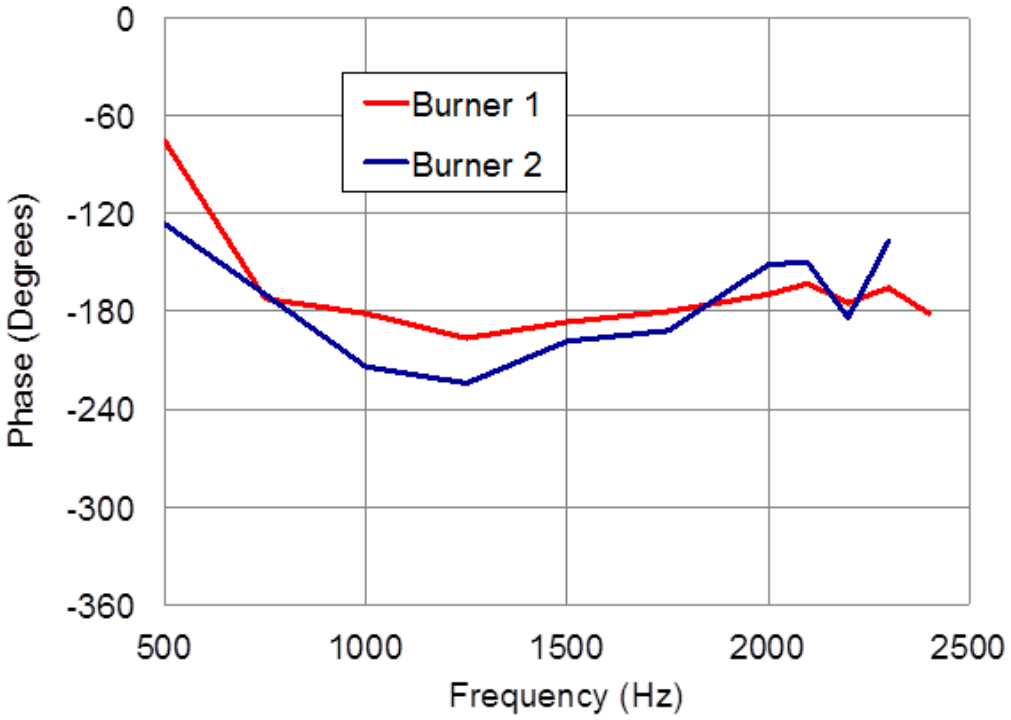

Figure 2.9 Comparison of flame transfer function phase with different burners.

2.4.2 Boiler 1 Feedback Loop Model Results

Switching the burner alleviated the instability. Figure 2.10 shows a schematic of a typical burner and Table 2.4 shows the primary dimensions for both Burners 1 and 2. With Burner 1, the boiler exhibited the combustion oscillation. Burner 1 consisted of a perforated metal cylinder with a ceramic fabric sock. A ring diffuser is positioned 12.5 cm (5 in) from the burner base. Burner 2 had a higher flow resistance and consisted of three layers; two perforated cylinders with a small gap between them and a sintered metal sock wrapping the outer cylinder. Both burners are similar in diameter but Burner 1 is 5 cm (2 in) longer. In Burner 2, a distributor panel is located at the attachment point. The panel incorporated a pattern of 5 mm (0.2 in) and 11 mm (0.43 in) circular holes.

If no inlet or vent pipe was attached, combustion-driven oscillations were not produced (Table 2.1). However, oscillations were induced if the intake or exhaust openings were partially blocked with masking tape (see Figure 2.11). The tape

has low mass so the acoustics will not be affected appreciably. However, the blockage will reduce the flow rate. A similar reduction in flow rate is achieved by adding length to the intake and/or exhaust pipes. By adding additional lengths to the intake and exhaust pipes, it was determined that the combustion oscillations primarily occurred for intake flow rates around 6.5 m/s. Flow rate was measured using an anemometer.

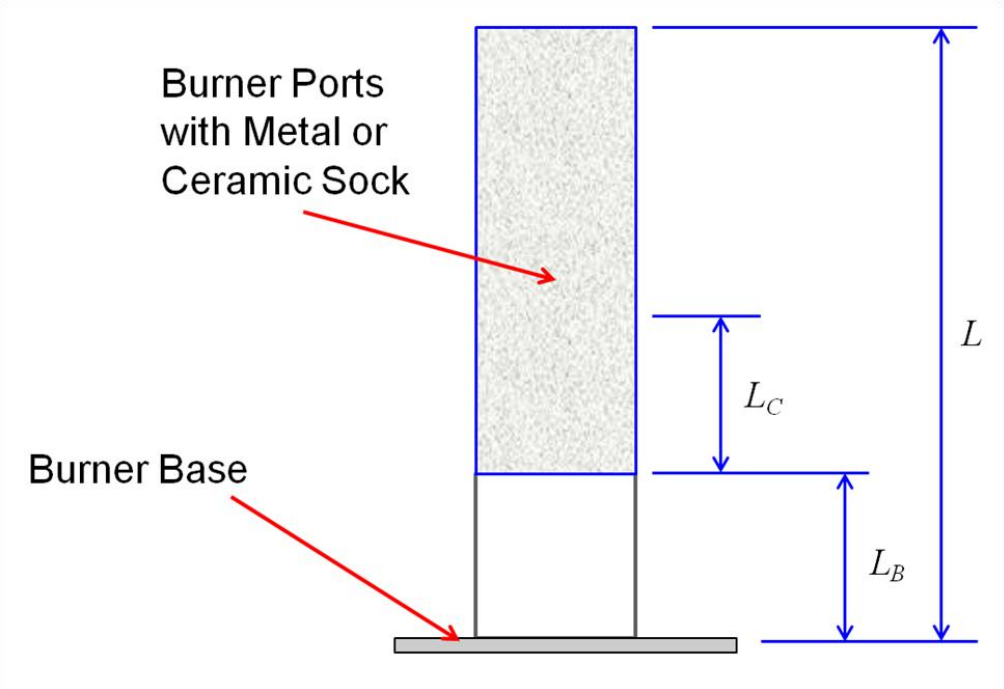

Figure 2.10 Schematic showing the configuration of the burner.

Table 2.4 Overall dimensions of Burners 1 and 2.

No.	Burner 1		Burner 2	
	in	cm	in	cm
L_B	2.0	5.0	2.8	7.2
L	13.6	34.5	11.5	29.2
d	1.9	4.8	2.5	6.3

Figure 2.11 Photograph showing partially blocked intake.

The feedback loop stability model for Boiler 1 was determined using the calculated impedances downstream and upstream, and the measured flame transfer functions [33]. The impedance was determined using the approach discussed in CHAPTER 3. The impedance of the burner was added to the upstream impedance at the burner attachment. Plane wave propagation was assumed inside the burner. This appears reasonable since the speed of sound is very different inside and outside the burner due to the high temperatures. Accordingly, there is a significant difference in characteristic impedance between the higher and lower temperature gas media.

Since the oscillation occurred above 2000 Hz, the acoustic wavelength will be on the order of 15 cm (6 in). At high frequencies, the dimensions of the burner itself will be important (i.e., small compared to an acoustic wavelength). As shown in Figure 2.10, L_B is the distance from the burner base to the lower burner port openings, and L_C is the distance from the lower burner port openings to the approximate center of the burner port surface (the approximate center of the flame which is the acoustic source). No visualization techniques were used so the dimension of L_c is an estimate. For Burner 1, 12.5 cm (5 in) was assumed for L_C.

The combined length of tube ($L_B + L_C$) can be considered as a duct with cross-sectional area equal to that of the burner. Using the methods described in Reference [34], a transfer matrix can be developed for the combined length with four-pole parameters A, B, C, and D. The burner can be treated as a transfer impedance (Z_{tr}) which can be measured or predicted according to Wu et al. [35] and Liu et al. [36]. More details are presented in CHAPTER 3. In that case, the total upstream impedance can be expressed as

$$Z_u = \frac{(A + Z_{tr}C)Z_{att} + B + Z_{tr}D}{CZ_{att} + D} \tag{2.16}$$

where Z_{att} is the impedance at the burner attachment.

Using the simulation model, the length of the burner from the attachment point to the burner surface (L_B) was varied. Figure 2.12 compares $|Z \times H|$ for various selected lengths. Notice that the variation is significant around 2100 Hz. As shown in Figure 2.13, the effect of switching from one burner port pattern to another on $|Z \times H|$ was also investigated but was found to be less significant. The results suggest that the geometry of the burner is more important than the burner port pattern or the material selected for the sock (i.e., sintered metal or ceramic fiber) placed over the burner port cylinder.

The plots of magnitude and phase for $Z \times H$ and $1/G_f$ are shown in Figure 2.14 and Figure 2.15 for Burner 1 and Figure 2.16 and Figure 2.17 for Burner 2. Thermo-acoustic instabilities are possible when the magnitude of $Z \times H$ exceeds $1/G_f$ and when the phases of $Z \times H$ and $1/G_f$ are equivalent. The results indicate that a combustion oscillation is possible at 2100 Hz for the selected ($L_B + L_C$). However, this selected length is somewhat arbitrary so the validation of the model is inconclusive.

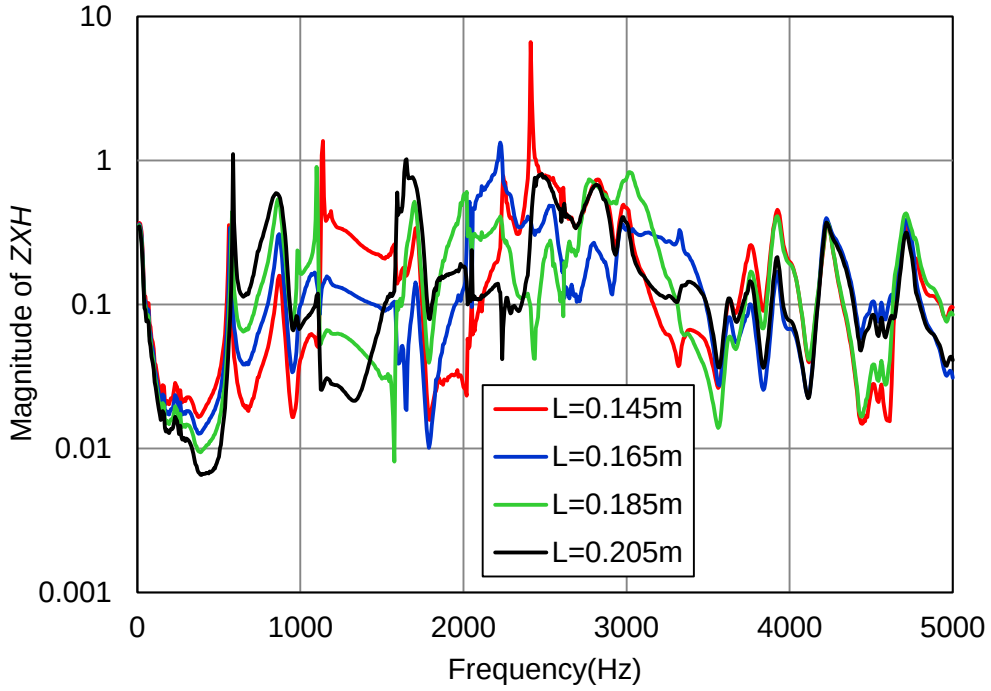

Figure 2.12 Effect of varying distance from burner attachment on $|Z \times H|$.

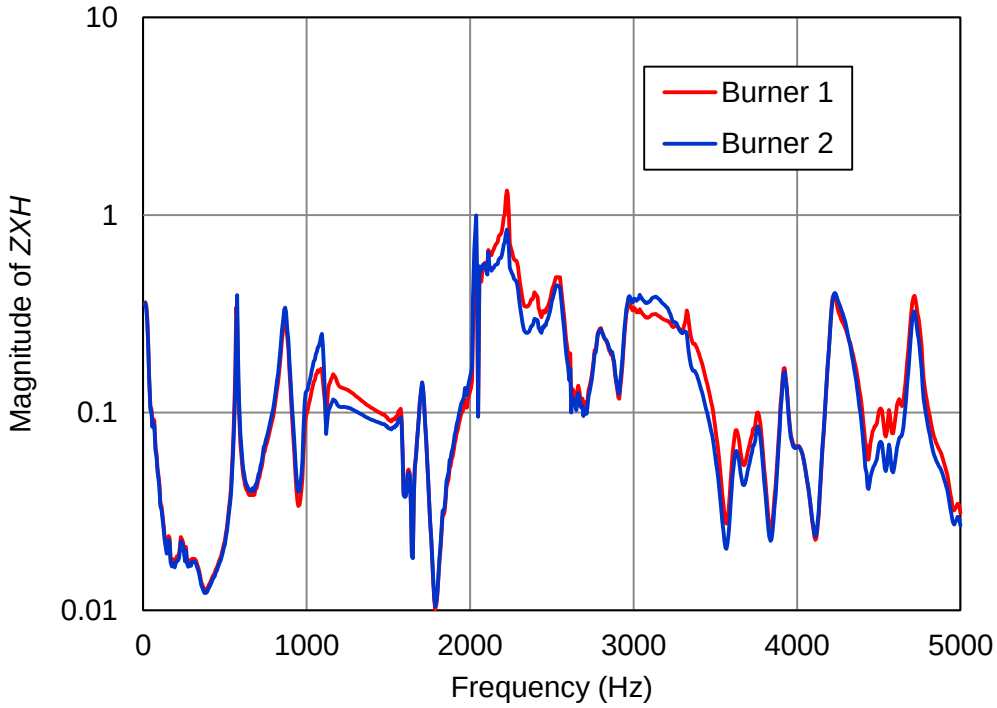

Figure 2.13 Effect of switching burner surface on $|Z \times H|$.

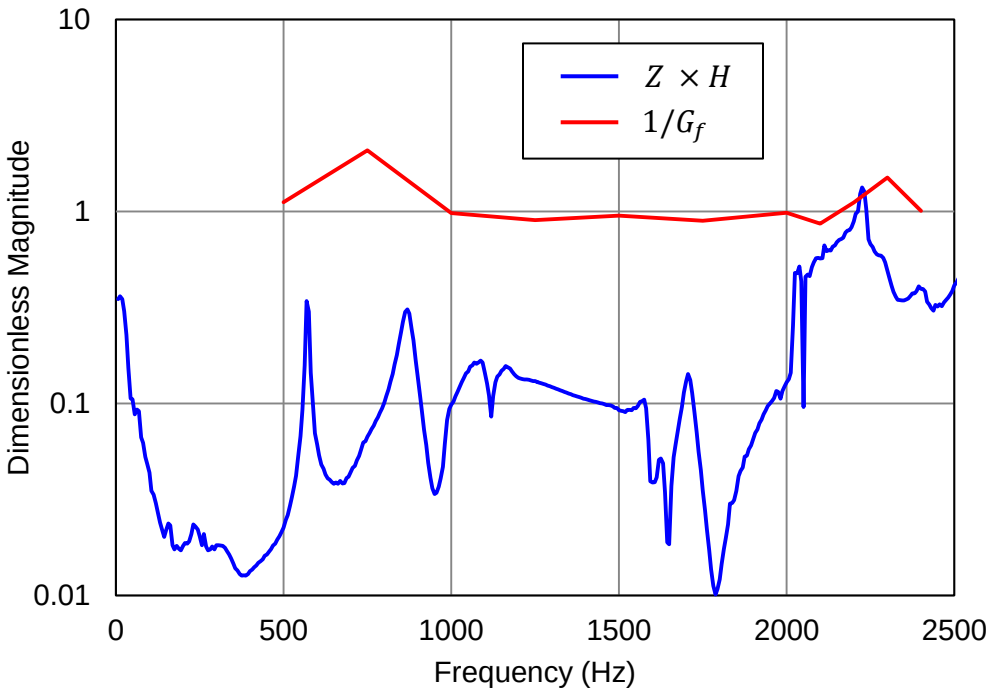

Figure 2.14 Magnitude of $Z \times H$ and $1/G_f$ with Burner 1.

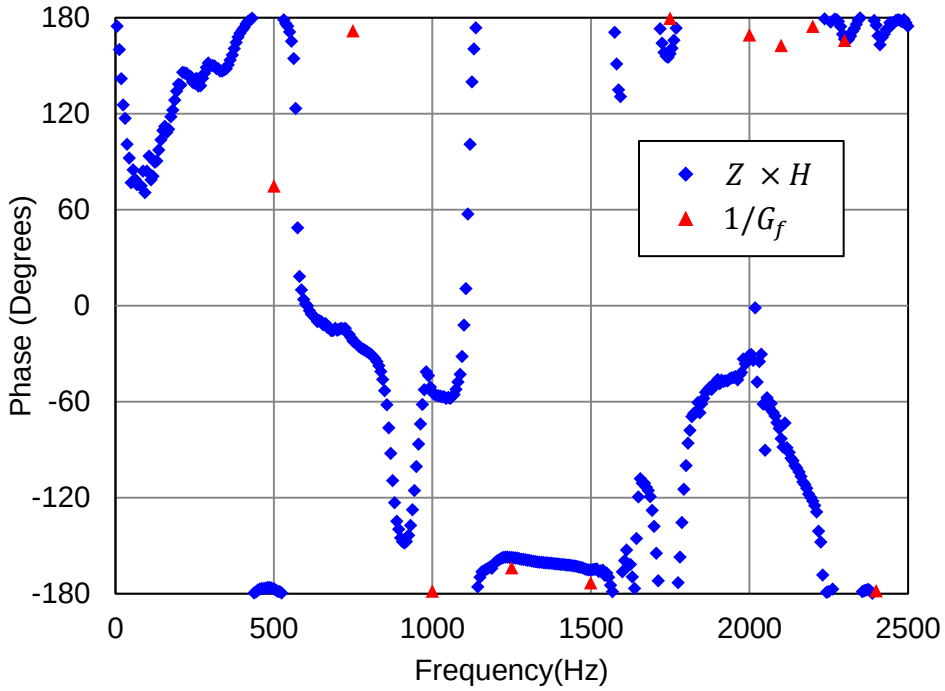

Figure 2.15 Phase of $Z \times H$ and $1/G_f$ with Burner 1.

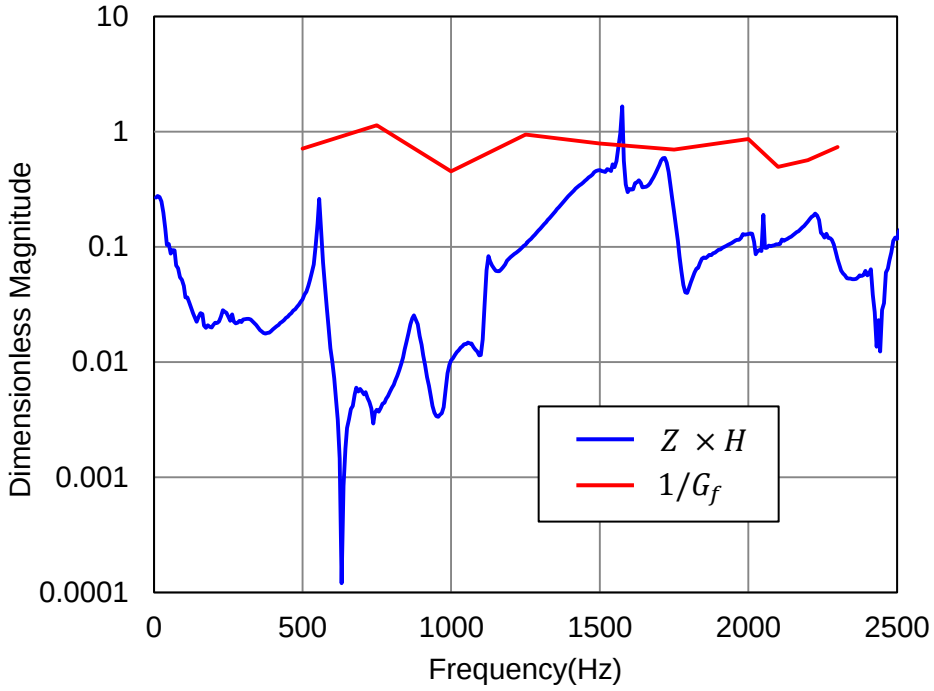

Figure 2.16 Magnitude of $Z \times H$ and $1/G_f$ with Burner 2.

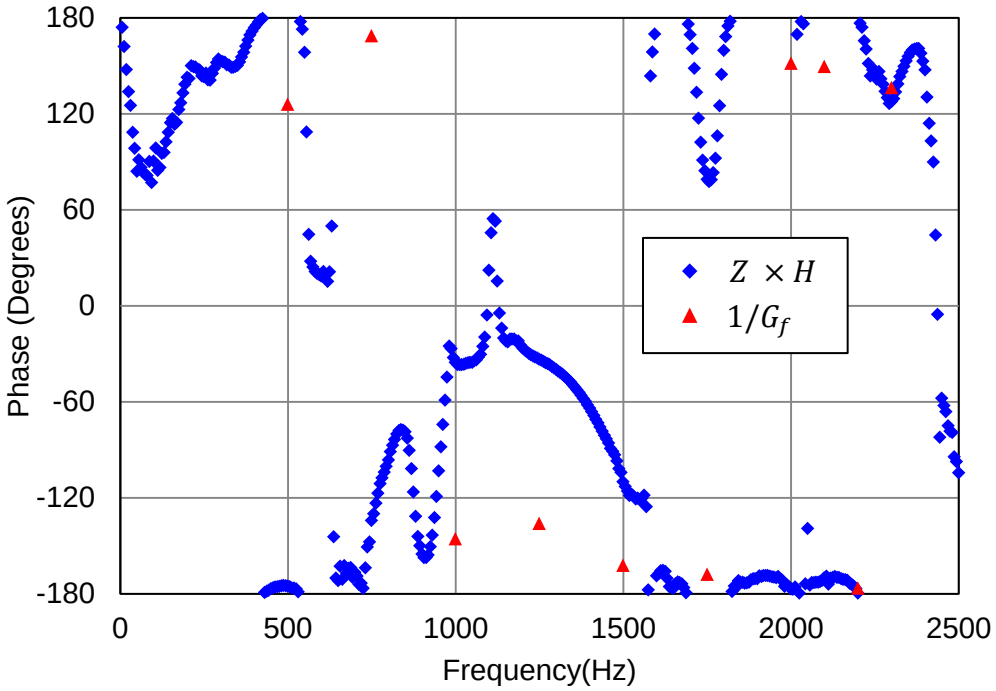

Figure 2.17 Phase of $Z \times H$ and $1/G_f$ with Burner 2.

As noted earlier, the geometry was different between Burners 1 and 2 (see Table 2.4) and the results from Figure 2.12 demonstrate that small changes to the overall geometry can greatly affect $|Z \times H|$ at high frequencies. Accordingly, the model suggests that the difference in burner geometry may have alleviated the instability. However, the validation of the model is inconclusive, and further experimental work is recommended to investigate the effect of burner geometry on combustion oscillations.

2.5 Low-Order Model for Equivalence Ratio Oscillations

2.5.1 Feedback Loop Stability Model

Combustion oscillations can also be produced by a fluctuating equivalence ratio [21, 7]. Sattelmayer [21] developed a model, which combined the effects of equivalence ratio and mixture flow fluctuations. However, the model assumed a simple geometry for the combustor and a flat burner. Moreover, the model was judged to be overly complex for the HVAC community since it requires the solution of 16 simultaneous equations.

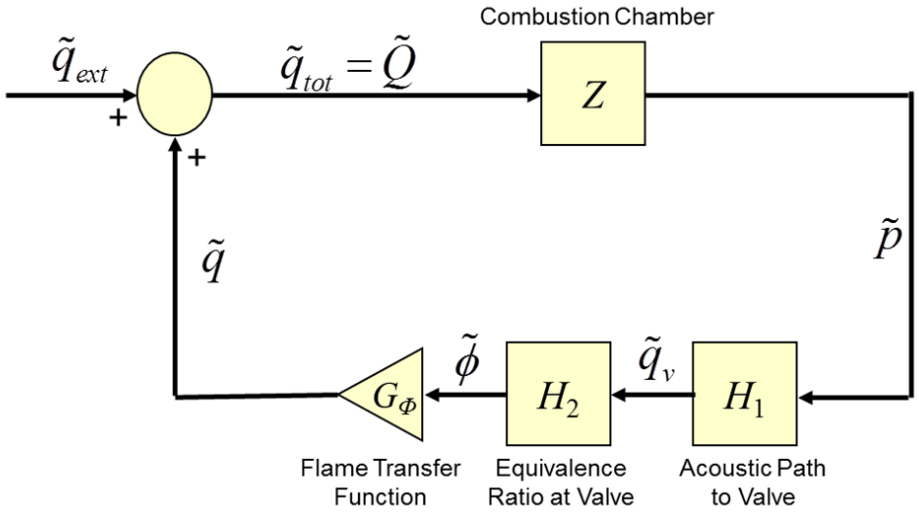

Figure 2.18 Feedback loop stability model for equivalence ratio oscillations.

It was decided to develop a feedback loop model similar to that shown earlier. Though Sattelmayer showed that combustion oscillations could result from a

combination of the two mechanisms (mixture flow and equivalence ratio fluctuations), one mechanism is more likely to be dominant. Moreover, solutions to combustion oscillation problems in equipment will be targeted for one or the other mechanism and not for a combination of the two. Hence, a separate feedback loop for equivalence ratio fluctuations was developed and no attempt was made to merge the two models into a unified model. In fact, Sattelmayer [21] demonstrated that a unified model was nonlinear.

The model is shown in Figure 2.18. Z and H_1 are both purely acoustic transfer functions. Z is the combustion chamber impedance and is identical to that used in the mixture flow model and H_1 relates the fluctuating velocity ($\tilde{q}_v$) at the gas valve to the fluctuating pressure ($\tilde{p}$) at the burner. H_2 describes the relationship between the equivalence ratio ($\tilde{\phi}$) to the fluctuating velocity at the gas valve. The flame transfer function (G_ϕ) should also be defined in terms of the equivalence ratio fluctuations. Accordingly,

$$G_\phi = \frac{\tilde{q}}{\tilde{\phi}} \tag{2.17}$$

where $\tilde{q}$ is the fluctuating heat release.

In this case, combustion oscillations can occur if

$$|Z| \cdot |H_1| \cdot |H_2| \cdot \left|G_\phi\right| > 1 \tag{2.18}$$

which can be restated as:

$$|Z| \cdot |H_1| > \frac{1}{|H_2| \cdot \left|G_\phi\right|} \tag{2.19}$$

if

$$\angle Z + \angle H_1 + \angle H_2 + \angle G_\phi = 0 \tag{2.20}$$

2.5.2 Acoustic Model of the System

For equivalence ratio perturbations, Z is identical to that described in Section 2.2.2. However, the acoustic model of the intake system is now described by the transfer function H_1 which relates the fluctuating particle velocity ($\tilde{q}_v$) at the gas valve to the fluctuating pressure ($\tilde{p}$) at the flame. Figure 2.19 illustrates the variables considered. The determination of H_1 is detailed in Section 2.5.4.

2.5.3 Fluctuating Equivalence Ratio at Gas Valve

The combustion intensity between a fuel and an oxidizer depends on their relative molar (or volume) concentrations. When their concentration ratio is chemically correct, all the reactants can be totally consumed by the reaction so that the combustion intensity is as high as possible. This combustion mode of burning is called the stoichiometric combustion. The stoichiometric combustion generates the products with the highest value of heat. In the C-H-O-N system, these products are water (gas or liquid phase), carbon dioxide, and nitrogen.

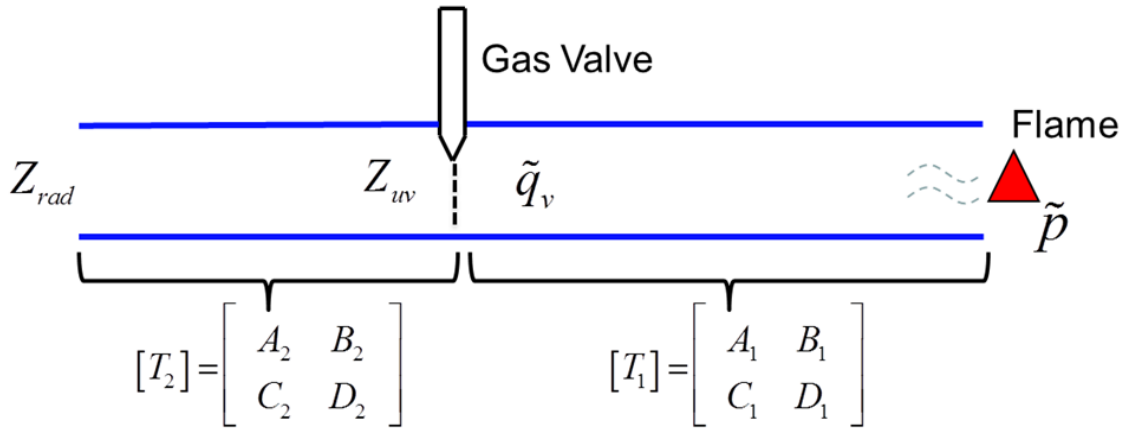

Figure 2.19 Schematic showing the variables relating the sound pressure at the flame to the volume flow velocity at the fuel intake.

To measure the relative molar concentration of fuel and oxidizer in a mixture, we define a fuel-oxidizer ratio, m_f/m_a as the ratio of the mass of fuel to the mass of oxidizer in the mixture. Similarly, if air is the oxidizer then m_a is the mass of air.

To specify the deviation of practical combustion from stoichiometric burning, the equivalence ratio ϕ is defined as

$$\phi = \frac{\left(m_f/m_a\right)_{act}}{\left(m_f/m_a\right)_{stoi}} \tag{2.21}$$

where the subscripts "*act*" and "*stoi*" designate the actual and stoichiometric states. The actual fuel and oxidizer (i.e., air) molar concentrations are obtained from measurements.

From Equation (2.21), $\phi = 1$ corresponds to stoichiometric combustion, and $\phi < 1$ and $\phi > 1$ respectively correspond to fuel-lean and fuel-rich combustion. Note that the air-to-fuel equivalence ratio is sometimes used, which is simply the reciprocal of the current definition of ϕ.

Oscillations of air and fuel lead to a fluctuation of equivalence ratio. The equivalence ratio can be decomposed into a constant portion ($\bar{\phi}$) and fluctuating portion ($\tilde{\phi}$). Thus, the equivalence ratio can be expressed as

$$\phi = \bar{\phi} + \tilde{\phi} \tag{2.22}$$

The fluctuating portion is

$$\tilde{\phi} = \frac{\left(m_f/m_a\right)_{act}}{\left(m_f/m_a\right)_{stoi}} - \frac{\left(\bar{m}_f/\bar{m}_a\right)_{act}}{\left(m_f/m_a\right)_{stoi}} \tag{2.23}$$

Using the definitions $m_f = \bar{m}_f + \tilde{m}_f$ and $m_a = \bar{m}_a + \tilde{m}_a$, Equation (2.23) can be rearranged and the fluctuating part of the equivalence ratio can then be expressed as

$$\frac{\tilde{\phi}}{\bar{\phi}} = \frac{\tilde{m}_f/\bar{m}_f - \tilde{m}_a/\bar{m}_a}{1 + \tilde{m}_a/\bar{m}_a} \tag{2.24}$$

where $\bar{m}_f$ and $\tilde{m}_f$ denote the constant and fluctuating mass of fuel respectively, $\bar{m}_a$ and $\tilde{m}_a$ denote the constant and fluctuating mass of air individually.

It is reasonable to assume that the acoustic impedance is large at the gas injection since the cross-sectional area of the injection port is small compared to the main duct. In that case, there will be no fuel fluctuation, which implies a constant fuel mass flow. In addition, the fluctuation part of the air mass is small compared to the total amount of air mass flow. Equation (2.24) can then be simplified as

$$\frac{\tilde{\phi}}{\bar{\phi}} = -\frac{\tilde{m}_a}{\bar{m}_a} = -\frac{\rho\tilde{q}_v}{\rho\bar{q}_v} = -\frac{\tilde{q}_v}{\bar{q}_v} \tag{2.25}$$

where $\bar{q}_v$ and $\tilde{q}_v$ represent the constant and fluctuating parts of mass flow rate respectively.

It follows that the transfer function relating the fluctuation of equivalence ratio to the acoustic particle velocity (H_2) can be expressed as

$$H_2 = -\frac{\tilde{\phi}}{\tilde{q}_v} = -\frac{\bar{\phi}}{\bar{q}_v} \tag{2.26}$$

It should be noticed that H_2 is constant with frequency and is defined in terms of the constant parts of the equivalence ratio and mass flow rate, which are easily measured.

2.5.4 Determination of H_1

The transfer function between the particle velocity at the gas valve and the source pressure (H_1 as identified in Section 2.5.1) can be derived using silencer transfer matrices. The transfer matrix between the flame and gas valve is defined as T_1 and between the gas valve and inlet opening as T_2 as shown in Figure 2.19.

The impedance of the pipe at the gas valve (Z_{uv}) can be determined from the transfer matrix between the gas valve and inlet opening T_2, and the impedance at the inlet opening (Z_{rad}). CHAPTER 3 describers the theory in details. Z_{uv} can be expressed as

$$Z_{uv} = \frac{A_2 Z_{rad} + B_2}{C_2 Z_{rad} + D_2} \tag{2.27}$$

where A_2, B_2, C_2 and D_2 are the four-pole parameters for T_2. This impedance is in parallel with the impedance of the gas valve. However, it can be assumed that the impedance of the gas valve is much larger than Z_{uv} since the area of the gas valve opening is much smaller than the area of the inlet pipe. It follows that the transfer function (H_1) relating the volume velocity fluctuations at the gas valve to the sound pressure at the flame can be expressed as

$$H_1 = \frac{\tilde{q}_v}{\tilde{p}} = \frac{1}{A_1 Z_{uv} + B_1} \tag{2.28}$$

Details about determining transfer matrices can be found in Reference [34].

2.5.5 Prediction of the Flame Transfer Function

In the case of equivalence ratio fluctuations, the flame transfer function (G_ϕ) is defined as the ratio of the fluctuating heat release to the fluctuating equivalence ratio. Sattelmayer [21] expressed the flame transfer function as

$$G_\phi = e^{-j\omega\tau} \frac{u_b}{\bar{\phi}} \left(\frac{\rho_u}{\rho_d} - 1 \right) \tag{2.29}$$

where u_b is the mean flow velocity at the burner, ρ_u and ρ_d are the gas densities at the upstream and downstream of burner respectively.

A time delay parameter (τ) is defined as

$$\tau = \frac{L}{u} \tag{2.30}$$

where L is the distance from the gas valve to the burner surface and u is the mean flow velocity.

Equation (2.25) assumes that the fluctuating equivalence ratio is the same at both the gas valve and burner surface. However, Sattelmayer [21] showed that the fluctuating equivalence ratio changes due to convective effects as the air-fuel

mixture travels from the valve to the burner. Nevertheless, it was found that these changes are minimal at lower frequencies.

2.6 Boiler 2 – Equivalence Ratio Fluctuations

Boiler 2 was a much larger 147 kW (500,000 BTU/hour) capacity propane gas boiler with a stainless steel heat exchanger. Coils were arranged cylindrically in both the upper and lower parts of the heat exchanger. The cause of the oscillation was a fluctuating equivalence ratio. This was determined in the following manner. The manufacturer increased the distance between the gas supply and the burner until the combustion oscillation was eliminated. In doing so, the acoustics of the intake should not change significantly since the gas valve has a small effect on the acoustic impedance. However, the flame transfer function relating the fluctuating heat release to the fluctuating equivalence ratio will change significantly. Especially, note the dependence of time delay on the distance from the gas valve to the burner. Ultimately, the manufacturer opted to change the intake system and the gas valve to eliminate the instability.

Table 2.5 and Table 2.6 list the operating conditions. Table 2.5 indicates whether or not combustion oscillations occurred. For Boiler 2, there was only a single port where a thermocouple could be inserted into the combustion chamber. Consequently, the temperature was only measured in the upper combustion chamber. Temperature at the outlet is typically in the neighborhood of 40°C (105°F). However, temperature will have a minimal effect on the acoustics at low frequencies.

Figure 2.20 demonstrates the setup for temperature measurements. The thermocouple was positioned in combustion chamber 17, 9 and 2 inches from burner surface respectively. Additionally, temperature at inlet and outlet of water and intake of air were recorded. Temperature measurements are tabulated in Table 2.7. The number indicates the operating condition number in Table 2.5 and Table 2.6.

Table 2.5 Operating conditions for Boiler 2.

No.	Combustion Driven Oscillation	Frequency (Hz)	Intake Duct Length (in)	Exhaust Duct Length (in)	Gas Rate (BTU/hr)	Equivalency Ratio
1	NO		0	94	4.86E+05	0.45
2	YES	11.4	0	94	4.77E+05	0.43
3	YES	10.2	128	94	4.48E+05	0.35
4	YES	10.1	248	94	4.36E+05	0.31
5	YES	10.9	504	94	4.72E+05	0.38
6	YES	10.4	0	224	4.49E+05	0.40
7	YES	9.2	0	344	4.32E+05	0.39
8	YES	8.3	0	475	4.13E+05	0.37
9	YES		0	94		

Table 2.6 Operating conditions for Boiler 2 Continued.

No.	Air Fuel Ratio	Intake Flow Rate (ft/s)	Exhaust Flow Rate (ft/s)	Note
1	34.7	32.8	68.2	Partially block exhaust
2	36.3	33.8	41.0	Reducing flow rate eliminates problem
3	44.6	38.7	55.1	
4	50.3	42.7	62.3	
5	41.1	38.1	41.7	
6	39.0	33.8	29.5	
7	40.0	33.8	43.6	
8	42.2	33.8	43.0	
9				Added sleeve at end of exhaust

Table 2.7 Temperature measurements for Boiler 2.

No.	Temperatures (°F)					
	Combustion Chamber (17 in from Burner Surface)	Combustion Chamber (9 in from Burner Surface)	Combustion Chamber (2 in from Burner Surface)	Water Inlet	Water Outlet	Inlet Air
1	1635	1778	1402	131	150	76
2	1568	1711	1451	106	125	71
3	1673	1800	1441	110	124	71
4	1729	1815	1530	117	132	71
5	1693	1816	1537	121	139	72
6	1635	1747	1692	124	140	75
7	1632	1681	1505	126	142	75
8	1611	1574	1535	128	143	76

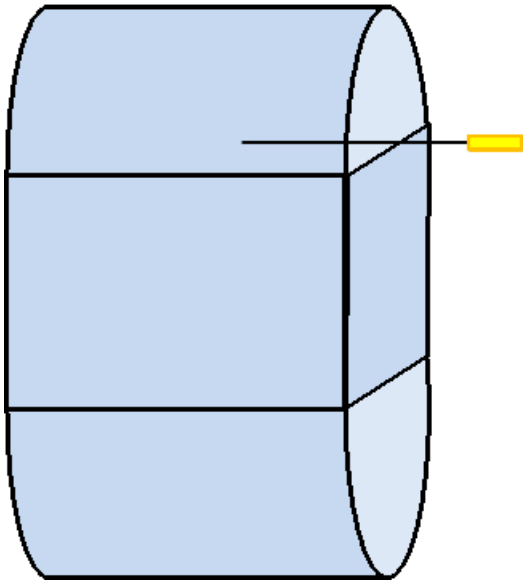

Figure 2.20 Schematic showing thermocouple insertion points for Boiler 2.

2.7 Results for Boiler 2

2.7.1 Boiler 2 Prediction of Flame Transfer Function

In the case of Boiler 2, the flame transfer function was calculated. Since the instability occurred at close to 10 Hz, it was difficult to measure the flame transfer function with any accuracy. The flame transfer functions for mixture flow and equivalence ratio fluctuations were determined using Equations (2.13) and (2.29) respectively. The parameters for each model are shown in Table 2.8 and Table 2.9 respectively. The two different transfer functions are compared in Figure 2.21 and Figure 2.22 up to 100 Hz. The equivalence ratio flame transfer function is somewhat sensitive to the input parameters provided. Many of these like the flame height and flame propagation velocity are estimated.

Table 2.8 Parameters used in Equation (2.13) for mixture flow fluctuations.

Variable	Symbol	SI	English
Density of unburned mixture	ρ_u	1.21 kg/m^3	4.37E-5 lb/in^3
Density of combustion products	ρ_d	0.325 kg/m^3	1.16E-5 lb/in^3
Flame height	H	1 cm	0.39 in
Mean gas velocity	V_0	10.3 m/s	40.6 in/s
Flame propagation velocity	S_L	40 cm/s	15.7 in/s
Time delay	τ_0	3.4E-4 s	3.4E-4 s
Attenuation parameter	τ_1	0.003 s	0.003 s
Empirical constant	T_0	5.3	5.3
Empirical constant	T_1	0.12 cm$^{3/2}$	4.4E-4 in$^{3/2}$
Offset term	A_0	0.001	0.001

Table 2.9 Parameters used in Equation (2.29) for equivalence ratio fluctuations.

Variable	Symbol	SI	English
Density of unburned mixture	ρ_u	1.21 kg/m^3	4.375E-5 lb/in^3
Density of Combustion products	ρ_d	0.325 kg/m^3	1.16E-5 lb/in^3
Time delay	τ	0.084 s	0.084 s
Mean flow velocity at burner	u_b	24.4 m/s	961 in/s
Mean flow velocity at gas valve	u_v	10.3 m/s	406 in/s
Mean equivalence ratio at burner	φ_b	0.9	0.9
Mean equivalence ratio at gas valve	φ_v	0.9	0.9
Distance from gas valve to burner	L	1.03 m	40.6 in
Mean velocity	u	12.2 m/s	480.3 in/s

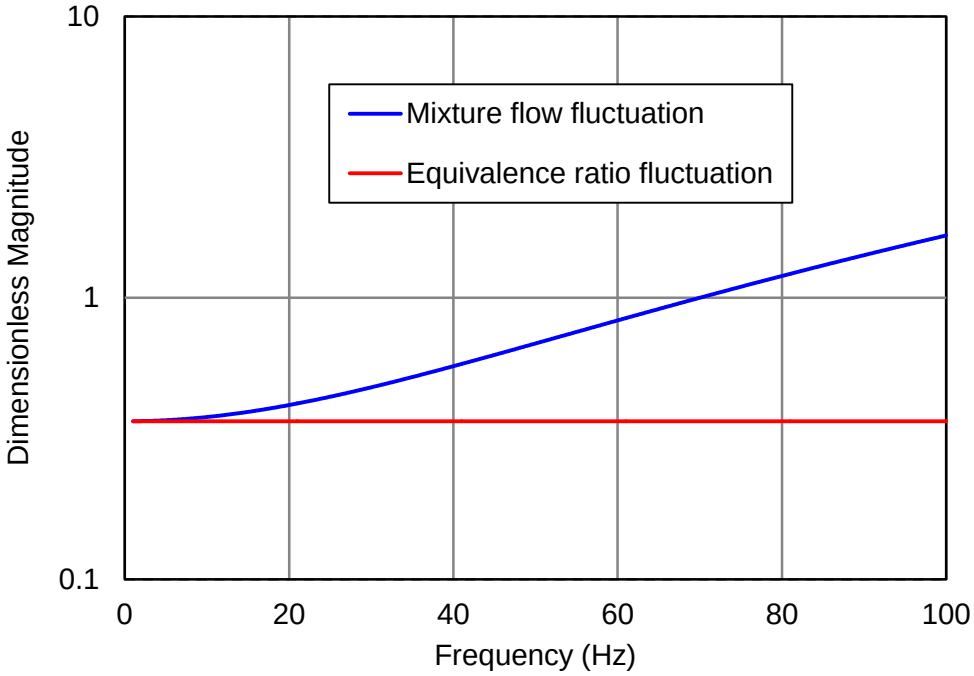

Figure 2.21 Comparison of magnitude of flame transfer function.

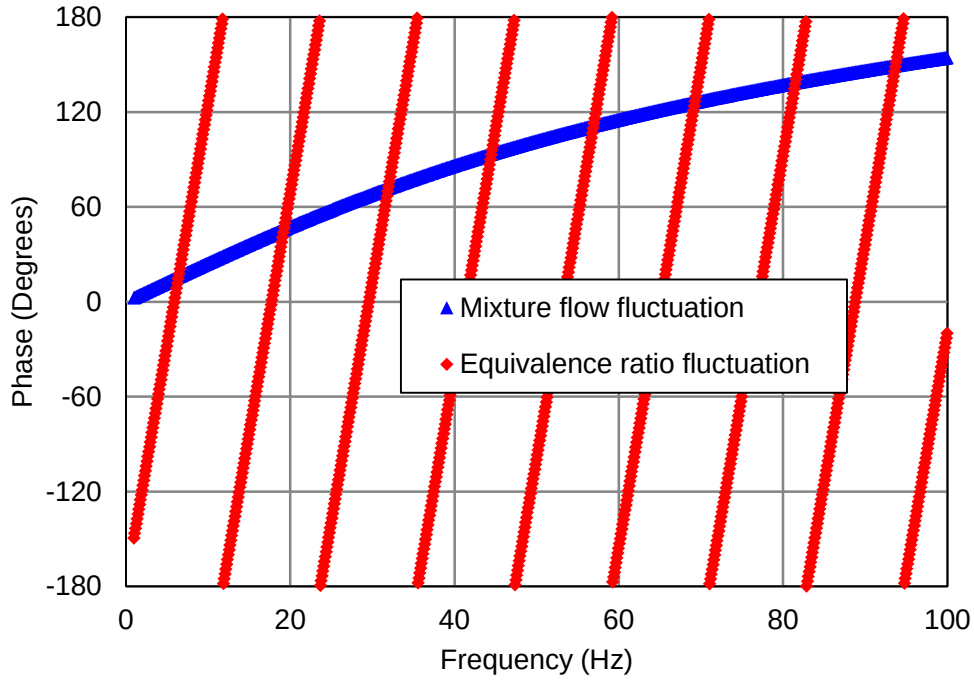

Figure 2.22 Comparison of phase of flame transfer function.

2.7.2 Boiler 2 Feedback Loop Model Results

The frequency of the oscillation was approximately 10 Hz and the entire unit vibrated violently. The frequency of oscillation was determined by measuring the vibration of the boiler with an accelerometer. The frequency of oscillation was most affected by increasing the vent length, which decreased the instability frequency.

For Boiler 2, both mixture flow and equivalence ratio fluctuations were considered for the feedback stability model. The downstream impedance was modeled and accounted for the elevated temperatures in the combustion chamber. In this case, the length from the burner base to the center of the burner port cylinder ($L_B + L_C$) was not included since it is very short compared to an acoustic wavelength of 34.3 m (112.5 ft) at low frequencies (i.e., 10 Hz). Additionally, the burner transfer impedance was found to be unimportant at low frequencies. The flame transfer functions for both fluctuating mixture and equivalence ratio fluctuations were found using Equations (2.13) and (2.29) respectively. The values used in Equations (2.13) and (2.29) are shown in Table 2.8 and Table 2.9 respectively.

Table 2.10 Comparison of measured and predicted instability.

No.	Intake Length		Vent Length		Measured Frequency (Hz)	Equivalence Ratio Model (Hz)	Mixture Flow Model (Hz)
	Inch	Meter	Inch	Meter			
2	0	0.00	94	2.39	11.4	11.8	21.5
3	128	3.25	94	2.39	10.2	13.5	16.5
4	248	6.30	94	2.39	10.1	14.9	24.8
5	504	12.80	94	2.39	10.9	13.3	17.2
6	0	0.00	224	5.70	10.4	11.8	16.4
7	0	0.00	344	8.75	9.2	11.7	13.8
8	0	0.00	475	12.06	8.3	11.0	11.5

Table 2.10 compares the combustion instability frequencies identified using the mixture flow and equivalence ratio models to the frequencies that were measured. The numbers correspond to operating conditions in Table 2.5 and Table 2.6. The results point to a fluctuating equivalence ratio as the primary cause of the instability. There are some differences between the prediction and measurement. However, these differences are expected for a couple reasons. First, the boiler

vibrated violently which implies that structural resonances were strongly coupled to the acoustic resonance. This is likely to result in a frequency shift. Additionally, the phase of the flame transfer function for equivalence ratio fluctuations (Equation (2.29)) is sensitive to the inputs, which are estimates. Accordingly, the model suggests that modifying the fuel intake system best solves the problem. The results also indicate that equivalence ratio fluctuations are more likely to be a concern at low frequencies.

Figure 2.23 and Figure 2.24 show the magnitude and phase for $Z \times H_1$ and $1/(H_2 \times G_\phi)$ (for equivalence ratio oscillations) for Case 2 in Table 2.1. Combustion instabilities are possible if the magnitude of $Z \times H_1$ exceeds $1/(H_2 \times G_\phi)$ and when the phases are equivalent. Figure 2.25 and Figure 2.26 show the magnitude and phase $Z \times H$ and $1/G_f$ for mixture flow fluctuations for Case 2. Figure 2.27 and Figure 2.28 show the magnitude and phase for $Z \times H_1$ and $1/(H_2 \times G_\phi)$ (for equivalence ratio oscillations) for Case 3 in Table 2.1. Figure 2.29 and Figure 2.30 show the magnitude and phase $Z \times H$ and $1/G_f$ for mixture flow fluctuations for Case 3.

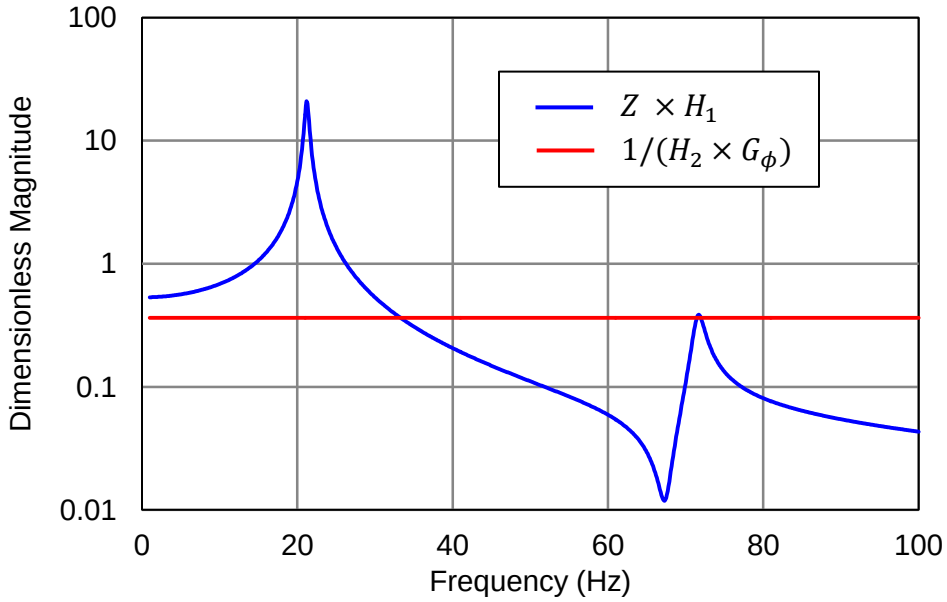

Figure 2.23 Magnitude of $Z \times H_1$ and $1/(H_2 \times G_\phi)$ for case 2.

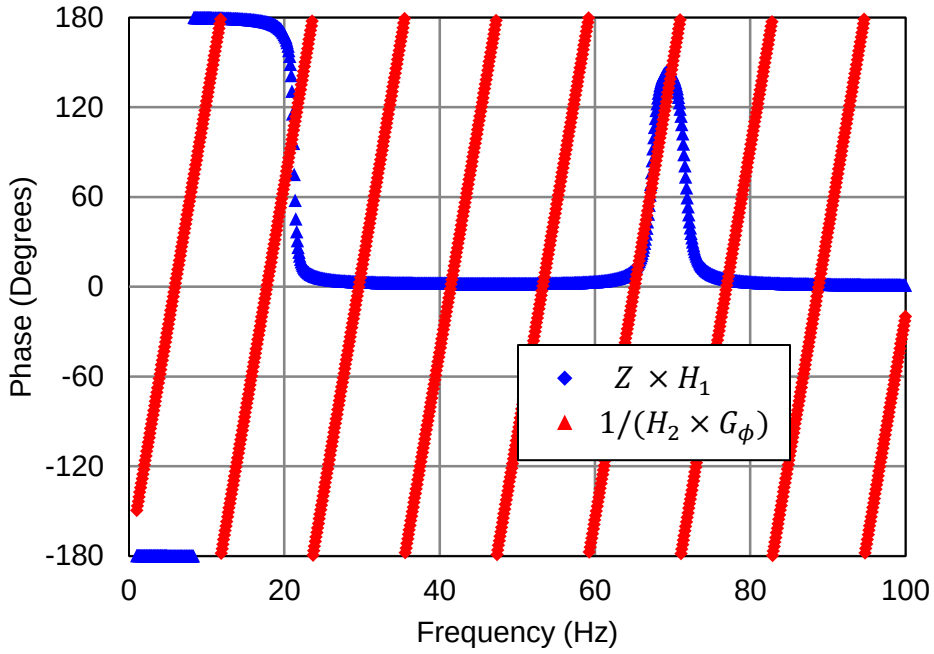

Figure 2.24 Phase of $Z \times H_1$ and $1/(H_2 \times G_\phi)$ for case 2.

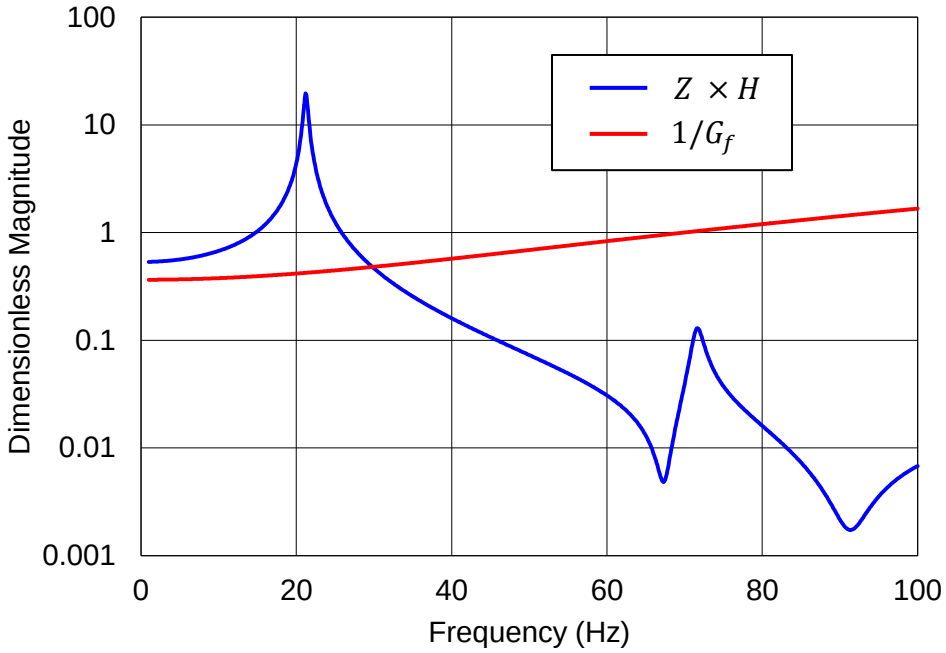

Figure 2.25 Magnitude of $Z \times H$ and $1/G_f$ for case 2.

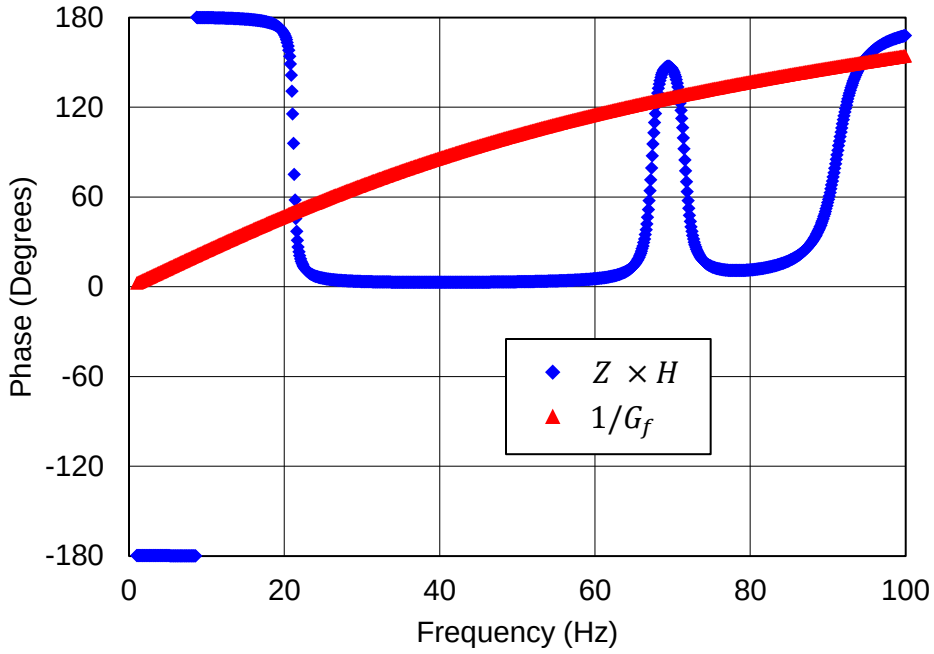

Figure 2.26 Phase of $Z \times H$ and $1/G_f$ for case 2.

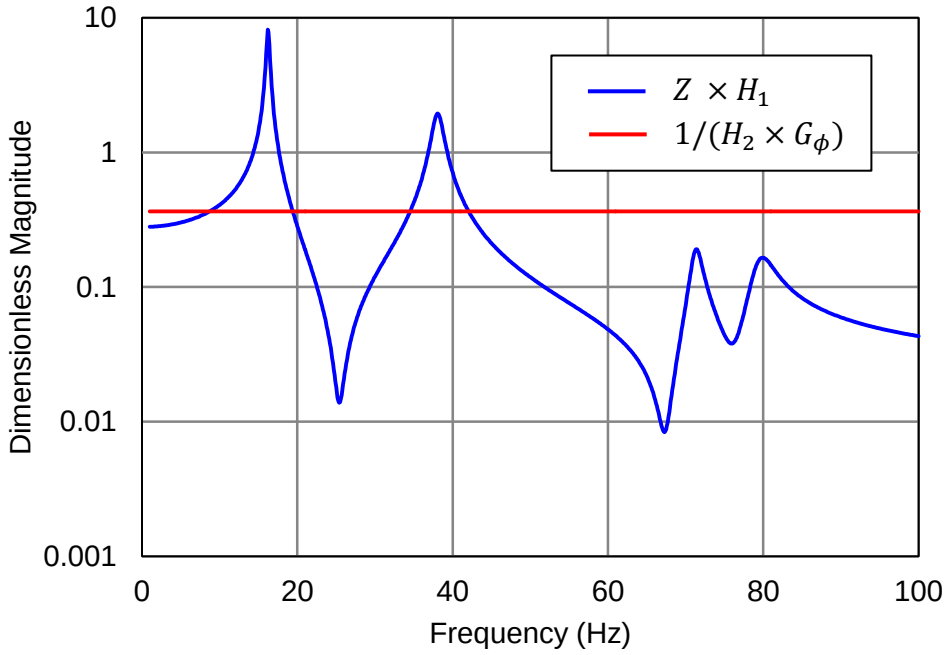

Figure 2.27 Magnitude of $Z \times H_1$ and $1/(H_2 \times G_\phi)$ for case 3.

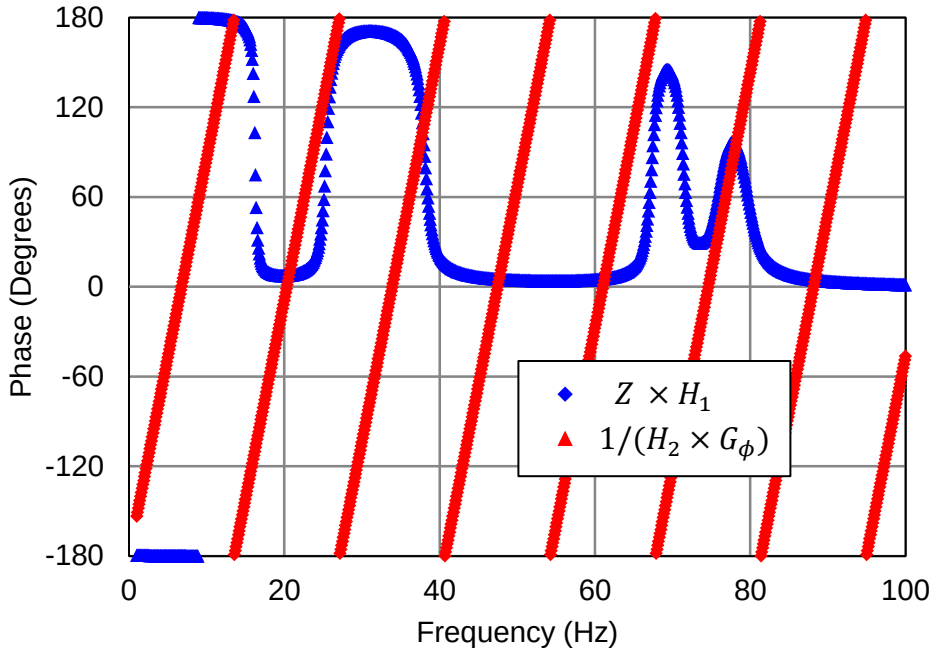

Figure 2.28 Phase of $Z \times H_1$ and $1/(H_2 \times G_\phi)$ for case 3.

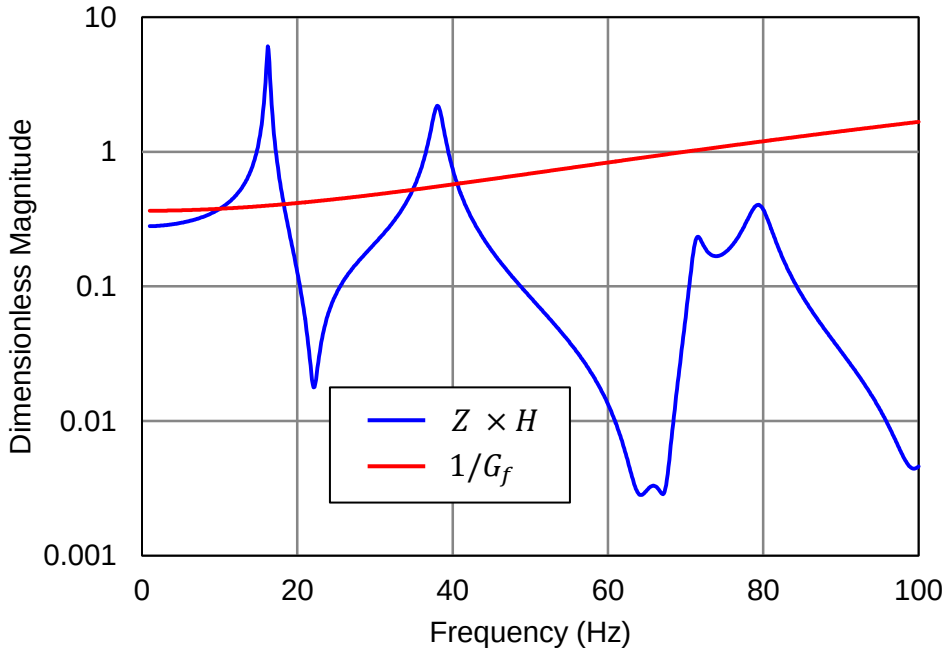

Figure 2.29 Magnitude of $Z \times H$ and $1/G_f$ for case 3.

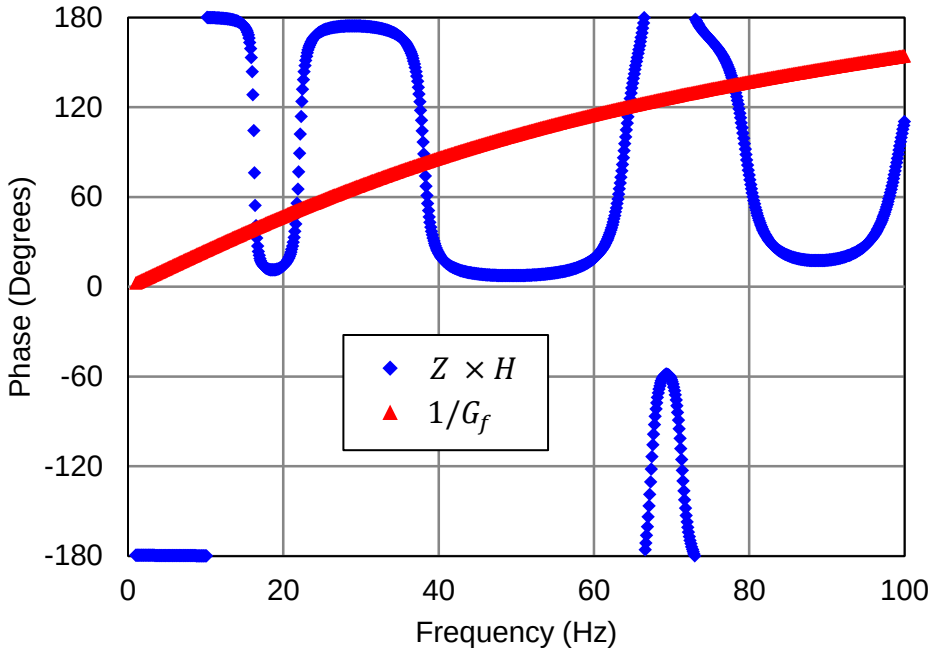

Figure 2.30 Phase of $Z \times H$ and $1/G_f$ for case 3.

2.8 Summary

Combustion oscillations are produced when sound produced by the flame is reflected from the combustion chamber towards the mixture chamber. The amount of reflection depends primarily on the geometry of the combustion chamber and attached ductwork. The reflection feeds back to the flame and disturbs it. The fluctuating flame oscillates the sound pressure in the combustion chamber which in turn fluctuates the mixture flow and equivalence ratio.

The low-order model originally developed by Baade [6] for identifying and preventing combustions oscillations was applied to two boilers. The original model has been enhanced by including a feedback loop to deal with equivalence ratio fluctuations. In each case, the model identified probable causes and possible solutions. CHAPTER 3 details the measurement and simulation of the downstream impedance for both boilers.

For Boiler 1, the instability was resolved by switching burners. By applying the model, it was determined that the higher acoustic resistance of the new burner

could provide some benefit. However, the primary reason that the second burner resolves the problem is likely the difference in geometry. The model showed that the upstream impedance is significantly affected by small changes to the burner geometry.

For Boiler 2, the instability was resolved by switching gas valves. The model identified equivalence ratio fluctuations as the primary cause of the instability. However, the model also indicated that oscillations could occur due to mixture flow fluctuations as well but at higher frequencies.

The research demonstrated the usefulness of the feedback loop stability model as a diagnostic tool. In each case, the model pointed towards a probable cause for the instability.

CHAPTER 3 MEASUREMENT AND SIMULATION OF ACOUSTIC LOAD IMPEDANCE FOR BOILERS

3.1 Introduction

What we know as sound is a result of fluid density or pressure fluctuations. The distinctive feature of these fluctuations is that they propagate rapidly away from the source at a speed that depends on the type of fluid [37]. The disturbance propagates as a wave with no net mass transport and the propagation speed is known as the speed of sound. The acoustic wavelength is the speed of sound (343 m/s or 1125 ft/s at room temperature for air) divided by the frequency of the disturbance.

If noise is produced in a duct or pipe system, the sound pressure will be constant across the duct cross-section at low frequencies. This is known as plane wave propagation, and will occur if the cross-sectional dimensions are less than half an acoustic wavelength. For a square cross-section, the plane wave cut-off frequency is equal to $c/2d$ where c is the speed of sound and d is a characteristic dimension of the duct cross-section. Similarly, Eriksson [38] showed that the cut-off frequency for a circular duct is $c/1.71d$ (d is the diameter in this case).

When a sound wave encounters an abrupt geometric change or an obstacle, the wave will at the very least be partially reflected. For example, a silencer uses cross-sectional area changes to reflect sound back towards the source. Sound is also reflected from the end of a pipe or duct due to the abrupt change in geometry. In the case of plane wave propagation, the sound field consists of an incident and a reflected wave. The superposition of these two waves results in a standing wave where the positions of high and low amplitude sound pressure inside a duct do not change.

Combustion oscillations are a common happening in boilers, furnaces, and water heaters. Oscillations in the burning rate result in a perturbation of the acoustic particle velocity. For the most part, the flame is a benign sound source.

However, the sound reflected back from the combustion chamber produces a standing wave that will perturb the mixture flow or composition. At certain frequencies, a sympathetic resonance develops resulting in a tone.

Changing the geometry of the system can eliminate these tones. Changes might include modifications to the combustion chamber, or the intake and vent pipe lengths. Additionally, problems have been solved by adding small holes into pipes [15, 16].

The acoustic metric that is most relevant to the combustion oscillation problem is the acoustic impedance. In fact, the acoustic impedance upstream and downstream of the flame is used as an input in the feedback loop model developed by Baade [6, 15] and Baade and Tomarchio [16]. In Reference [39], the feedback loop stability model developed by Baade is applied to two boilers that exhibited combustion oscillation problems.

The acoustic impedance relates the perturbation in particle velocity ($\tilde{u}$) directed away from the source to the acoustic pressure ($\tilde{p}$) and can be expressed as

$$Z = \frac{\tilde{p}}{S\tilde{u}} \tag{3.1}$$

where S denotes the cross-sectional area.

Hence, a relationship between the acoustic pressure and volume velocity of the source (i.e. flame) can be established by measuring or calculating the acoustic impedance at the location of the flame. The next section details how the upstream and downstream impedances are in parallel with each other at the source. The sections that follow describe how the acoustic impedance can be measured and simulated.

3.2 Determination of Acoustic Impedance

3.2.1 Measurement of Acoustic Impedance

Acoustic impedance is most commonly measured using the two-microphone method [40]. The two-microphone method is shown schematically in Figure 3.1.

A loudspeaker is placed at one end of the tube and the sound pressure is measured at the two microphone locations. The microphone closest to the source is the reference and the transfer function between the two microphones (H_{12}) is measured. The transfer function can be used to determine the sound pressure reflection coefficient (R) using the equation

$$R = \frac{H_{12} - e^{-jks}}{e^{jks} - H_{12}} \tag{3.2}$$

where k is the acoustic wavenumber and s the microphone spacing.

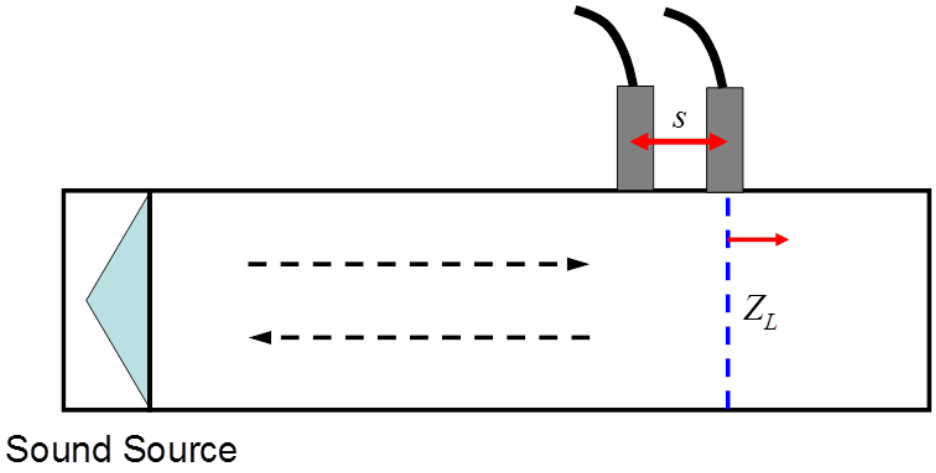

Figure 3.1 Schematic showing the two microphone measurement.

The acoustic load impedance (Z_L) can then be determined from the reflection coefficient via

$$Z_L = \frac{\rho c}{S_t}\frac{1+R}{1-R} \tag{3.3}$$

where ρ is the mass density of air and c the speed of sound, S_t is the area of the tube.

Both the upstream and downstream impedances (Z_u and Z_d) shown in Figure 2.2 can be measured in this way.

Instrumentation is used to measure quantities that are harmonic in time. Accordingly, there will be a time lag between quantities. Accurate measurement of the phase is crucial to acquiring an accurate measurement of the impedance (Z_L). Phase differences between the microphones, pre-amplifiers, and the channels of the spectrum analyzer can lead to errors in the measurement of the load impedance. The phase between the microphones can be calibrated by switching the positions between the two microphones for an identical source and load, as explained in the ASTM Standard [40].

The Spectronics impedance tube and software [41] were used to acquire all the data in this work. The impedance tube is brass and the microphone holders are well sealed to prevent sound leakage. The source is a compression driver loudspeaker (JBL 2426J). For Boiler 2, the compression driver was replaced with a bookshelf loudspeaker in order to boost the source energy at low frequencies.

It is also important to insure that the signal to noise ratio is high. The field sound pressure should be substantially higher than the background noise in the pipe or tube. Standards recommend that the sound pressure level in the tube is at least 10 dB higher than the background noise though 20-30 dB is preferred [42].

3.2.2 Calculation of Impedance using Transfer Matrix Theory

The upstream and downstream acoustic impedances (Z_u and Z_d) can be determined using a model based on transfer matrix theory [28, 43, 44]. Transfer matrix theory relates the sound pressure and particle velocity at the inlet to that at the outlet of a component. The main assumption is that plane acoustic waves can be assumed at the inlet and outlet of each component though sound waves need not be planar within the components. Provided that each component in the upstream or downstream piping system can be modeled as a transfer matrix, the impedance can be determined after multiplying the transfer matrices together. The numerical computing software MATLAB® [45] was used for all calculations.

A transfer matrix $[T]$ is composed of four-pole parameters A, B, C, and D. These four pole parameters relate the sound pressure and particle velocity at the inlet and outlet of a particular duct section. This can be expressed mathematically as

$$\begin{Bmatrix} \tilde{p}_1 \\ S_1\tilde{u}_1 \end{Bmatrix} = \begin{bmatrix} A & B \\ C & D \end{bmatrix} \begin{Bmatrix} \tilde{p}_2 \\ S_2\tilde{u}_2 \end{Bmatrix} \tag{3.4}$$

where $\tilde{p}_1$ and $\tilde{p}_2$ are sound pressures and $\tilde{u}_1$ and $\tilde{u}_2$ are particle velocities as defined in Figure 3.2 for an arbitrary duct component.

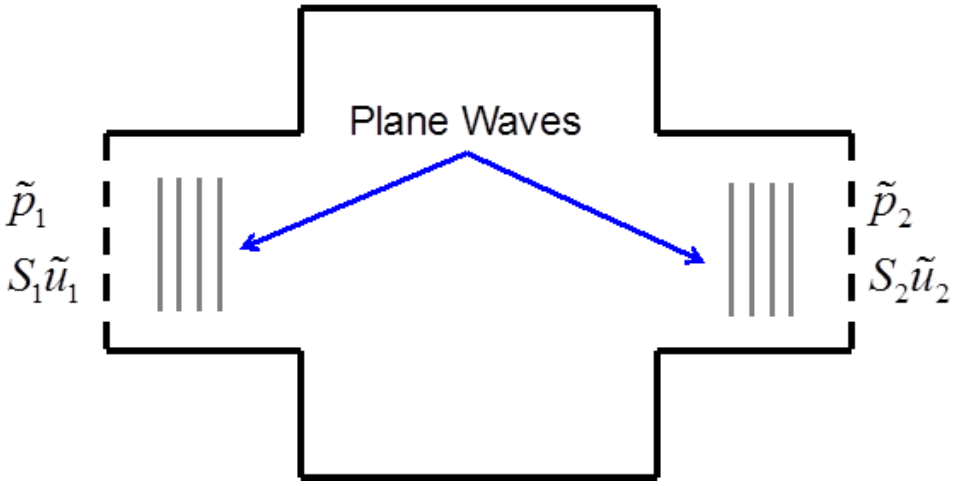

Figure 3.2 Arbitrary duct component with inlet and outlet variables.

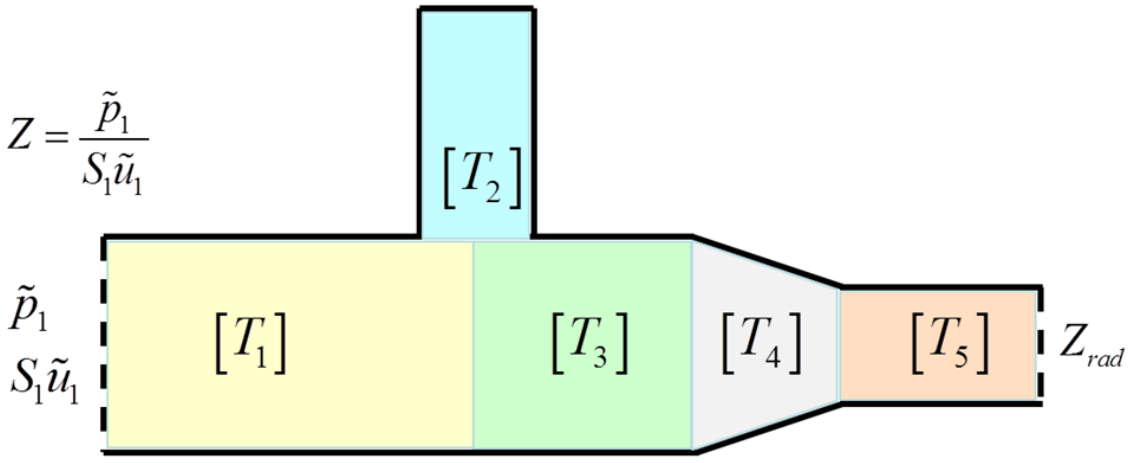

Figure 3.3 Schematic showing transfer matrices for a duct system.

Figure 3.3 shows a schematic for duct system. The transfer matrix for the complete system $[T]$ can be found by multiplying each of the transfer matrices together. Thus,

$$[T] = [T_1][T_2][T_3][T_4][T_5] \tag{3.5}$$

for the case shown in Figure 3.3. The impedance at the left hand side can be determined from the four-pole parameters A_T, B_T, C_T, and D_T for the system transfer matrix $[T]$ and the radiation impedance at the end of the duct or piping system (Z_{rad}). The impedance can be expressed as

$$Z = \frac{A_T Z_{rad} + B_T}{C_T Z_{rad} + D_T} \tag{3.6}$$

3.2.3 Four-pole Matrices for Common Duct Elements

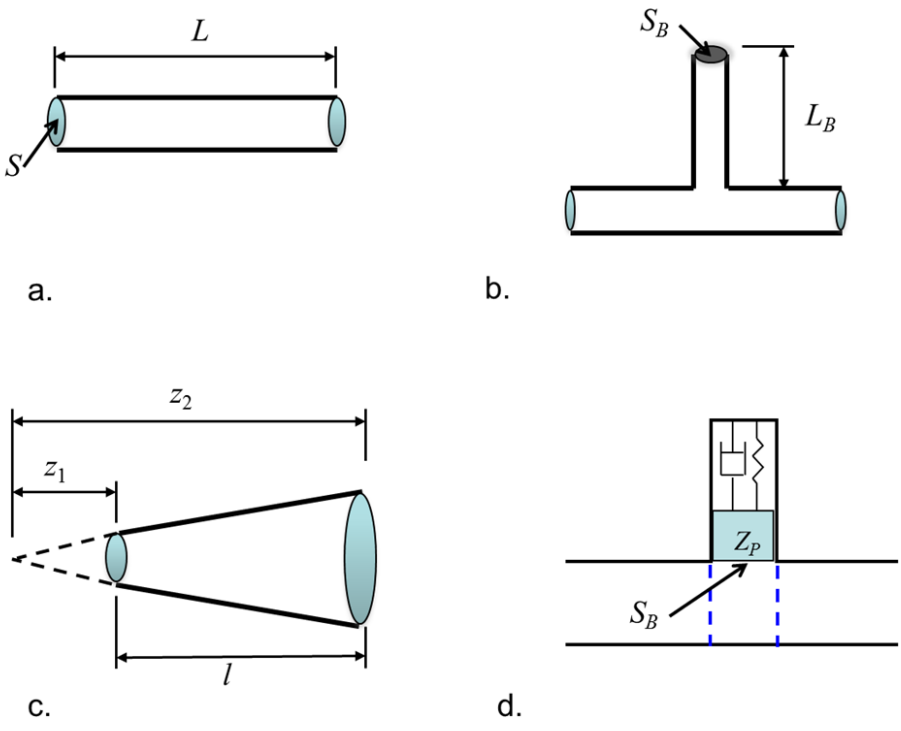

Figure 3.4 Common transfer matrices for heating equipment: a) straight pipe, b) quarter wave tube, c) cone and d) structural element modeled as a side branch.

The most commonly used duct elements in boilers, furnaces and water heaters are shown in Figure 3.4 [28]. The transfer matrix for a straight duct (Figure 3.4a) or tube can be expressed as

$$T_{tube} = \begin{bmatrix} \cos(kL) & j\frac{\rho c}{S}\sin(kL) \\ j\frac{S}{\rho c}\sin(kL) & \cos(kL) \end{bmatrix} \tag{3.7}$$

The transfer matrix for a quarter wave tube (Figure 3.4b) or structural element modeled as a side branch (Figure 3.4d) can be expressed as

$$T_{quarter} = \begin{bmatrix} 1 & 0 \\ 1/Z_p & 1 \end{bmatrix} \tag{3.8}$$

For the case of a quarter wave tube,

$$Z_p = -j\rho c\cot(kL_B)\,/S_B \tag{3.9}$$

The impedance (Z_p) for a vibrating plate which is modeled as a side branch can be found in the next section 3.2.6.

The transfer matrix for a cone (Figure 4c) can be expressed as [46]

$$T_{cone} = \begin{bmatrix} A_{cone} & B_{cone} \\ C_{cone} & D_{cone} \end{bmatrix} \tag{3.10}$$

where

$$A_{cone} = \frac{z_2}{z_1}\cos(kl) - \frac{\sin(kl)}{kz_1} \tag{3.11}$$

$$B_{cone} = j\frac{\rho c}{S_D}\frac{z_2}{z_1}\sin(kL) \tag{3.12}$$

$$C_{cone} = j\frac{S_D}{\rho c}\left(\frac{z_1}{z_2}\left(1+\frac{1}{k^2 z_1 z_2}\right)\sin(kL) - \left(1-\frac{z_1}{z_2}\right)\frac{\cos(kL)}{kz_2}\right) \tag{3.13}$$

$$D_{cone} = \frac{\sin(kL)}{kz_2} + \frac{z_1}{z_2}\cos(kl) \tag{3.14}$$

In Figure 3.3, a straight duct is used to model $[T_1]$, $[T_3]$ and $[T_5]$. A quarter wave tube is used to model $[T_2]$ and a cone to model $[T_4]$.

Figure 3.5 illustrates how a quarter wave tube can be configured as an extended outlet (or inlet). For an extended inlet or outlet, the Equation (3.9) can be used but L_B must be adjusted to include near field effects at the flanged end [47]. Accordingly,

$$L_B = l + \delta_e \tag{3.15}$$

where

$$\delta_e = \frac{8a_s}{3\pi}H(\alpha), H(\alpha) = \begin{cases} 0.875(1-\alpha)(1.371-\alpha), & 0.5 < \alpha < 1 \\ 1 - 1.238\alpha, & 0 < \alpha < 0.5 \end{cases} \tag{3.16}$$

and

$$\alpha = \sqrt{S/S_B} \tag{3.17}$$

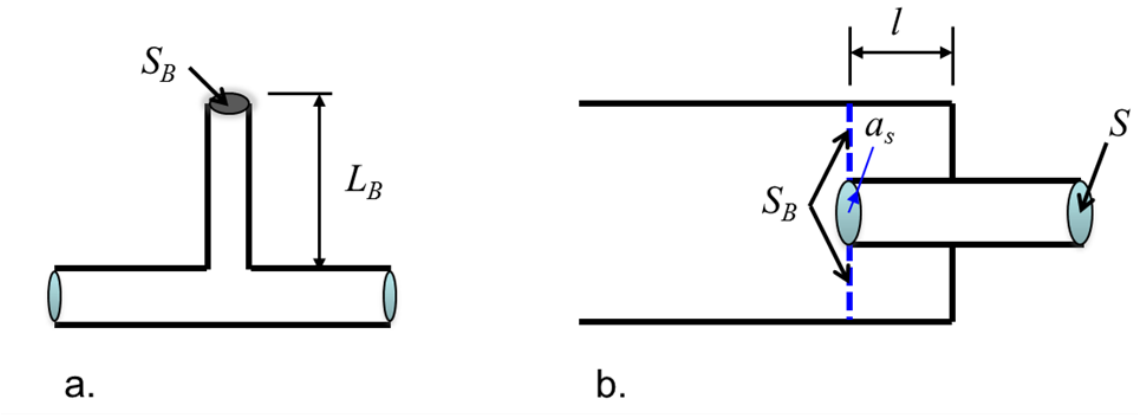

Figure 3.5 a) Quarter wave tube and b) quarter wave tube as extended outlet.

3.2.4 Measurement of Transfer Impedance of Burners

The upstream impedance (Z_u) should include the impedance of the burner itself. The burner can be treated as a series or transfer impedance since the thickness of the burner element is very small compared to an acoustic wavelength. The approach described below is commonly used to predict the impedance of perforates [48, 49].

The transfer impedance can be expressed as

$$Z_{tr} = \frac{\tilde{p}_1 - \tilde{p}_2}{S\tilde{u}} \tag{3.18}$$

where $\tilde{p}_1$ and $\tilde{p}_2$ are the respective sound pressures on opposing sides. Particle velocity ($\tilde{u}$) is assumed continuous on both sides of the sample. Figure 3.6 illustrates the concept. The transfer matrix can be expressed as

$$\begin{Bmatrix} \tilde{p}_1 \\ S\tilde{u}_1 \end{Bmatrix} = \begin{bmatrix} 1 & Z_{tr} \\ 0 & 1 \end{bmatrix} \begin{Bmatrix} \tilde{p}_2 \\ S\tilde{u}_2 \end{Bmatrix} \tag{3.19}$$

which can be incorporated into the low-order acoustic model.

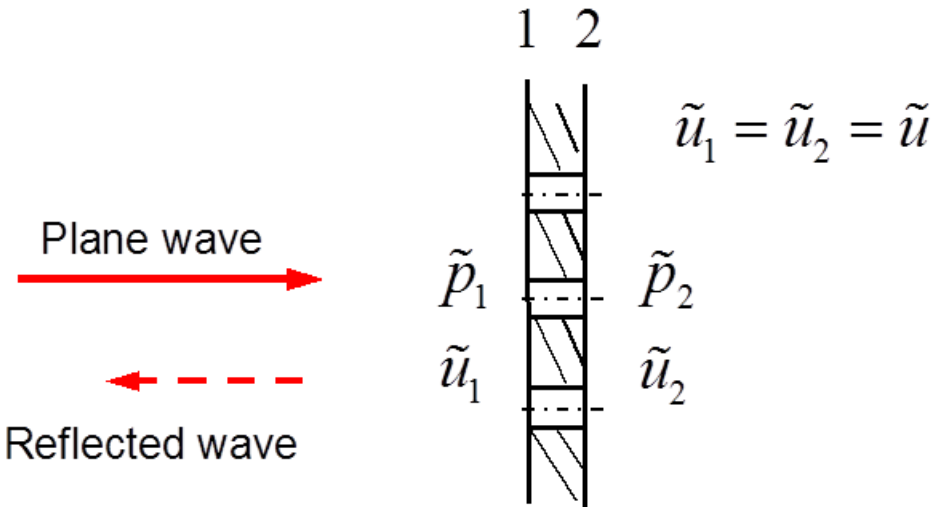

Figure 3.6 Schematic of perforate (burner) showing important variables.

Mechel et al. [48] demonstrated that the real part of the transfer impedance (the acoustic resistance) of a perforate depends on the Mach number and that the static flow resistance could be used to approximate the transfer impedance at low frequencies. Normally, the imaginary part of the transfer impedance (the transfer reactance) is negligible at low frequencies. Hence, the static flow resistance can be measured using ASTM C522 [50] at low frequencies and used directly.

However, the transfer impedance is more accurately measured using an impedance tube. This can be accomplished using the approach illustrated in Figure 3.7. The impedance at the surface of the sample can be measured twice using the two-microphone approach, once with the sample (Z_1) and the second without (Z_2) [35]. The transfer impedance is the difference between the two measurements. Normally, it is best to place some absorption at the end of the tube to eliminate any strong tube resonances.

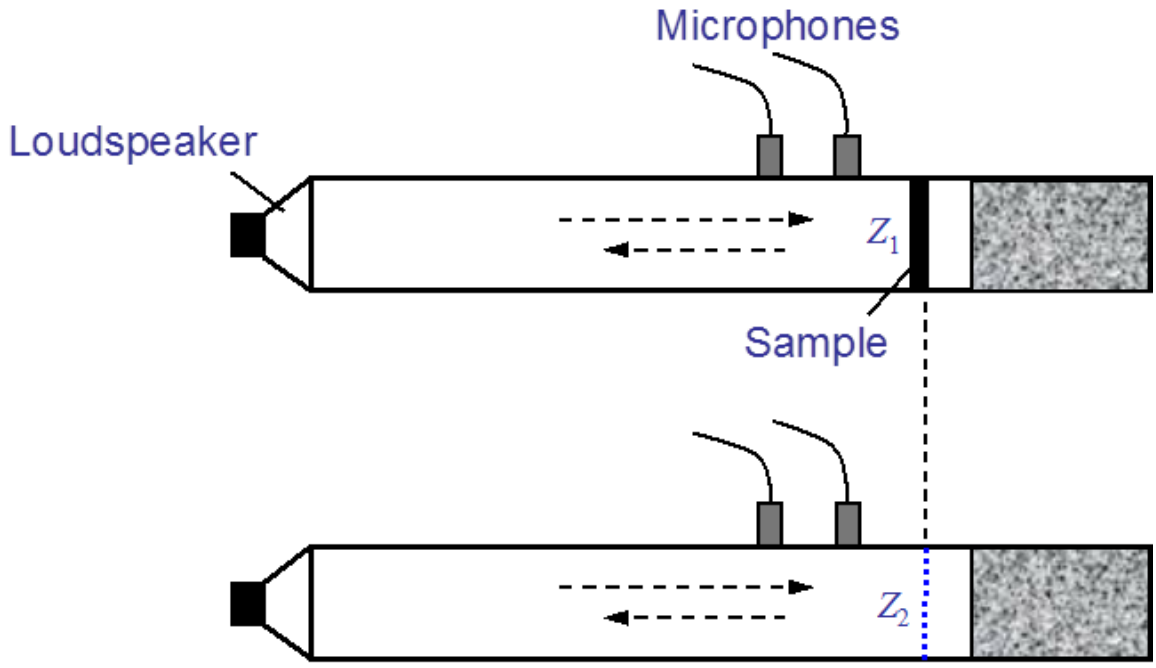

Figure 3.7 Schematic illustrating measurement of transfer impedance.

3.2.5 Calculation of Transfer Impedance of Burners

Burners are very similar to micro-perforated panel absorbers. Hole and slit dimensions are typically sub-millimeter in size. As a result, acoustic attenuation is expected due to viscous friction in the holes. Maa's theory [51, 52] has typically been used to characterize the transfer impedance of micro-perforated panels and was adopted for burners as well. Three parameters control the transfer impedance of a micro-perforate: pore diameter d, panel porosity σ, and thickness t. The transfer impedance sans flow (Z_{tr}) can be expressed as

$$Z_{tr} = \frac{\Delta\tilde{p}}{S\tilde{u}} = \frac{32\eta t}{S\sigma\rho c d^2}\left(\left(1+\frac{\beta^2}{32}\right)^{1/2} + \frac{\sqrt{2}}{8}\beta\frac{d}{t}\right) + j\left(\frac{\omega t}{\sigma c}\left(1+\left(3^2+\frac{\beta^2}{2}\right)^{-1/2} + 0.85\frac{d}{t}\right)\right) \quad (3.20)$$

where ω is the angular frequency, c is the speed of sound, η is the viscosity, and β is a perforate constant dependent on the properties of the fluid. β is given as

$$\beta = d\sqrt{\omega\rho/4\eta} \quad (3.21)$$

where ρ is the mass density of air. The real part of the transfer impedance will increase with flow. In that case, the transfer impedance with flow can be expressed as [53]

$$Z_{tr,flow} = Z_{tr} + \frac{KM}{S\sigma} \quad (3.22)$$

where M is the Mach number and K is a constant (0.044 and 0.079 for grazing and normal flow respectively).

For some burners, both porosity and hole or slit dimensions are difficult to measure using traditional means. Additionally, many burners have a metal fabric cover. In these cases, effective dimensions for the hole size and the porosity can be obtained by curve fitting the data to Maa's equation. Porosity and hole diameter can be assumed in Maa's equation. Then, the predicted transfer impedance is compared to that measured in a least square sense. The transfer impedance of different combinations of porosity and hole diameter are calculated

until optimum values were determined. This method has been documented in Reference [36].

One application of this method is to extrapolate the measured data to lower frequencies. For example, transfer impedance measured using the aforementioned subtraction method at low frequencies is noisy due to measurement difficulties (low source strength and microphone spacing). By applying this method, the fitted transfer impedance at low frequencies is much smoother than the measured data. Fitted data is compared to measured data with good agreement for a typical burner in Figure 3.8. The burner sample is inserted in the picture. The normalized transfer impedance is the magnitude of the transfer impedance defined in Equation (3.20) multiplied by $S/\rho c$.

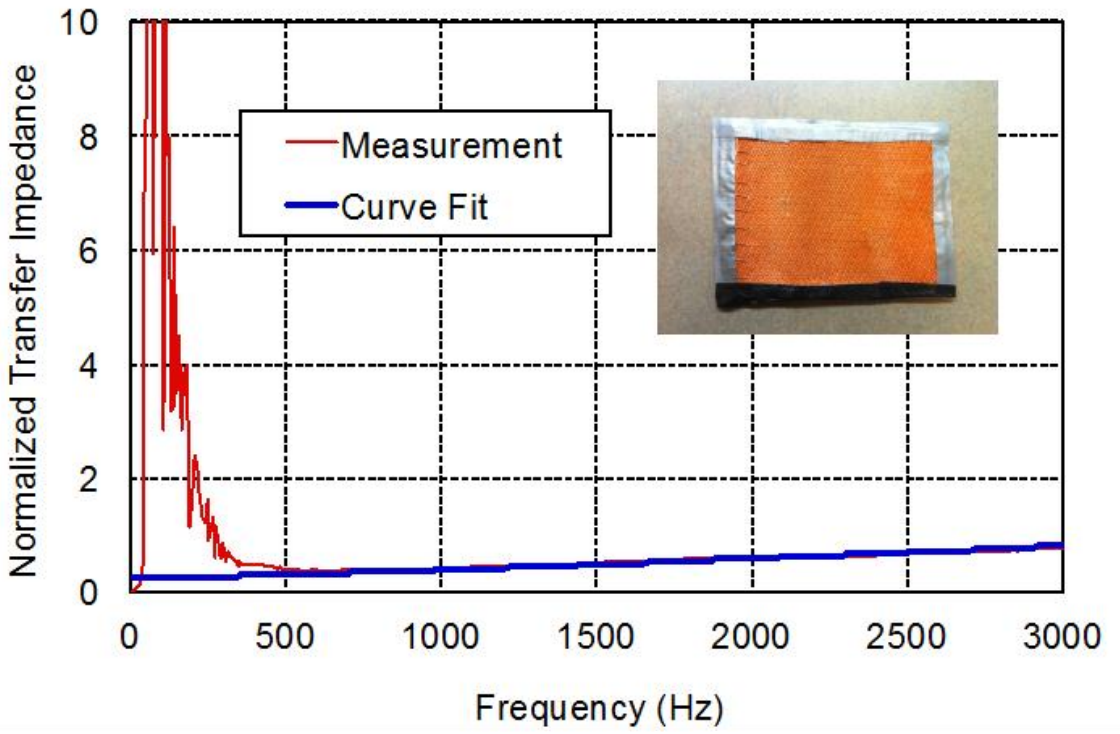

Figure 3.8 Comparison of measured to fitted data for the transfer impedance.

3.2.6 Inclusion of Structural Vibration in Transfer Matrix

It has been observed in practice that stiffening or adding damping to panels can eliminate combustion oscillations in some cases. This is especially the case for

combustion chambers with thin flat plates. A simple model (Figure 3.4d) can be used to include the structural vibration of the plate. The plate can be treated as a side branch or parallel impedance similar to a quarter wave tube if it is assumed that the sound pressure is constant across the panel. This assumption should be appropriate at low frequencies since the acoustic wavelength is long compared to the panel dimension.

The impedance of the panel can be determined by considering the plate as being simply supported [54]. The natural frequencies of the plate are then

$$\omega_{mn} = \pi^2 \left(\left(\frac{m}{a} \right)^2 + \left(\frac{n}{b} \right)^2 \right) \sqrt{\frac{D}{\rho_p h}} \tag{3.23}$$

where m and n denote the number of harmonics along the x and y-coordinate directions respectively. a and b are the length and width of the plate and h is the thickness. ρ_p is the density of the plate. At low frequencies, the mode most likely to couple strongly with the acoustics is the first mode ($m = 1$ and $n = 1$). The flexural rigidity of the plate (D) is defined as

$$D = \frac{E h^3}{12(1 - \nu^2)} \tag{3.24}$$

where E is the elastic modulus and ν is the Poisson's ratio.

The modal participation factors (η_{mn}) can be determine using

$$\eta_{mn} = \Lambda_{mn} e^{-j\phi_{mn}} \tag{3.25}$$

where

$$\Lambda_{mn} = \frac{F_{mn}}{\omega_{mn}^2 \sqrt{(1 - (\omega/\omega_{mn})^2)^2 + 4\zeta_{mn}^2 (\omega/\omega_{mn})^2}} \tag{3.26}$$

where ω is angular frequency and ζ_{mn} modal damping coefficient.

The modal damping coefficient is best determined experimentally. A frequency response function can be measured using an impact hammer and an accelerometer. The modal damping coefficient can be determined by identifying the peak amplitude and the half power frequencies from the frequency response function. See Ewins [55] for more information.

F_{mn} can be determined using

$$F_{mn} = \frac{4p\big(1-\cos(m\pi)\big)\big(1-\cos(n\pi)\big)}{\rho h m n \pi^2} \tag{3.27}$$

where p is the pressure which can be set to 1 for determining the impedance. The phase lag is defined as

$$\phi_{mn} = \tan^{-1}\frac{2\zeta_{mn}(\omega/\omega_{mn})}{1-(\omega/\omega_{mn})^2} \tag{3.28}$$

The vibrational velocity for the first mode can then be expressed as

$$\tilde{u}(x,y) = j\omega\eta_{11}\sin\left(\frac{\pi x}{a}\right)\sin\left(\frac{\pi y}{b}\right) \tag{3.29}$$

Then, the branch impedance can be approximated as

$$Z_p = \frac{-p}{avg(\tilde{u})S_p} \tag{3.30}$$

where S_p is the area of the plate.

The velocity of the plate ($\tilde{u}$) was averaged in a root mean square sense and the phase was averaged as well. The branch impedance (Z_p) found in Equation (3.30) can then be inserted into Equation (3.8).

3.2.7 Calculation of Transfer Matrix using Acoustic FEM

In some cases, the combustion chamber cannot be simulated using the transfer matrices described earlier because the geometry is too complex or the plane wave cut-off frequency has been exceeded. For example, sand-cast combustion

chambers have a complicated geometry and it is difficult to model the chamber using plane wave approximations. More importantly, the cut-off frequency is exceeded in all combustion chambers above the cut-off frequency. However, transfer matrix theory can still be used if it is assumed that plane waves exist at the inlet and outlet to the combustion chamber. However, analytical solutions for the transfer matrices above the plane wave cut-off are not available in the literature for most geometries. Accordingly, the transfer matrix itself should be determined using a deterministic method like the acoustic finite (FEM) or boundary element method (BEM).

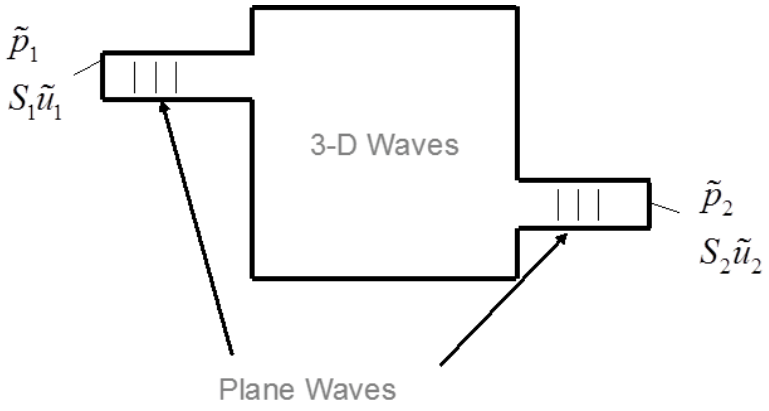

Figure 3.9 Schematic of a combustion chamber.

A schematic of a combustion chamber is shown in Figure 3.9. When using numerical methods, it is normally easier to first find modified four-pole parameters [56, 57, 58] which are defined as

$$A^* = \tilde{p}_1|_{\tilde{u}_1=1,\tilde{u}_2=0} \quad B^* = \tilde{p}_1|_{\tilde{u}_1=0,\tilde{u}_2=-1}$$
$$C^* = \tilde{p}_2|_{\tilde{u}_1=1,\tilde{u}_2=0} \quad D^* = \tilde{p}_2|_{\tilde{u}_1=0,\tilde{u}_2=-1} \qquad (3.31a,b,c,d)$$

To determine these modified four-pole parameters, two BEM/FEM analyses need to be completed. The four-pole parameters can be found by applying a unit velocity on the left end ($\tilde{u}_1 = 1$). Then, a subsequent analysis should be performed with a unit velocity on the right end ($\tilde{u}_2 = -1$). The first run is used to determine both A^* and C^*. The second run is used to find B^* and D^*. The

BEM/FEM model should include a length of duct on both the inlet and outlet sides in order to ensure plane wave behavior so that the transfer matrix approach is valid.

The four pole parameters in Equation (3.31a,b,c,d) can then be obtained from the modified four pole parameters using the expression

$$A = \frac{A^*}{C^*} \quad B = \frac{1}{S_2}\left(B^* - \frac{A^* D^*}{C^*}\right)$$
$$C = \frac{S_1}{C^*} \qquad D = -\frac{S_1}{S_2}\frac{D^*}{C^*} \tag{3.32a,b,c,d}$$

3.2.8 Measurement of the Transfer Matrix

The geometry for some components like blowers is too difficult to simulate using plane wave methods or even acoustic FEM. For complicated cases, transfer matrices should be measured using either the two-load [59] or two-source [60] methods. For the two-source method, the duct component is excited first on the inlet side and then on the outlet side using a source such as a loudspeaker. In the similar two-load method, the load or termination is changed.

A schematic illustrating the two-load method, which was used in this work, is shown in Figure 3.10 and a photograph of the measurement setup for a blower is shown in Figure 3.11. Transfer functions are measured between microphone 1 and the other 3 microphones for each of the two load cases. The acoustic load (i.e., impedance) is most easily modified by adding sound absorbing material to the end of the tube as illustrated in Figure 3.10. The use of ASTM 2611 [61] contains the recommended algorithm for determining the four-pole matrices. The essentials of the algorithm are presented next.

The transfer matrix can be determined in the following manner from the measurements. The incident pressure amplitudes upstream and downstream are expressed as

$$P_A = j\frac{e^{-jkl_1} - H_{21}e^{-jk(l_1+s_1)}}{2\sin ks_1} \quad P_B = j\frac{H_{21}e^{jk(l_1+s_1)} - e^{jkl_1}}{2\sin ks_1}$$
$$P_C = j\frac{H_{31}e^{jk(l_2+s_2)} - H_{41}e^{jkl_2}}{2\sin ks_2} \quad P_D = j\frac{H_{41}e^{-jkl_2} - H_{31}e^{-jk(l_2+s_2)}}{2\sin ks_2} \tag{3.33a,b,c,d}$$

where H_{21}, H_{31}, and H_{41} are the respective transfer functions assuming microphone 1 is used as a reference for phase. l_1, l_2, s_1 and s_2 are dimensions between microphones and the sample as shown in Figure 3.10. The sound pressure and particle velocity at the inlet and outlet to the sample can be expressed as

$$p_1 = P_A + P_B \quad u_1 = (P_A - P_B)/\rho c$$
$$p_2 = P_c e^{-jkd} + P_D e^{jkd} \quad u_2 = \left(P_C e^{-jkd} - P_D e^{jkd}\right)/\rho c \tag{3.34a,b,c,d}$$

and then the transfer matrix can be expressed as

$$\begin{Bmatrix} \tilde{p}_1 \\ S_1\tilde{u}_1 \end{Bmatrix} = \begin{bmatrix} \dfrac{p_{1a}u_{2b} - p_{1b}u_{2a}}{p_{2a}u_{2b} - p_{2b}u_{2a}} & \dfrac{1}{S_2}\dfrac{p_{1b}p_{2a} - p_{1a}p_{2b}}{p_{2a}u_{2b} - p_{2b}u_{2a}} \\ S_1\dfrac{u_{1a}u_{2b} - u_{1b}u_{2a}}{p_{2a}u_{2b} - p_{2b}u_{2a}} & \dfrac{S_1}{S_2}\dfrac{p_{2a}u_{1b} - p_{2b}u_{1a}}{p_{2a}u_{2b} - p_{2b}u_{2a}} \end{bmatrix} \begin{Bmatrix} \tilde{p}_2 \\ S_2\tilde{u}_2 \end{Bmatrix} \tag{3.35}$$

where the subscripts a and b indicate the respective loads.

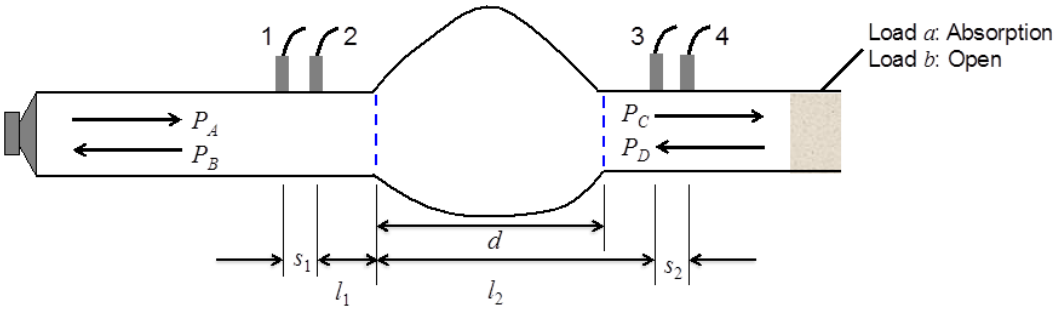

Figure 3.10 Schematic showing microphone setup for the two-load method.

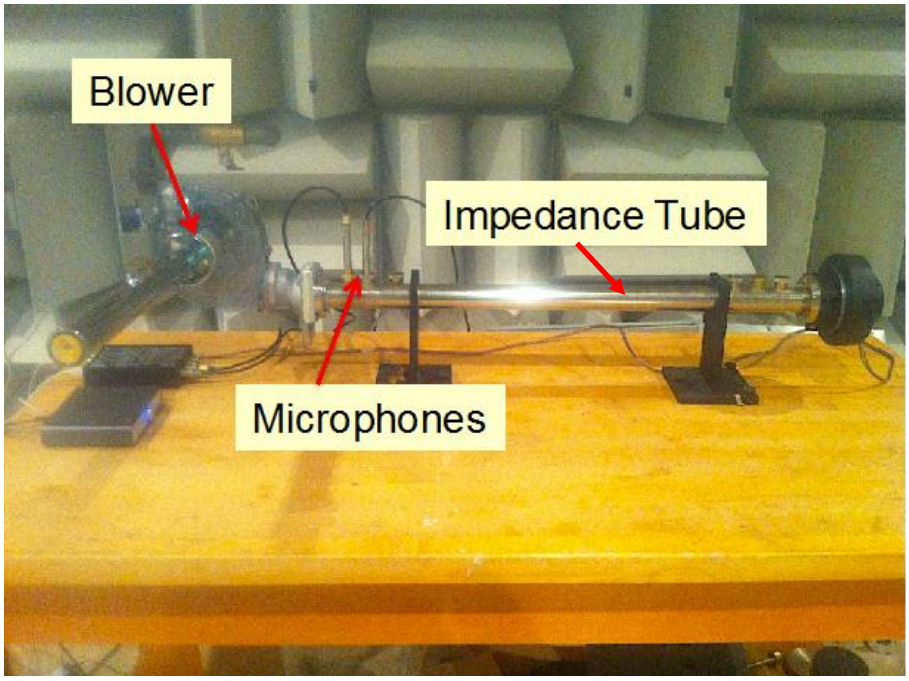

Figure 3.11 Photograph of measurement setup.

3.2.9 Determination of the Termination Impedance

The termination impedance (Z_{rad}) can be determined analytically for unflanged and flanged openings shown in Figure 3.12. The termination impedance for an unflanged opening [44, 62] is

$$Z_{rad} = \frac{\rho c(1+R)}{S(1-R)} \tag{3.36}$$

The reflection coefficient (R) is given as

$$R = -R_0 e^{-j2ka\zeta_0} \tag{3.37}$$

where a is the radius at the orifice, R_0 is the amplitude of the reflection coefficient and ζ_0 is the end correction. The amplitude of the reflection coefficient (R_0) is written as

$$R_0 = 1 + 0.01336ka - 0.59079(ka)^2 + 0.33576(ka)^3 - 0.06432(ka)^4, ka < 1.5 \tag{3.38}$$

and the end correction (ζ_0) as

$$\zeta_0 = \begin{cases} 0.6133 - 0.1168(ka)^2, & ka < 0.5 \\ 0.6393 - 0.1104ka, & 0.5 < ka < 2 \end{cases} \tag{3.39}$$

For the flanged or baffled opening [44, 63], the radiation impedance (Z_{rad}) is defined as

$$Z_{rad} = \frac{\rho c}{S}\left(R_1(2ka) - jX_1(2ka)\right) \tag{3.40}$$

where

$$R_1 = 1 - \frac{J_1(2ka)}{ka} \quad X_1 = \frac{H_1(2ka)}{ka} \tag{3.41a,b}$$

J_1 and H_1 are the Bessel function and Struve function of first order respectively.

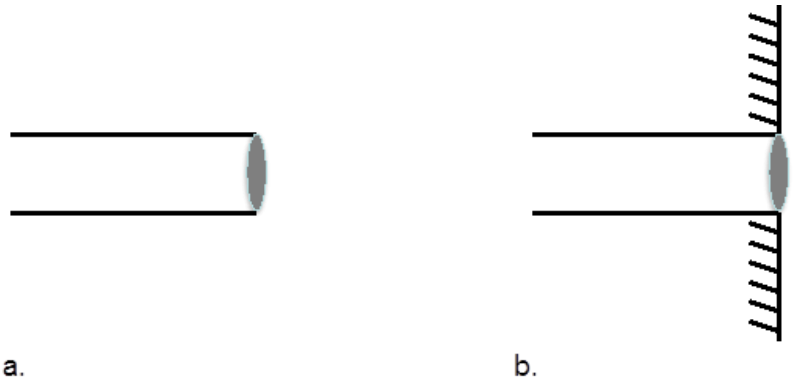

Figure 3.12 a) unflanged and b) flanged terminations.

3.3 Impedance Comparisons

The downstream impedance of three boilers was simulated and measured using the procedures described. Each of these boilers has distinguishing features that make them representative of the range of commercial boiler, water heater, and furnace applications. For Boiler 1, the combustion oscillation problem was at high frequencies (around 2100 Hz at elevated temperatures) and the geometry of the combustion chamber was very complicated. Acoustic FEM had to be relied

on in order to simulate the combustion chamber. For Boiler 2, the combustion oscillation problem occurred at low frequencies (around 10 Hz) and the geometry was simple. Consequently, plane wave methods were sufficient for the entire frequency range of interest. For Combustion chamber with thin panel, a panel resonance at approximately 220 Hz proved to be the source of the oscillation problem. Combustion chamber with thin panels was simulated using plane wave methods with the thin panel included as a side branch.

3.3.1 Downstream Impedance of Boiler 1

The combustion oscillation problem occurred at approximately 2100 Hz when the boiler was running lean. The predicted and measured impedances at room temperature compare well up to 1300 Hz. The speed of sound is proportional to the square root of absolute temperature. Accordingly, low frequencies at room temperature directly correspond to high frequencies at elevated temperatures. When realistic operating temperatures (approximately 800°F or 425°C) are included, the model should be acceptable up to and above 2100 Hz.

The downstream impedance of Boiler 1 was measured using ASTM E1050 [16]. See Section 3.2.1 for more details about the measurement. A 1.375-inch (35 mm) diameter impedance tube was used for the measurements and 0.5-inch (1.25 cm) condenser microphones (PCB 426E01) were used to measure the impedance. The microphone spacing was 1.35-inch (3.4 cm). All measurements were performed in a hemi-anechoic chamber in order to minimize background noise contamination.

The combustion oscillation occurred at approximately 2100 Hz. Consequently, the simulation model needed to be valid above the plane wave cut-off frequency of the combustion chamber. Hence an acoustic FEM model of the combustion chamber was created. As a first step, a simplified solid model of the combustion chamber was created and meshed. The acoustic FEM model is shown in Figure 3.13. A large acoustic resistance of 82,500 rayls was added to the inside surface of the combustion chamber in order to add a small amount of acoustic absorption. The transfer matrix was determined by applying a velocity of 1.0 m/s at the

burner inlet and then the exhaust in sequential runs. See Section 3.2.7 for the methodology.

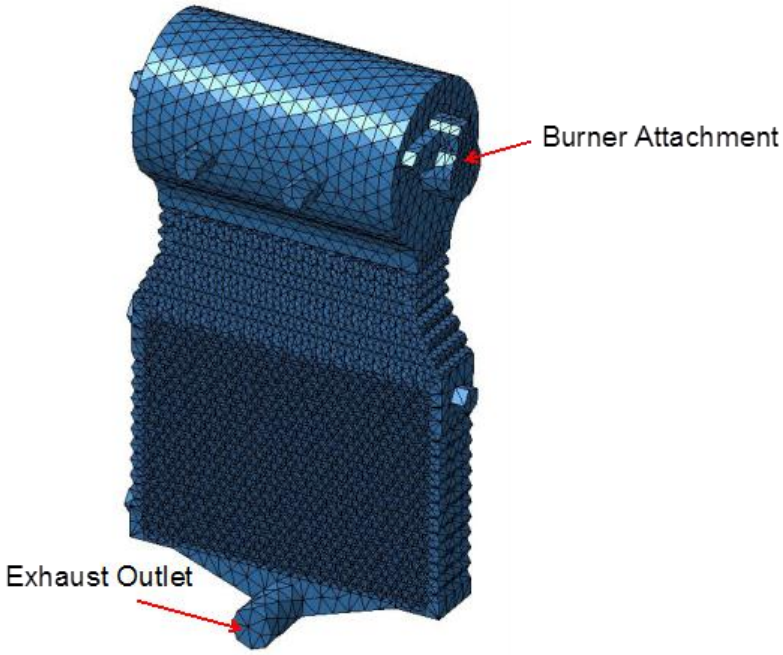

Figure 3.13 Acoustic FEM model of the Boiler 1 combustion chamber.

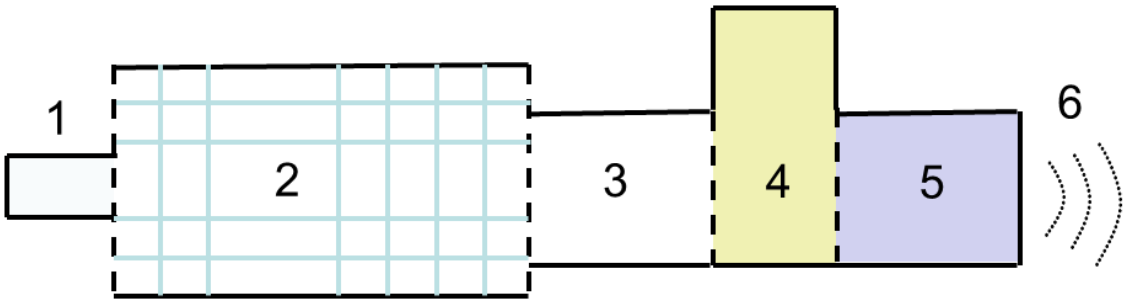

Figure 3.14 Schematic illustrating modeling approach for Boiler 1 downstream impedance.

Plane wave theory was used for each of the other elements in the model. A schematic of the model is shown in Figure 3.14. Table 3.1 shows the specific dimensions that were used for each of the elements.

The magnitude and phase of the impedance for a vent length of 1m or 35.4 in are compared in Figure 3.15 and Figure 3.16 respectively. These results are

representative of other vent lengths. Vent length had little impact on the impedance. The predicted and measured impedances at room temperature compare well up to 1300 Hz. At elevated temperatures, the speed of sound will increase and acoustic wavelengths will also increase as well. As a result, the model should be acceptable up to 2300 Hz.

Table 3.1 Dimensions and details of simulation model for Boiler 1 downstream impedance

No.	Description	Element Type	Area (cm^2)	Area (in^2)	Length (cm)	Length (in)
1	Impedance tube end	Duct	9.6	1.5	2.2	0.9
2	Combustion chamber	Acoustic FEM	46 to 20	7.1 to 3.1	N/A	N/A
3	Pipe from chamber to elbow	Duct	20	3.1	12	4.7
4	Elbow	Quarter Wave Tube	28	4.3	10	3.9
5	Vent pipe	Duct	20	3.1	90	35.4
6	Termination	Unflanged	20	3.1		

The magnitude and phase of the impedance for a vent length of 5.5m or 217 in are compared in Figure 3.17 and Figure 3.18 respectively.

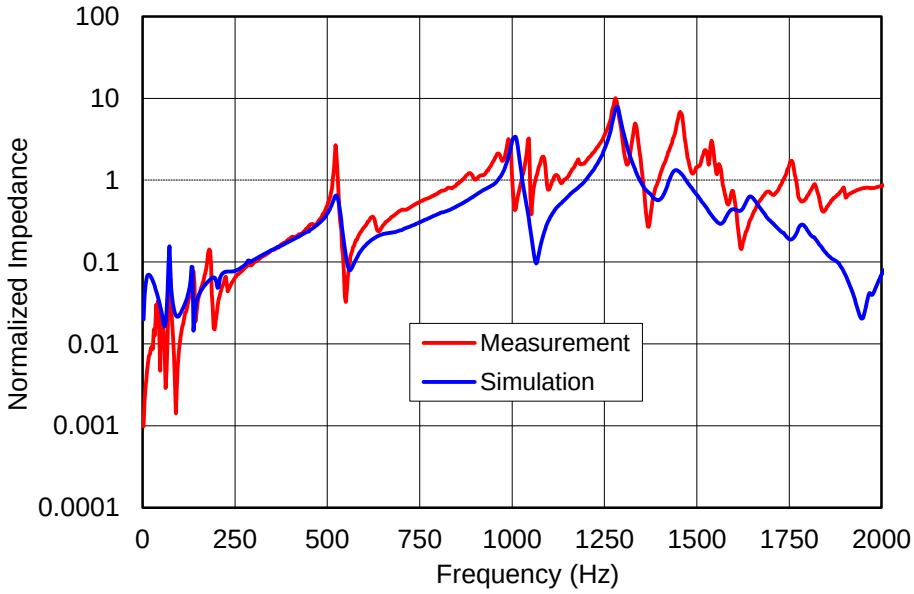

Figure 3.15 Comparison of the magnitude of the downstream impedance of Boiler 1 (vent length 1 m or 35.4 in).

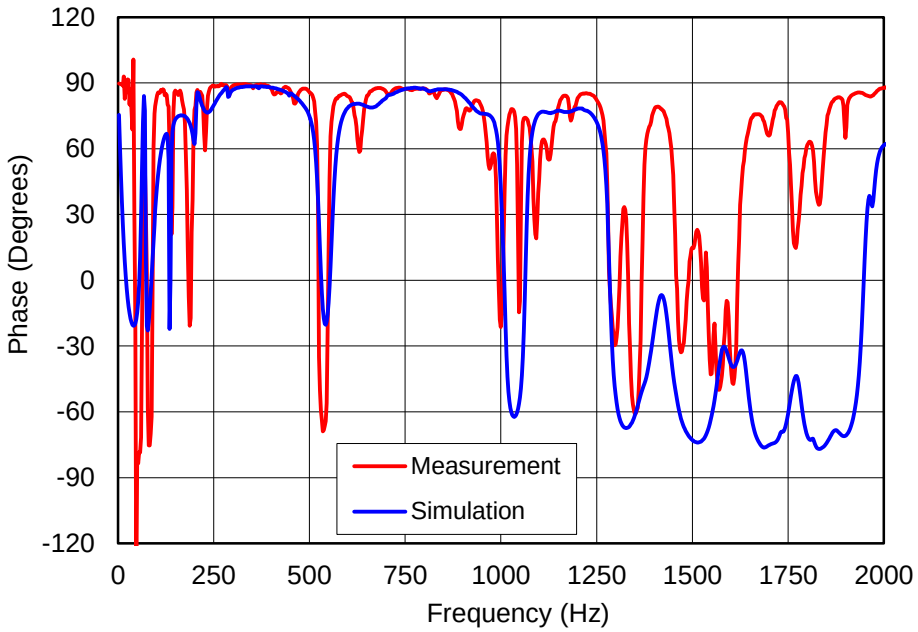

Figure 3.16 Comparison of the phase of the downstream impedance of Boiler 1 (vent length 1 m or 35.4 in).

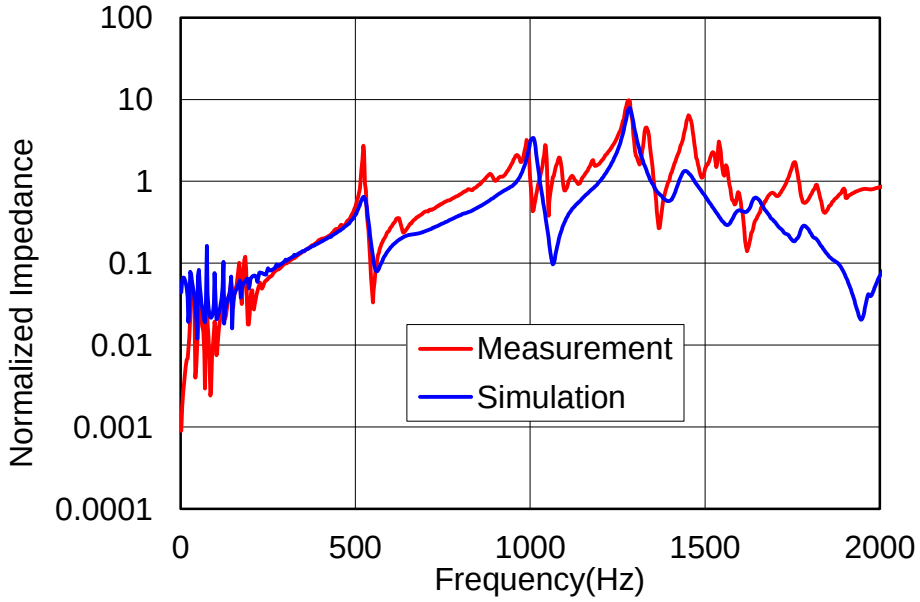

Figure 3.17 Comparison of magnitude of downstream impedance of Boiler 1 (vent length of 5.5 m or 217 in).

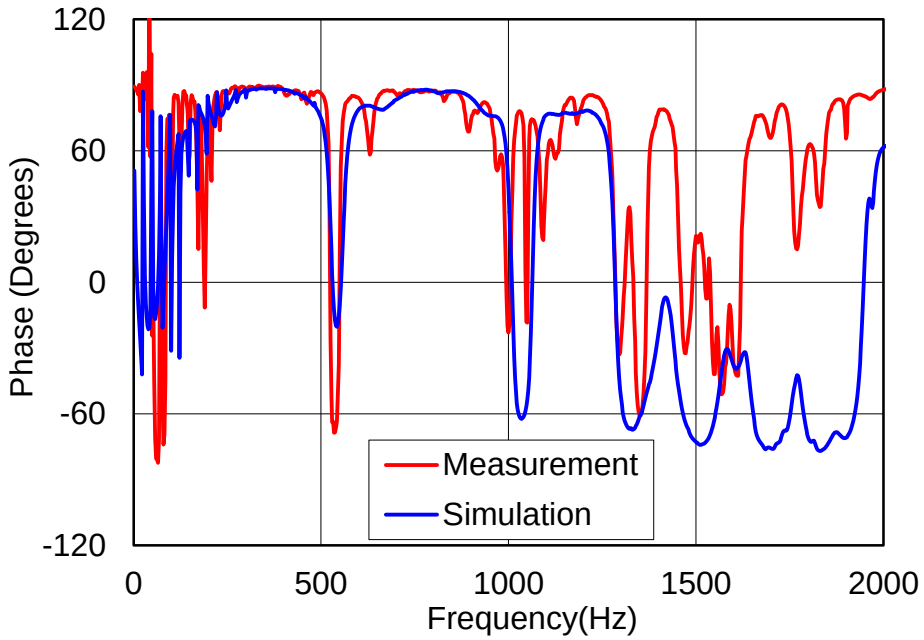

Figure 3.18 Comparison of phase of downstream impedance of Boiler 1 (vent length of 5.5m or 217 in).

3.3.2 Upstream Impedance of Boiler 1

The upstream impedance was measured in the same manner as downstream. In this case, the blower and gas valve assembly were too difficult to measure using either plane wave techniques or acoustic FEM. Hence, the transfer matrix for the assembly was measured using the method described in Section 3.2.8. A photograph of the measurement setup is shown in Figure 3.11. Not all components were determined by measurement. The intake pipe was modeled using plane wave theory. The simulation model for the system is shown in Figure 3.19 and details about the model and dimensions are provided in Table 3.2.

The magnitude and phase of the upstream impedance for an inlet pipe length of 0.4 m or 15.7 in are compared in Figure 3.20 and Figure 3.21 respectively. The inlet length had little effect on the upstream impedance. The simulation using the measured transfer matrix for the blower assembly compares well with measurement over most the frequency range.

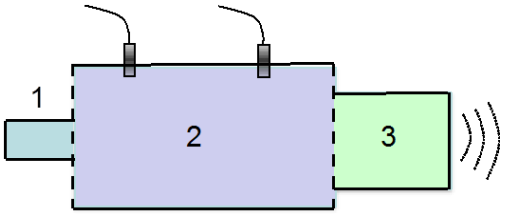

Figure 3.19 Schematic illustrating modeling approach for Boiler 1 upstream impedance.

Table 3.2 Dimensions and details of simulation model for Boiler 1 upstream impedance.

No.	Description	Element Type	Area (cm^2)	Area (in^2)	Length (cm)	Length (in)
1	Impedance tube end	Duct	9.6	1.5	1	0.4
2	Blower assembly	Measured 4-pole	40 to 17	6.2 to 2.6	N/A	N/A
3	Inlet pipe	Duct	20	3.1	65	25.6
4	Inlet opening	Quarter Wave Tube	20	3.1		

The magnitude and phase of the upstream impedance for with no inlet pipe are compared in Figure 3.22 and Figure 3.23 respectively.

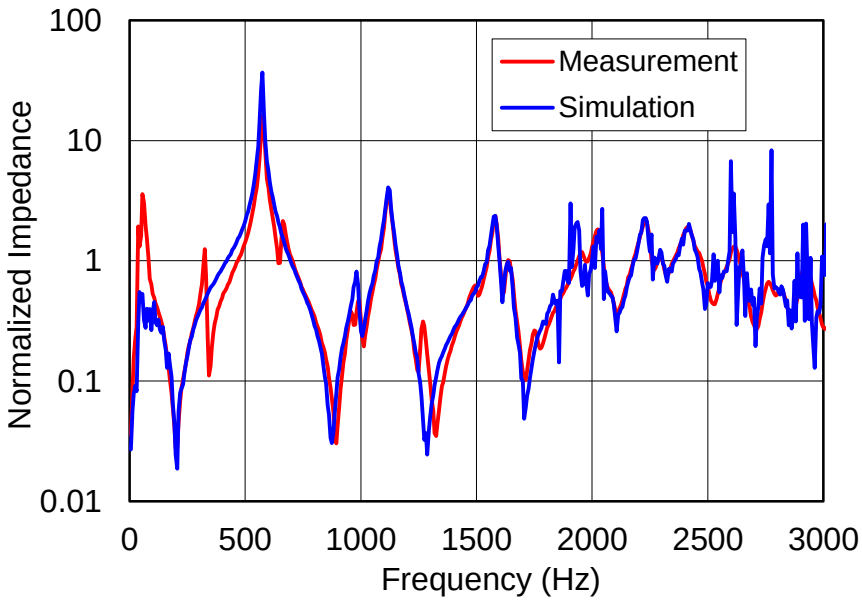

Figure 3.20 Comparison of the magnitude of the upstream impedance of Boiler 1 (vent length 0.4 m or 15.7 in)

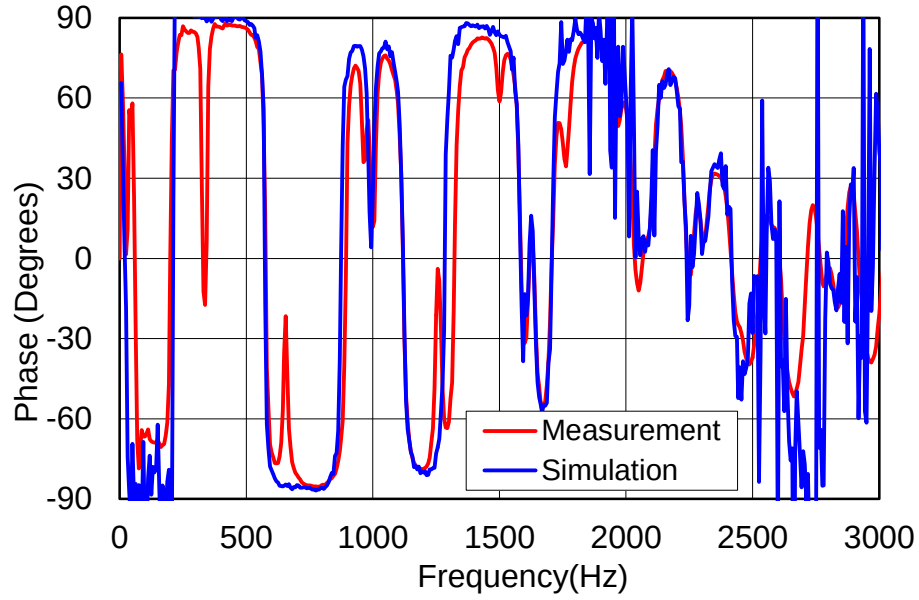

Figure 3.21 Comparison of the phase of the upstream impedance of Boiler 1 (vent length 0.4 m or 15.7 in).

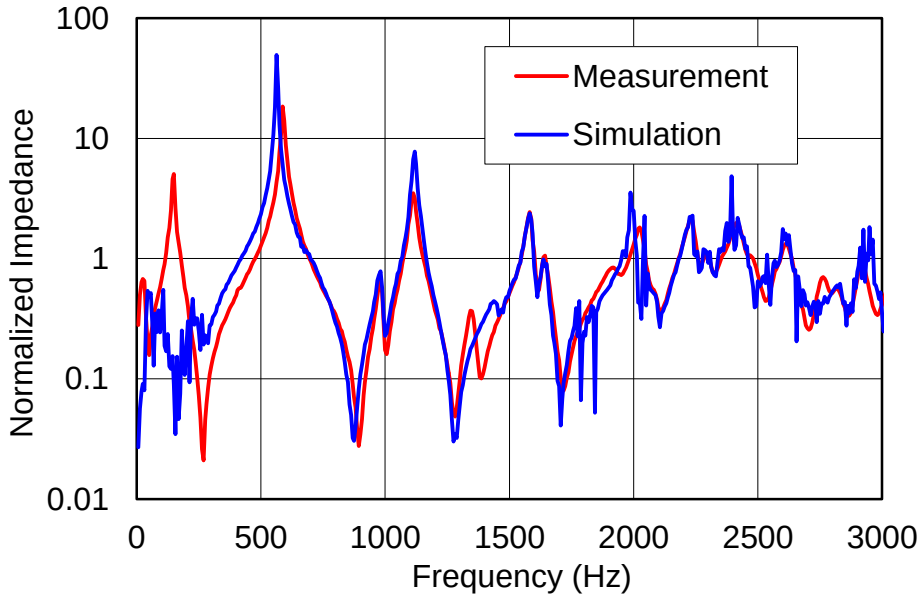

Figure 3.22 Comparison of magnitude of upstream impedance of Boiler 1 (no inlet pipe).

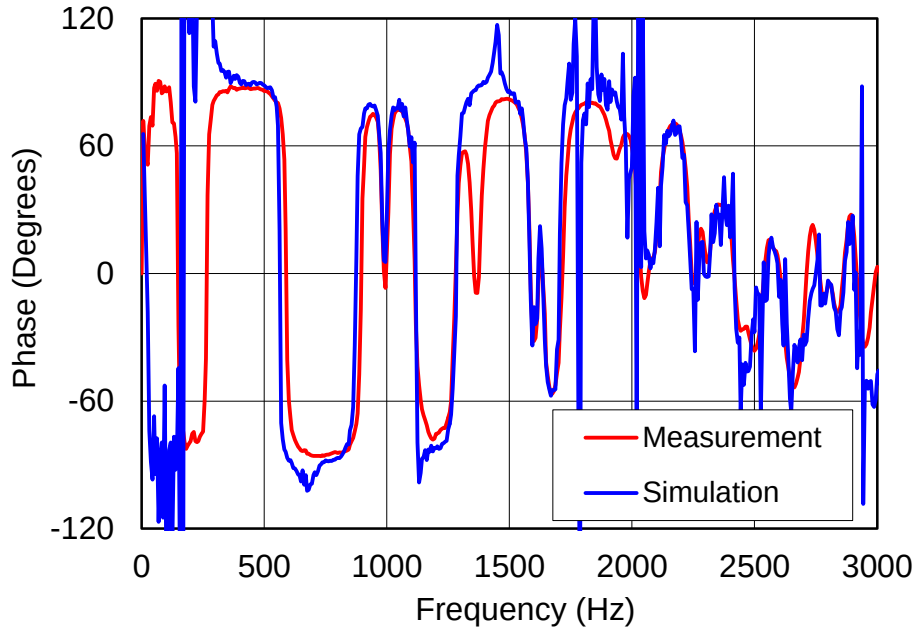

Figure 3.23 Comparison of phase of upstream impedance of Boiler 1 (no inlet pipe).

3.3.3 Measurement of Burner Transfer Impedance for Boiler 1

Switching burners eliminated the instability at 2100 Hz for Boiler 1. Both the original burner (Burner 1) and the new burner (Burner 2) are shown lit in Figure 3.24. Both burners are similar in diameter but Burner 1 is 5 cm (2 in) longer. Additionally, a ring diffuser is positioned 12.5 cm (5 in) from the burner attachment (Figure 3.24) whereas the diffuser in Burner 2 is at the attachment point. Burner 1 has a perforated metal inner layer and ceramic fabric outer layer as shown in Figure 3.25. Burner 2 consists of three layers: the inner cylinder is a perforated plate with large diameter holes. The outer two layers are in contact with one another and consist of a metallic mesh affixed to another perforated plate with higher porosity than the first plate but smaller perforations. The three layers are shown in Figure 3.26. For both burners, each layer was measured (with the exception of the inner layer of Burner 1) according to the methodology described in Sections 3.2.4 and 3.2.5 and fitted to Maa's equation. The effective parameters for each burner layer are shown in Table 3.3.

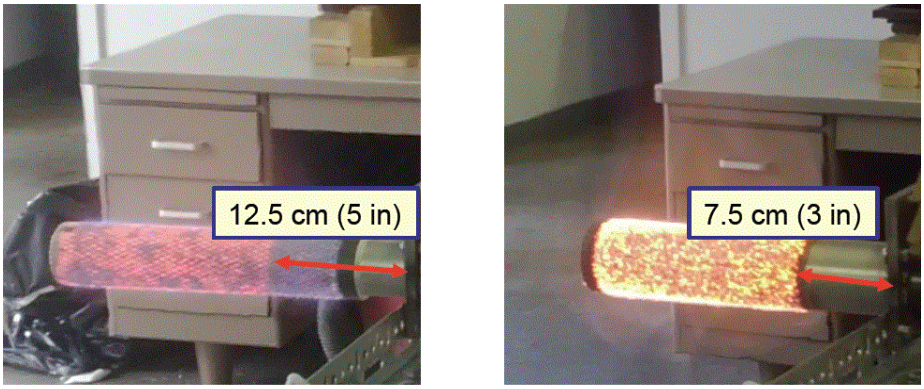

Figure 3.24 Photographs of Burners 1 and 2.

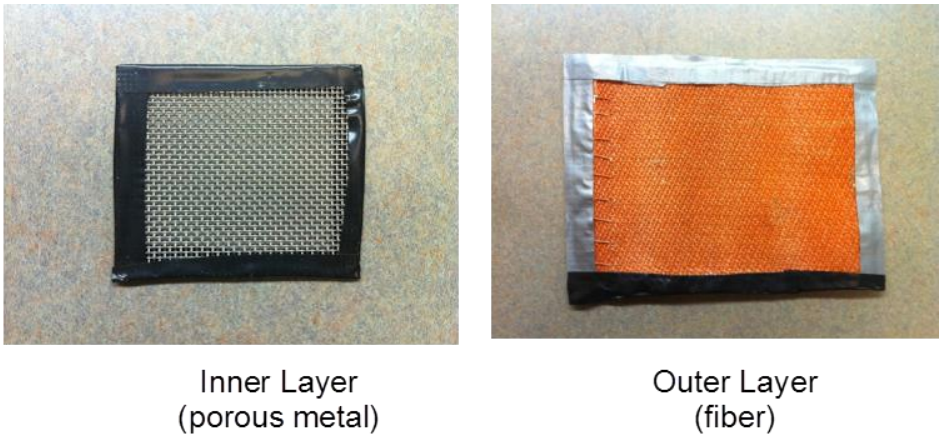

Figure 3.25 Inner and outer burner layers for Burner 1.

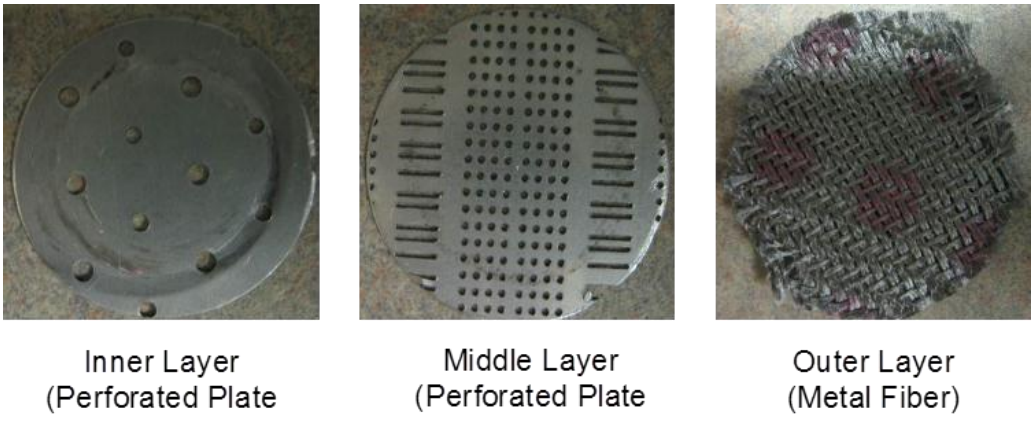

Figure 3.26 Three layers for Burner 2.

After determining the burner transfer impedance for each layer, the impedances were summed to determine the total transfer impedance. In the case of Burner 1, the inner layer is acoustically transparent because the porosity is so high and was ignored. The transfer impedance with flow was determined using Equation (2.24).

Table 3.3 Effective parameters for each burner layer.

Burner 1	**Effective Diameter**	**Effective Porosity**
Inner Layer	N/A	Over 90%
Outer Layer	0.22 mm (8.6 mils)	10.2%
Burner 2	**Effective Diameter**	**Effective Porosity**
Inner Layer	0.43 mm (16.9 mils)	4.4%
Middle Layer	0.31 mm (12.2 mils)	16.9%
Outer Layer	0.18 mm (7.1 mils)	36.1%

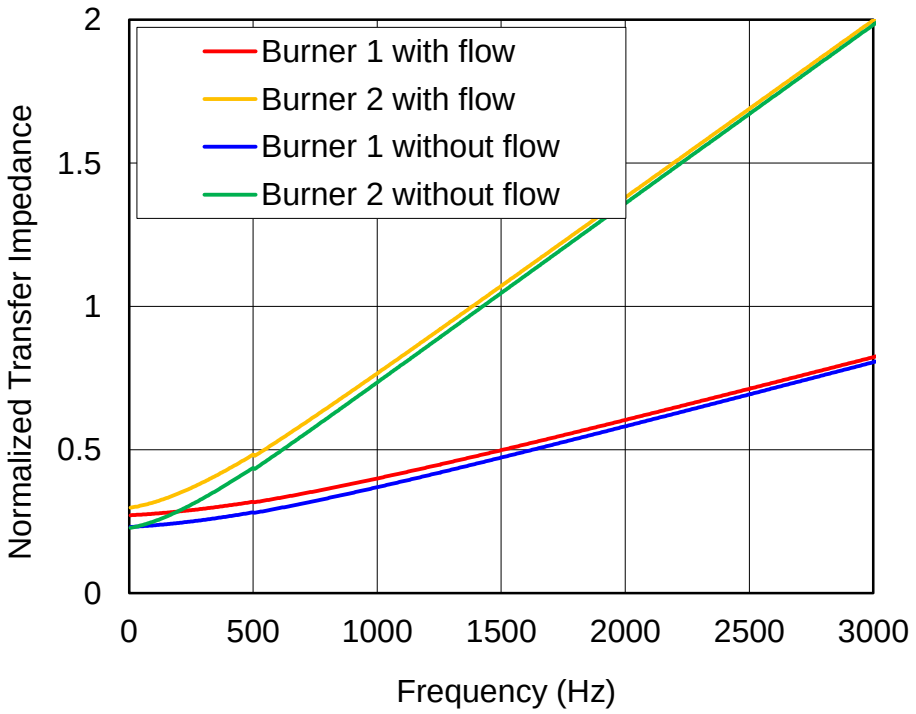

Figure 3.27 Normalized impedance magnitude for Burners 1 and 2 with and without flow.

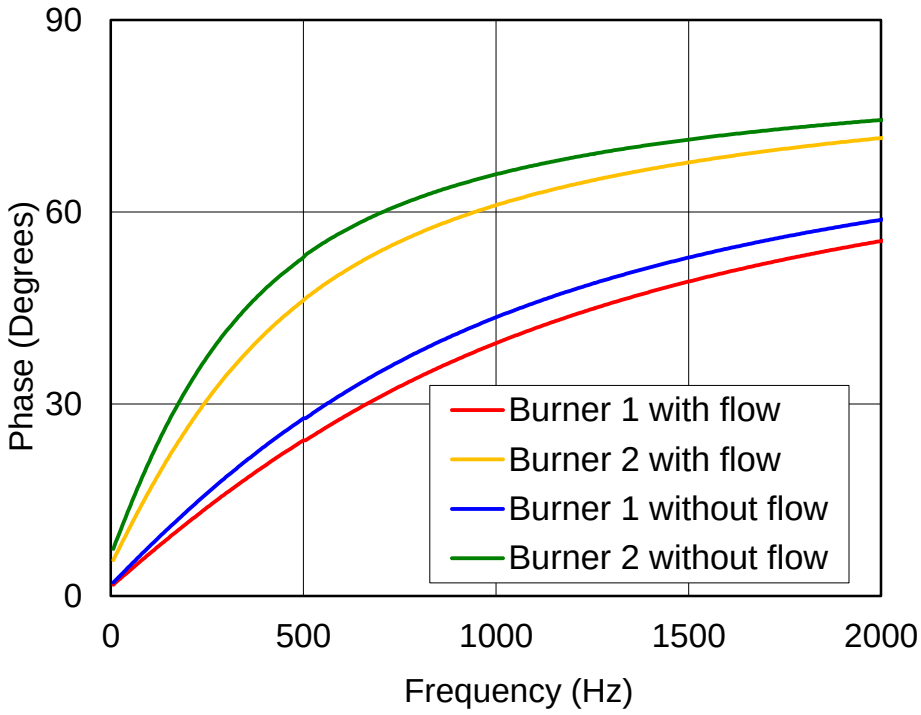

Figure 3.28 Normalized transfer impedance phase for Burner 1 and 2 with and without flow.

The transfer impedance magnitude and phase are compared for each burner with and without flow in Figure 3.27 and Figure 3.28. Notice that the acoustic impedance is higher for Burner 2. The increase in acoustic resistance should be beneficial in preventing combustion oscillations especially at higher frequencies.

3.3.4 Downstream Impedance of Boiler 2

The downstream impedance for Boiler 2 was measured using ASTM E1050 [40] and simulated using plane wave theory [28]. For Boiler 2, the instability occurred at close to 10 Hz, and plane wave theory was viable for the entire frequency range of interest.

Measuring the impedance at very low frequencies is challenging for a few reasons. Most loudspeakers do not put out sufficient sound energy below 100 Hz and condenser microphones do not measure sound pressure accurately

below 20 Hz. Additionally, background noise levels are high even in a hemi-anechoic chamber below 50 Hz.

Several steps were taken to improve the measurements so that the simulation model could be compared. A bookshelf loudspeaker was used rather than a compression driver to increase the sound energy at low frequencies, and the spacing between the microphones in the impedance tube was increased to 21.4 in to improve the accuracy of the measurement at low frequencies. Figure 3.29 shows the loudspeaker and impedance tube.

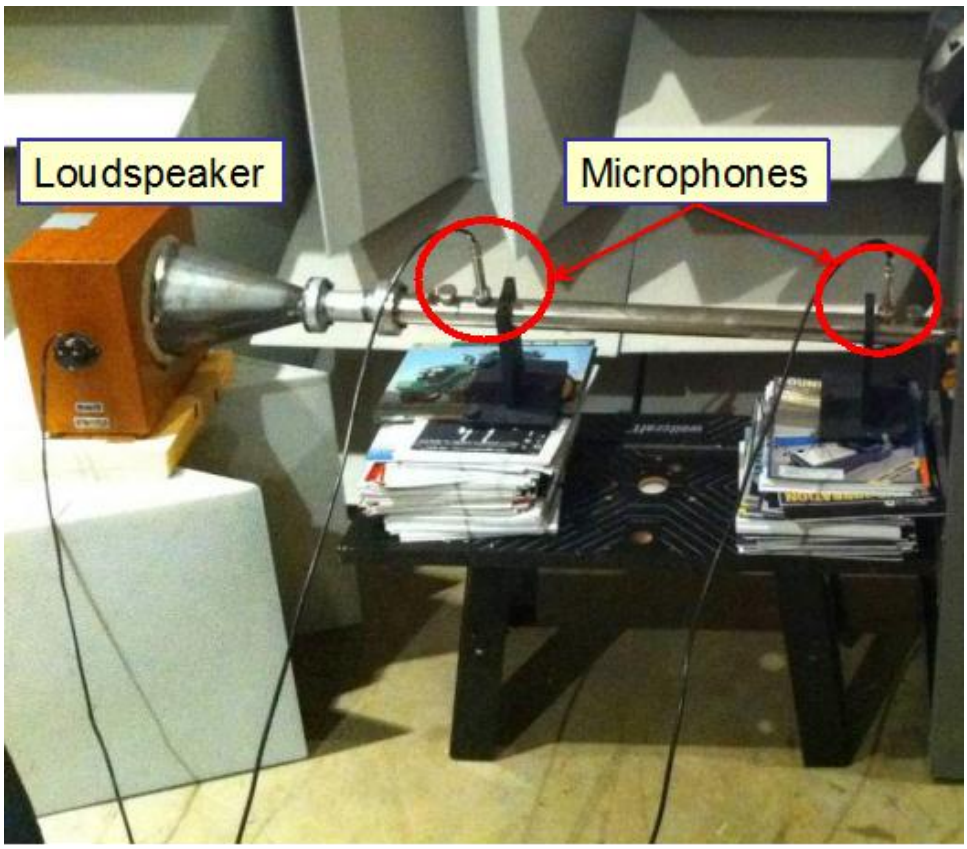

Figure 3.29 Impedance tube with bookshelf loudspeaker.

Additionally, the exhaust pipe was either removed entirely or only a short length was used. Though this does not match the boiler in operation, the first resonance frequency (also known as the Helmholtz frequency) of the combustion chamber was moved higher in frequency with a shorter exhaust pipe. Moving the first acoustic resonance higher in frequency (above 20 Hz) enables the

measurement to capture the first resonance. The measured first resonance can then be correlated with plane wave simulation. Figure 3.30 shows the impedance tube, boiler, and the exhaust pipe.

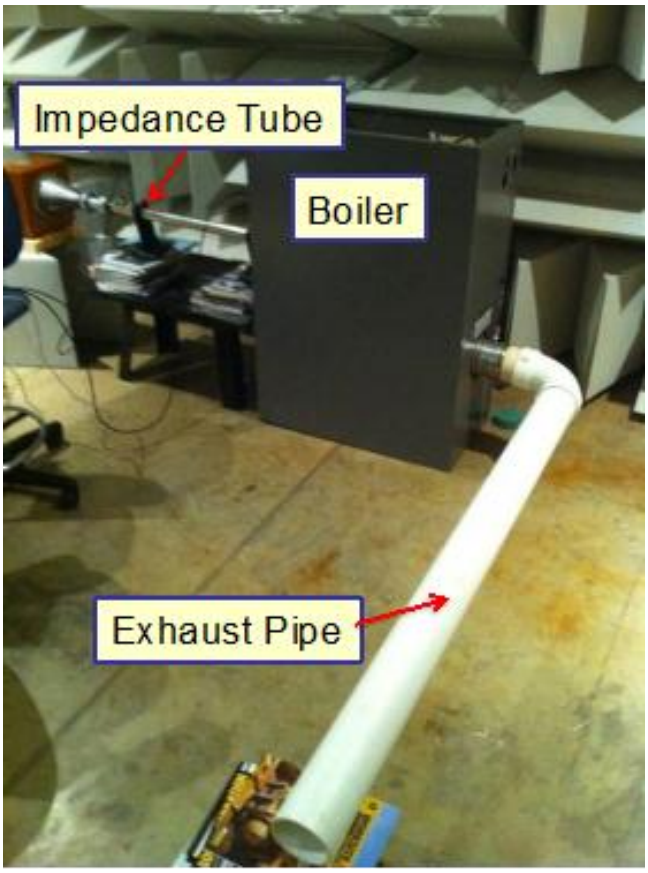

Figure 3.30 Impedance tube with Boiler 2.

The downstream impedance of Boiler 2 was modeled as shown in Figure 3.31. Detailed dimensions are shown in Table 3.4. For good agreement between measurement and simulation, it was important to model Element 4 as a quarter wave tube or extended outlet. Section 3.2.3 details the equations used for a quarter wave tube.

The magnitude and phase of the impedance for a vent length of 0 m (0 in) are shown in Figure 3.32 and Figure 3.33 respectively. As the results show, there is good agreement from 20 to 230 Hz. Below 20 Hz, the measurement is suspect due to the microphones used, background noise, and insufficient source strength.

Above 230 Hz, acoustic FEM should be used since the plane wave cut-off frequency is exceeded in the combustion chamber. The magnitude and phase of the impedance for a vent length of 1.8 m (71 in) are shown in Figure 3.34 and Figure 3.35 respectively.

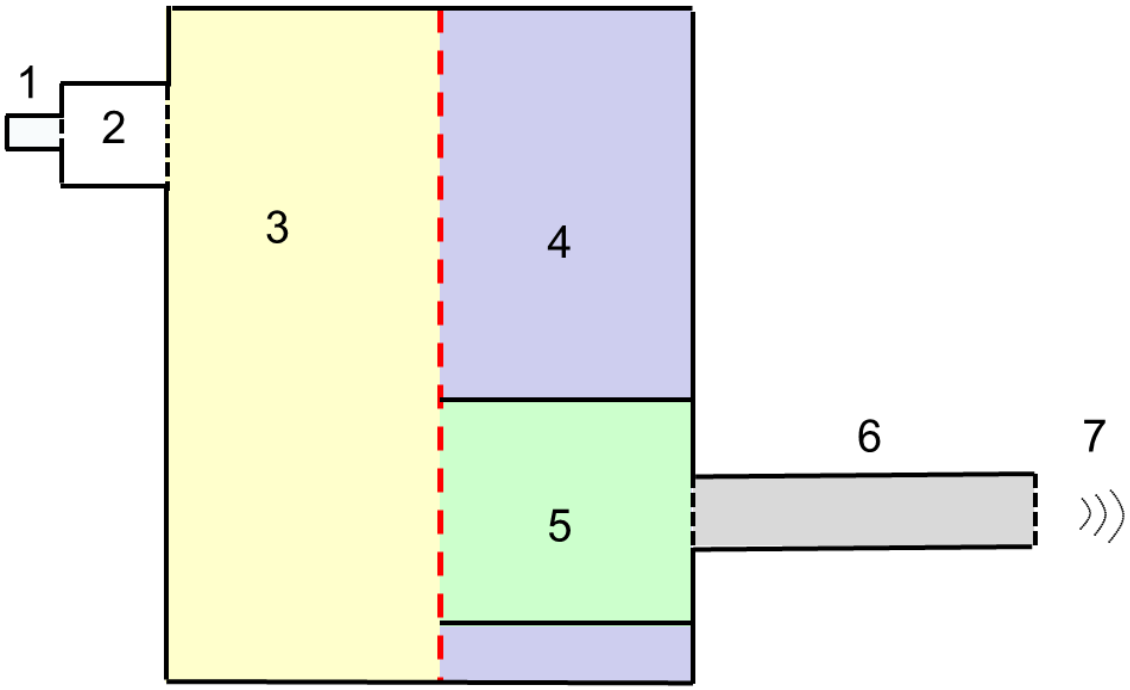

Figure 3.31 Schematic illustrating modeling approach for Boiler 2 downstream impedance.

Table 3.4 Dimensions and details of simulation model for Boiler 2 downstream impedance.

No.	Description	Element Type	Area (cm^2)	Area (in^2)	Length (cm)	Length (in)
1	Impedance tube end	Duct	9.6	1.5	2.2	0.9
2	Short duct at burner attachment	Duct	44	6.8	3.0	1.2
3	Left part of combustion chamber	Duct	1180	182.9	36.0	14.2
4	Right part of combustion chamber	Quarter Wave Tube	926	143.5	31.0	12.2
5	Outlet chamber	Duct	254	39.4	31.0	12.2
6	Vent	Duct	103	16.0	11.5	4.5
7	Termination	Unflanged	103	16.0		

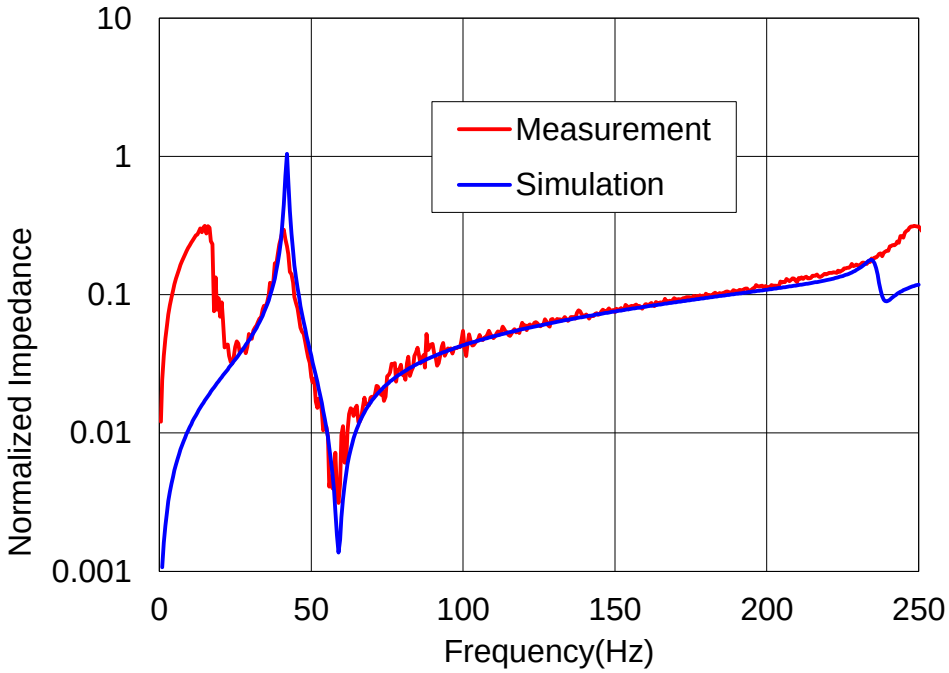

Figure 3.32 Comparison of magnitude of downstream impedance (no vent pipe).

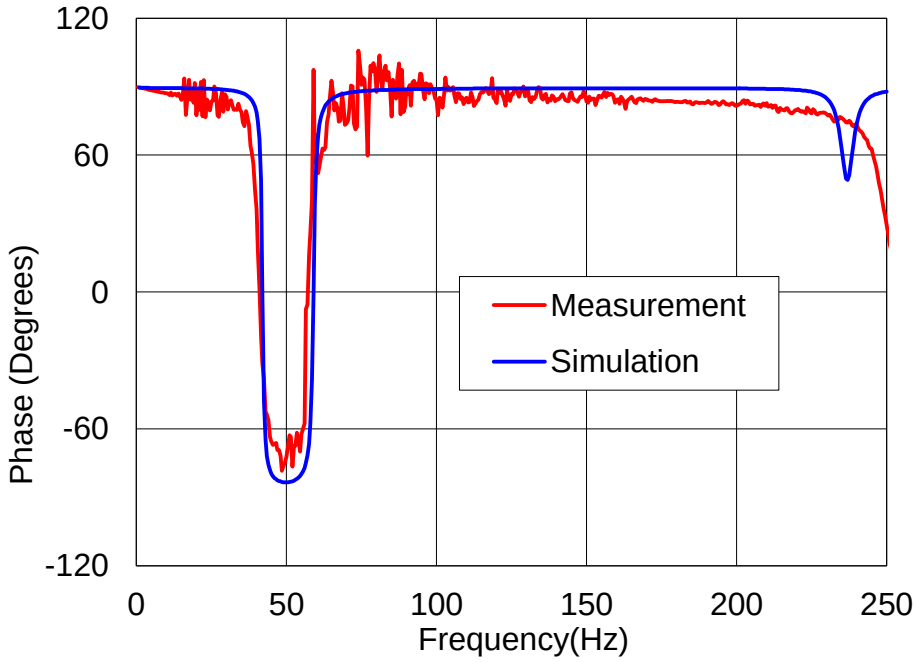

Figure 3.33 Comparison of phase of downstream impedance (no vent pipe).

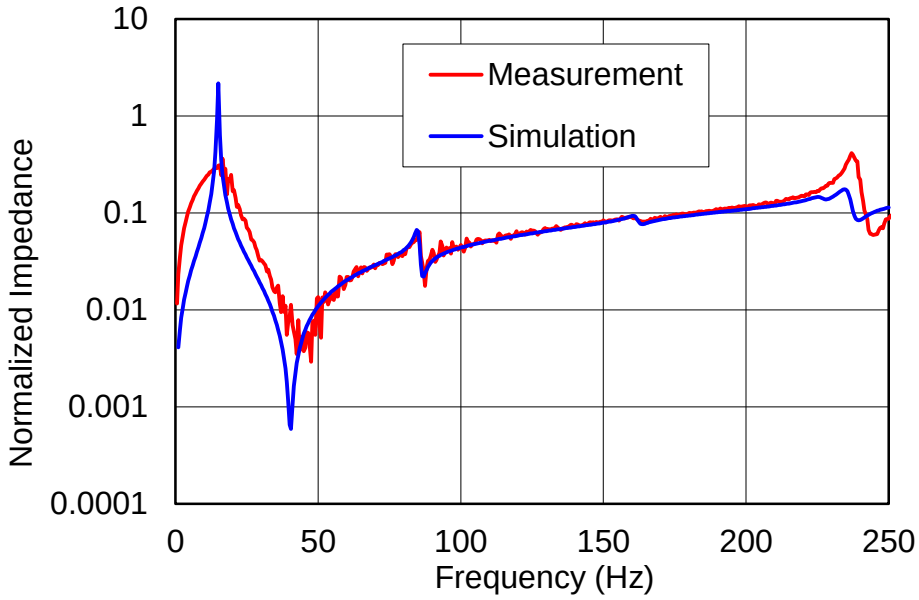

Figure 3.34 Comparison of magnitude of downstream impedance of Boiler 2 (vent length of 1.8 m or 71 in).

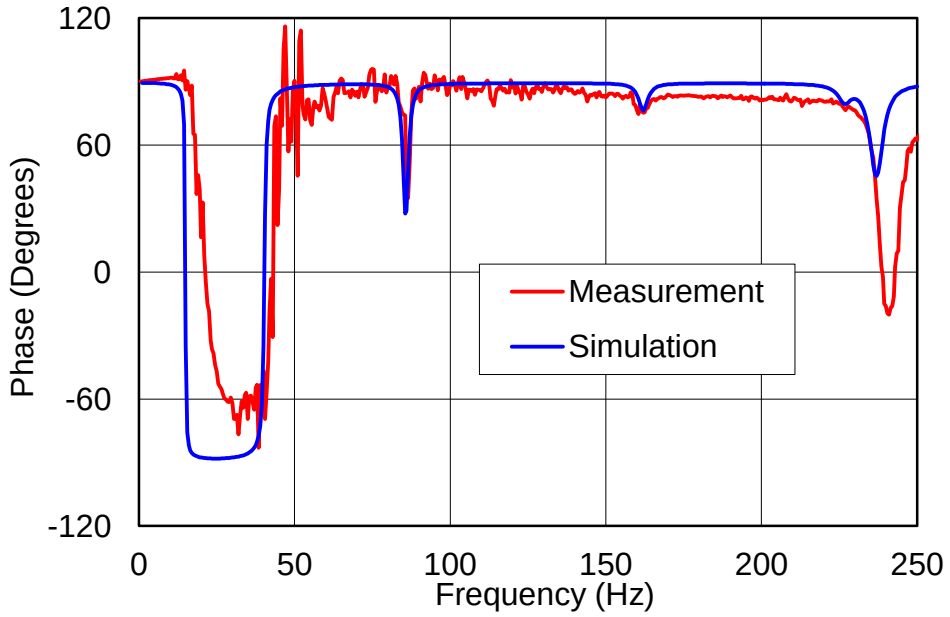

Figure 3.35 Comparison of phase of downstream impedance of Boiler 2 (vent length of 1.8 m or 71 in).

3.3.5 Upstream Impedance of Boiler 2

The upstream impedance for Boiler 2 was also modeled measured using ASTM E1050 [40] with a bookshelf loudspeaker and a microphone spacing of 0.54 m (21.4 in). Figure 3.36 shows the impedance tube attached to the intake system. The length of the intake pipe was varied.

The impedance was simulated using plane wave theory [28]. All components in the inlet system were modeled as ducts or cones. The cone element can be used for any element with a gradually increasing or decreasing cross-sectional area. The cross-section need not be circular. Figure 3.37 shows a schematic of the plane wave model and Table 3.5 shows the detailed dimensions.

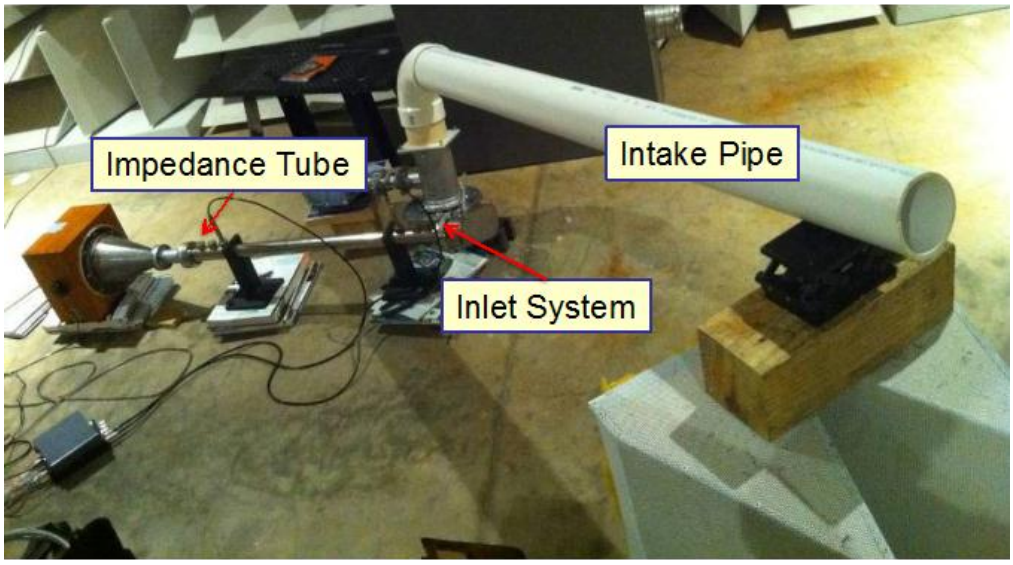

Figure 3.36 Impedance tube attached to intake system for Boiler 2.

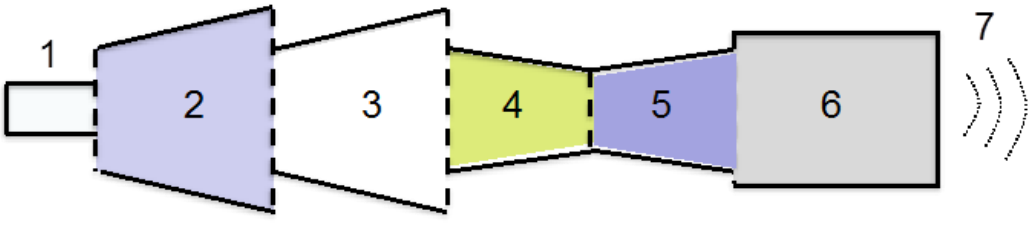

Figure 3.37 Schematic illustrating modeling approach for Boiler 2 upstream impedance

Table 3.5 Dimensions and details of simulation model for Boiler 2 upstream impedance

No.	Description	Element Type	Area (cm^2)	Area (in^2)	Length (cm)	Length (in)
1	Impedance tube end	Duct	9.6	1.5	1.8	0.7
2	Transition from burner to blower	Cone	38 to 57	5.9 to 8.8	30.0	11.8
3	Blower	Cone	34 to 50	5.3 to 7.8	65.0	25.6
4	Transition from blower to venturi	Cone	38 to 7	5.9 to 1.1	8.0	3.1
5	Transition from venturi to inlet pipe	Cone	7 to 79	1.1 to 12.2	8.0	3.1
6	Inlet pipe	Duct	81	12.6	32.0	12.6
7	Inlet	Unflanged	81	12.6		

The most challenging element was the blower, which was modeled as a cone. The length of the cone was tuned so that it would compare well with the measurement. A length of approximately 75% of blower circumference was ultimately selected.

Magnitude and phase comparisons of the impedance are shown in Figure 3.38 and Figure 3.39 respectively. The simulation results compared well with measurement above 20 Hz. The intake pipe length was 1.8 m (71 in) for the results shown though other intake lengths were considered as well.

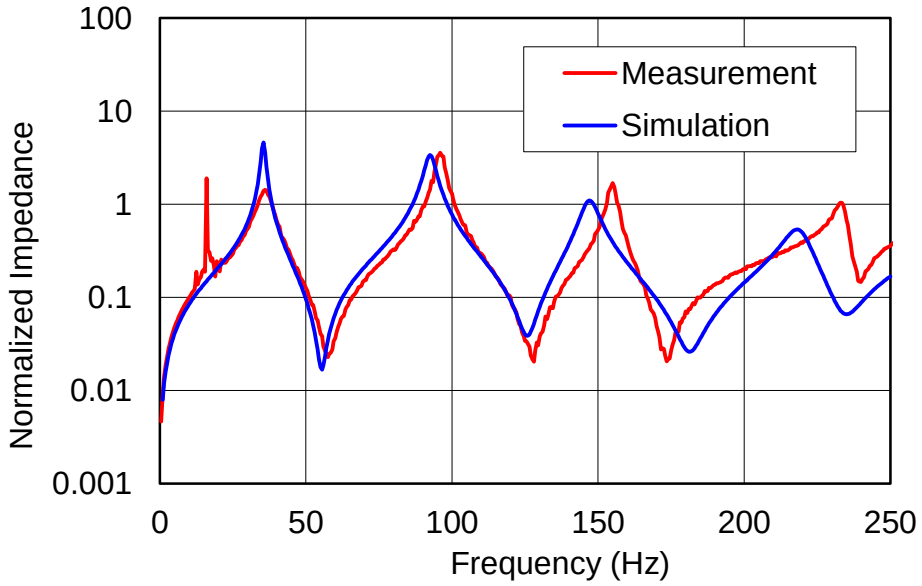

Figure 3.38 Comparison of magnitude of upstream impedance (1.8m or 71 inch inlet pipe).

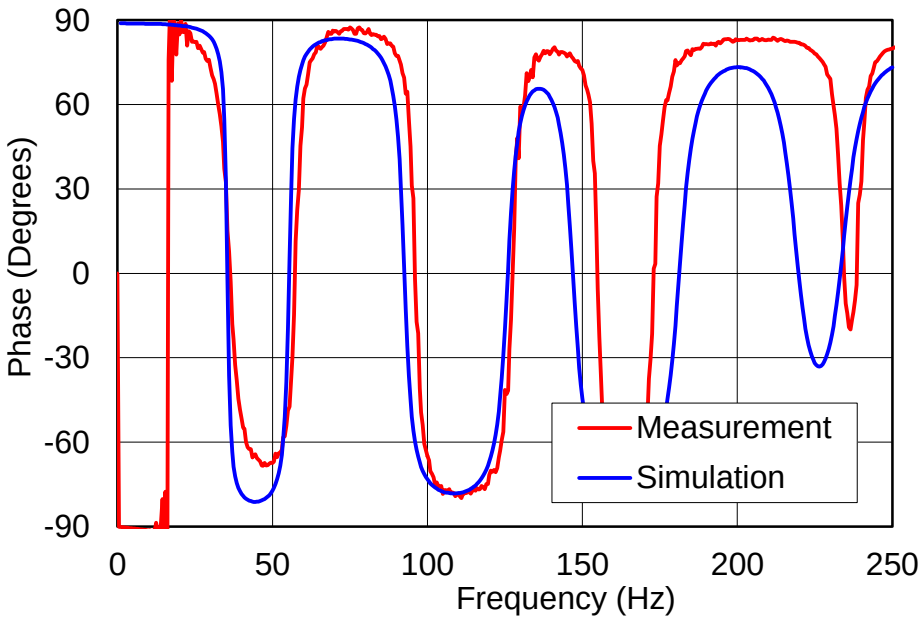

Figure 3.39 Comparison of phase of upstream impedance (1.8m or 71 inch inlet pipe).

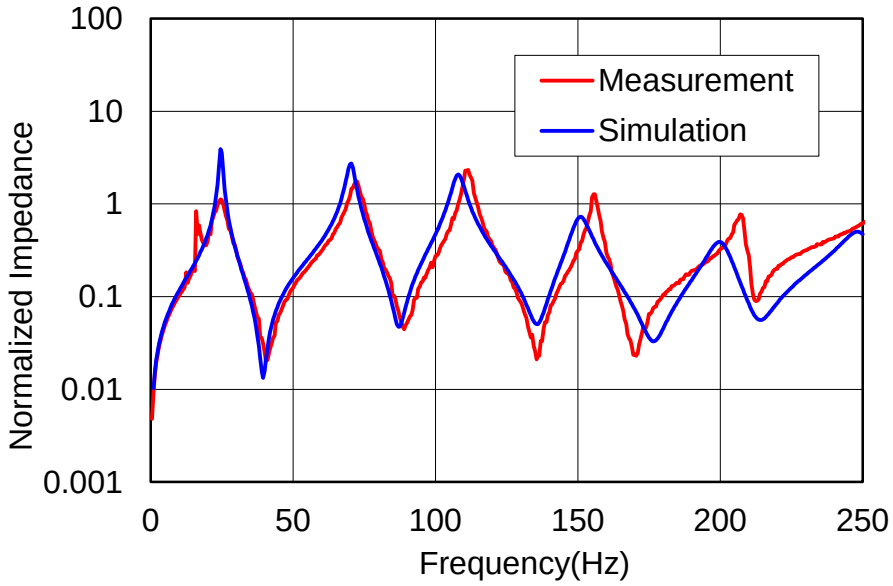

Figure 3.40 Comparison of magnitude of upstream impedance of Boiler 2 (2.9 m or 114 in intake pipe).

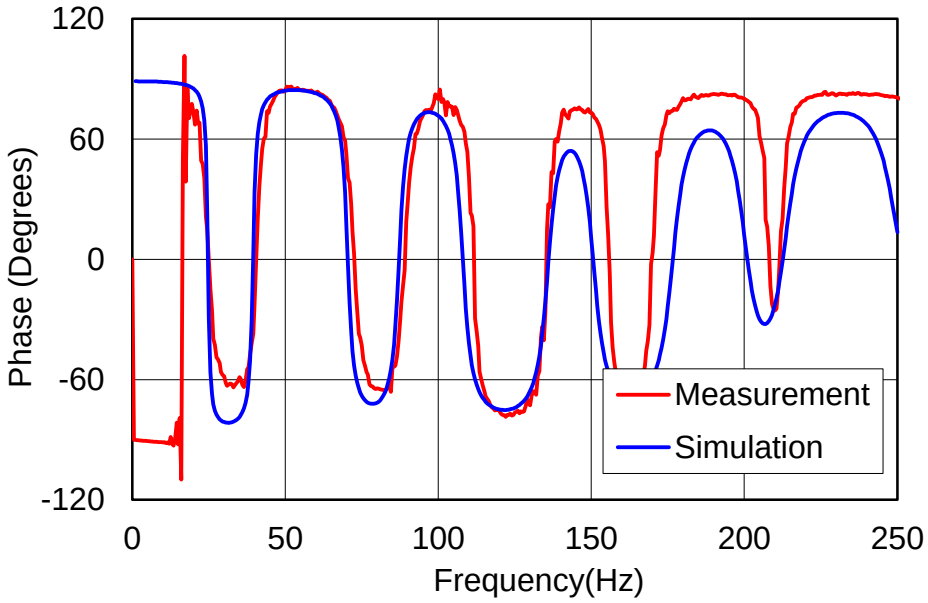

Figure 3.41 Comparison of phase of upstream impedance of Boiler 2 (2.9 m or 114 in intake pipe).

3.3.6 Combustion Chamber with Thin Panel

A combustion chamber was selected which had a thin and nearly flat panel on one side. The combustion chamber is shown in Figure 3.42. Since the plate was thin, it was believed that the vibration of the plate would affect the measured impedance at certain frequencies. The downstream impedance of the combustion chamber was measured and simulated to determine if this was indeed the case. The impedance for the combustion chamber was measured in a manner identical to the measurements for Boilers 1 and 2. A vent pipe was added to one end of the chamber.

A schematic of the plane wave model is shown in Figure 3.43. The thin plate was modeled as a side branch. The theoretical approach for dealing with a thin plate is detailed in Section 3.2.6. Table 3.6 provides details about the dimensions and individual transfer matrix elements. Table 3.7 summarizes the plate dimensions and material properties.

Figure 3.42 Combustion chamber with thin and nearly flat panel.

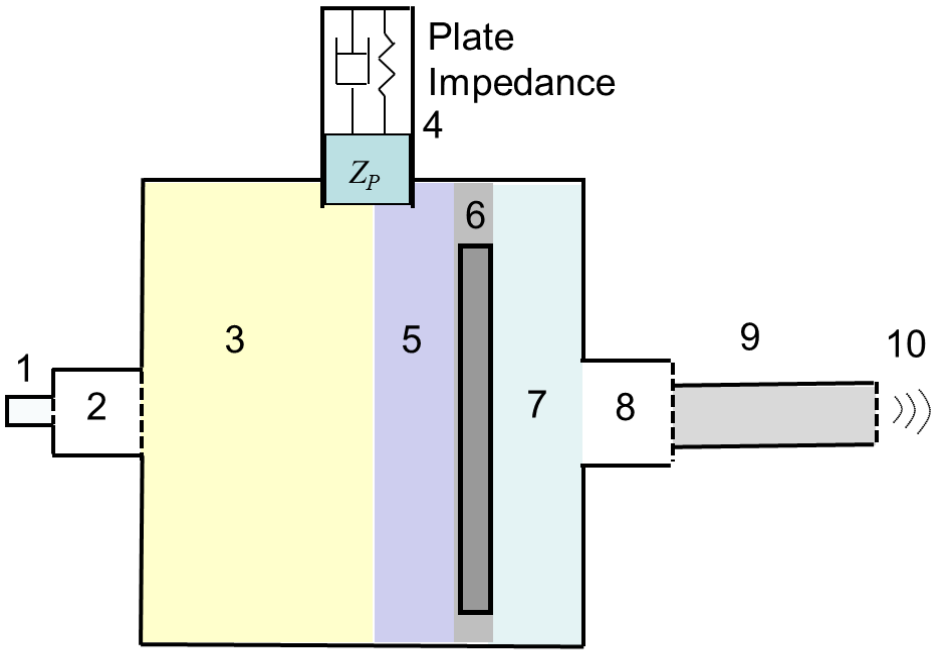

Figure 3.43 Schematic illustrating modeling approach for combustion chamber.

Table 3.6 Dimensions and details of simulation model for combustion chamber impedances.

No.	Description	Element Type	Area (cm^2)	Area (in^2)	Length (cm)	Length (cm)
1	Impedance tube end	Duct	9.6	1.5	1.8	0.7
2	Short duct at burner attachment	Duct	43	6.7	2.2	0.9
3	Combustion chamber (near burner)	Duct	60	9.3	8.7	3.4
4	Thin plate (side branch)	Side branch				
5	Combustion chamber (near plug)	Duct	60	9.3	4.7	1.9
6	Area around plug	Duct	39	6.0	1.4	0.6
7	Combustion chamber (behind plug)	Duct	60	9.3	2.7	1.1
8	Short duct at outlet	Quarter Wave Tube	13	2.0	0.7	0.3
9	Vent pipe	Duct	18	2.8	1.51	0.6
10	Termination	Unflanged	18	2.8		

Table 3.7 Dimensions and material properties for the thin panel.

Young's Modulus	Poisson's Ratio	Density	Thickness	Length	Width	Damping Loss Factor
19.3 Gpa	0.3	8000 kg/m^3	1.8 mm	0.20 m	0.19 m	0.01
2800 $kips/in^2$	0.3	0.289 lbs/in^3	0.071 in	7.8 in	7.5 in	0.01

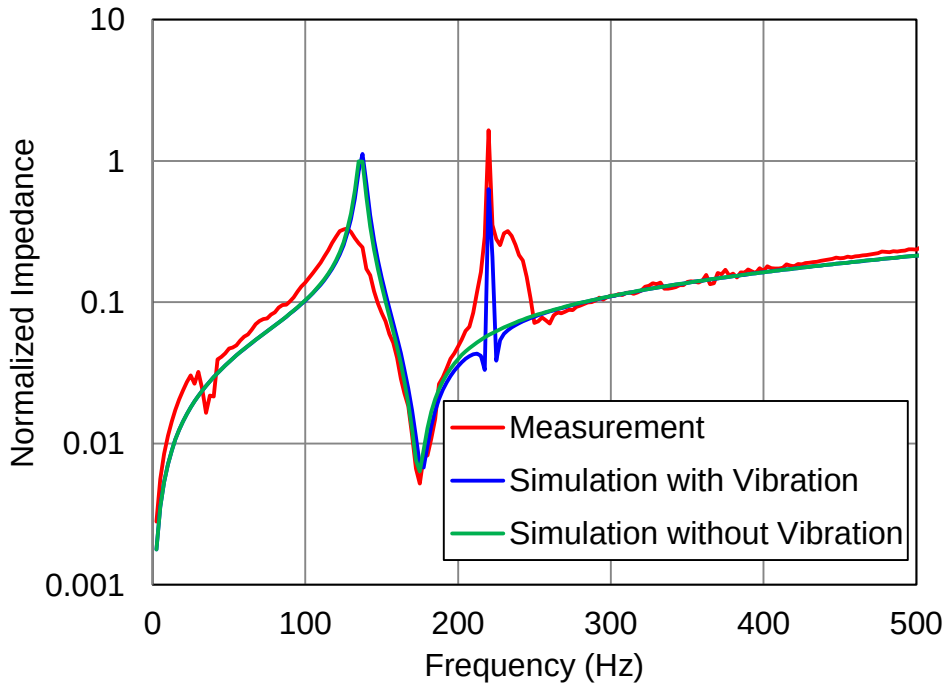

Figure 3.44 Comparison of magnitude of downstream impedance (no vent).

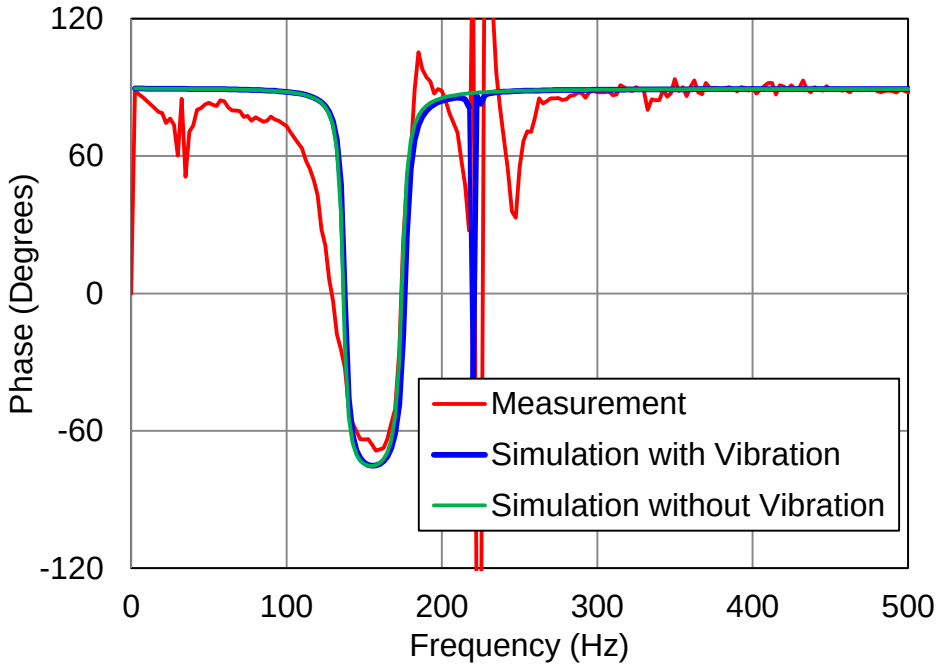

Figure 3.45 Comparison of phase of downstream impedance (no vent).

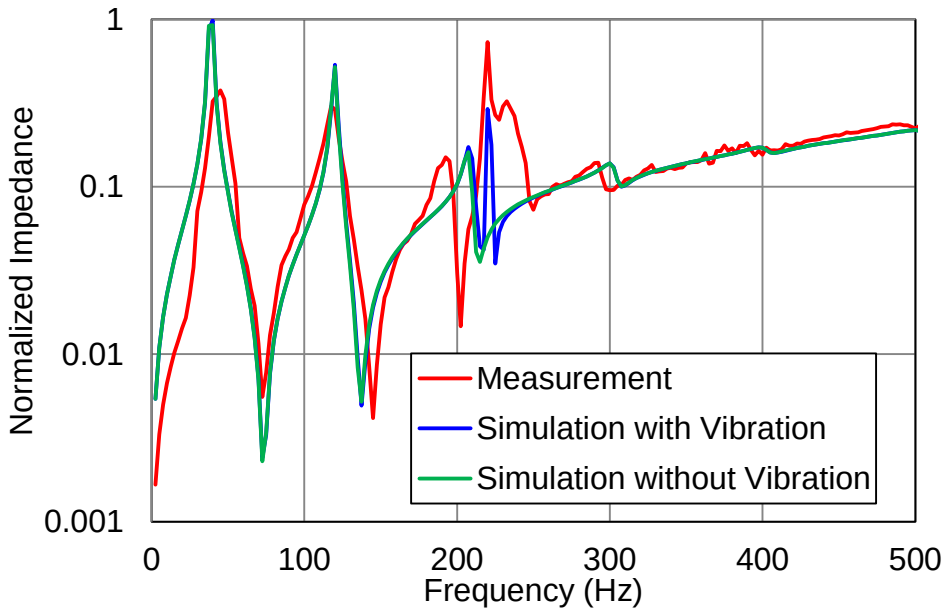

Figure 3.46 Comparison of magnitude of downstream impedance of a combustion chamber with a thin panel (vent length of 1.5 m or 59 in).

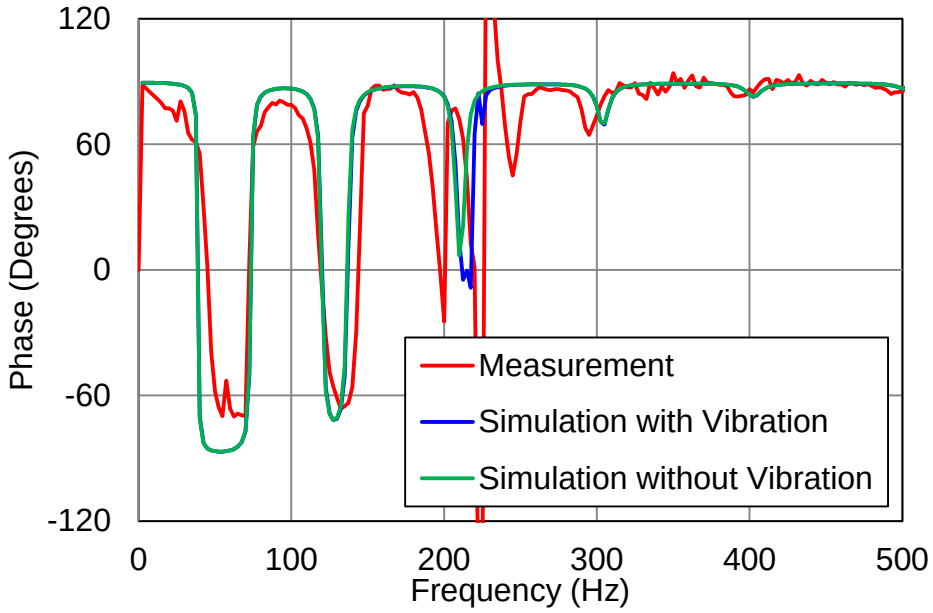

Figure 3.47 Comparison of phase of downstream impedance of a combustion chamber with a thin panel (vent length of 1.5 m or 59 in).

The magnitude phase of the impedance is compared in Figure 3.44 and Figure 3.45 for no vent case. Measured results are compared with simulation with and without Element 4 (the thin plate in Table 3.6). The results demonstrate that the resonance at 220 Hz is due to the thin plate and will be present regardless of the vent length. Additionally, the good agreement with simulation demonstrates that the effect of structural vibration can be incorporated into the plane wave model. The magnitude phase of the impedance is compared in Figure 3.46 and Figure 3.47 for the case with 1.5 m or 59 in long vent pipe.

3.4 Summary

The acoustic impedance is the ratio of sound pressure to the volume velocity at a given position. Accordingly, it is directly applicable to characterizing the sound pressure at the flame produced by volume velocity perturbations of the flame. This chapter presents the measurement technique and simulation procedure for determining the acoustic load impedance for boilers, water heaters, and furnace.

In the basis of transfer matrix theory, assuming the characteristic dimension of the system is less than a wave length, each component of the boiler system is analyzed as an acoustic element using four-pole parameters and is used to assemble the entire system. In case of complicated system with characteristic dimension exceeds the interested wave length, it is not suitable to employ the transfer matrix theory to simulate the system. Rather, numerical acoustics, such as FEM and BEM, becomes the appropriate analysis tool. By building a finite element model of the combustion chamber, the four-pole parameters are determined assuming plane wave propagation in the inlet and outlet pipes. In order to take burner into account, the transfer impedance of burners is characterized first experimentally and then curve-fitted using a nonlinear least square algorithm. In addition, the vibration of flexible panel is modeled as a side branch which could be incorporated into the impedance model. This chapter details the most commonly used duct elements and their transfer matrices. In additions, a transfer matrix element has been developed for combustion chambers consisting of thin and flat plates.

The acoustic impedance of boilers can be determined at room temperatures by experimentation. However, simulation is required to determine the impedance at elevated temperatures if the temperature is varied from element to element. In this study, simulation models for three combustion chambers have been correlated with measured results.

CHAPTER 4 A DESIGN APPROACH FOR PREVENTING AND SOLVING COMBUSTION OSCILLATION PROBLEMS

4.1 Introduction

The flame in a boiler, furnace, or water heater is a source of sound that is benign at most frequencies. However, it is very likely that the sound produced by the flame will excite either an acoustical or structural resonance at certain frequencies. Sound reflected back from the combustion chamber will produce a fluctuating mixture flow or equivalence ratio that will feed back onto the flame. As the sound power of the flame increases, a tone that is clearly abnormal and unacceptable will develop.

The previous two chapters detail efforts to further develop and validate a feedback loop stability model for combustion oscillations. The model that was used was originally developed by Baade [6] over 30 years ago. In CHAPTER 2, Baade's model is reviewed and enhanced. The model, as originally formulated, assumed that the root cause of the instability was a fluctuating mixture flow. A complementary model was developed for equivalence ratio fluctuations partially based on work by Sattelmayer [21]. The model was demonstrated to be useful for determining the cause of combustion oscillations for two commercial boilers.

CHAPTER 3 is a guide for determining the impedance upstream or downstream of the flame. This chapter provides a fairly exhaustive set of equations for modeling the individual acoustic elements that are commonly found in combustion chambers and intake systems. Moreover, the chapter details how to measure acoustic impedance if the geometry is difficult to model and directed readers to the appropriate measurement standards.

While the aforementioned chapters and other work [6, 15, 17] communicate the theory for the feedback loop stability model and how to implement it, most engineers working in the boiler, furnace, or water heater industry neither have the acoustic knowhow or time to apply the model to their specific problem.

The model is based on knowing the downstream (Z_D) and upstream (Z_U) impedances and the flame transfer function (G_f). However, most labs do not have the necessary equipment or knowhow in house. For example, an impedance tube or silencer simulation software is very useful for determining the upstream and downstream acoustic impedances but few manufacturers have this capability. Additionally, few, if any, burner manufacturers supply their customers with flame transfer functions and most manufacturers do not have access to a rig to measure the flame transfer functions. Accordingly, most manufacturers rely on solving problems in a trial-and-error fashion or hiring the few acoustical consultants who have some experience with thermo-acoustic instabilities.

This chapter presents steps that can be taken by engineers to prevent and treat combustion oscillations. Though the recommendations are based on having a basic understanding of Baade's low order model, the model need not be fully implemented for a particular design to take advantage of the tips presented herein. To my knowledge, the work by Baade and Tomarchio [16, 64] is the only one aimed directly at the practicalities of solving combustion oscillation problems.

4.2 The Design Process and Combustion Oscillations

The traditional design process consists of the following four steps:

1. Clarification of Task
2. Conceptual Design
3. Detailed Design
4. Prototyping

ISO/TR 11688-1 [65] and Bockhoff [66] discuss what may be done regarding noise control during each step of the process. For the most part, combustion oscillation problems are in no way addressed until the prototyping step. Even then, most manufacturers solve the problem in a trail-and-error fashion while not understanding the science. The goal of the current work is to indicate what may be accomplished at each step the design process. Table 4.1 summarizes the steps that can be taken during each step of the design process.

Table 4.1 Design process for preventing and diagnosing combustion instabilities.

1	**Clarification of Task**
	Log information from prior equipment (temperatures, instability frequencies, etc.)
	Obtain flame transfer functions from burner suppliers
2	**Conceptual Design**
	Dampen all structural resonances in the combustion chamber
	Add absorption to the combustion chamber
	Add absorption or sound reflecting elements upstream
3	**Detailed Design**
	Select dimensions for combustion chamber, exhaust, and inlet
	Develop the feedback loop stability model
	Identify and solve possible combustion instability frequencies a priori
4	**Prototyping**
	Perform operational tests varying exhaust and inlet length, air fuel ratio, and flow speed.
	Identify running combustion instability frequencies
	Add absorption or structural damping
	Drill holes below the flame in the combustion chamber
	Change the burner port size or air fuel ratio to stretch the flame
	Change the burner geometry for high frequency instabilities
	Change the intake system or gas valve for problems caused by equivalent ratio fluctuations

4.2.1 Clarification of Task

If combustion oscillations have occurred with similar products, they are likely to occur again. Hence, it will be very beneficial for management and engineering to make a commitment to addressing these issues when a new product is initiated. A few steps can be taken early on.

First, data from past equipment should be recorded. This would include air fuel ratios, flow rates, and temperatures in the combustion chamber and exhaust pipe. Also, it would be advantageous to record the instability frequencies of past problems that have occurred.

Secondly, it would be beneficial to require the burner suppliers to measure and provide flame transfer functions. The measured flame transfer function can then be integrated into the feedback loop model in later stages of the design process.

4.2.2 Conceptual Design

In the conceptual design step, design rules can be applied to dampen and minimize the number of resonances in the combustion chamber. Resonances are inescapable in any enclosed space, but many strong resonances can be avoided. A few design rules are listed below.

Dampen all Structural Resonances in the Combustion Chamber

It has been shown that structural resonances can sometimes lead to combustion oscillations [34, 67]. In CHAPTER 3, we showed that a structural resonance led to a peak at a single frequency in the downstream impedance. Figure 4.1 shows the measured downstream impedance for a combustion chamber with and without damping added to a panel. Notice that the impedance is much higher at 220 Hz if the panel is not damped. Accordingly, it is recommended that each panel in the combustion chamber have sufficient damping. The frequency response function for each panel can be measured by hitting each panel with an impact hammer and measuring the acceleration, and the damping for each mode can be determined [55].

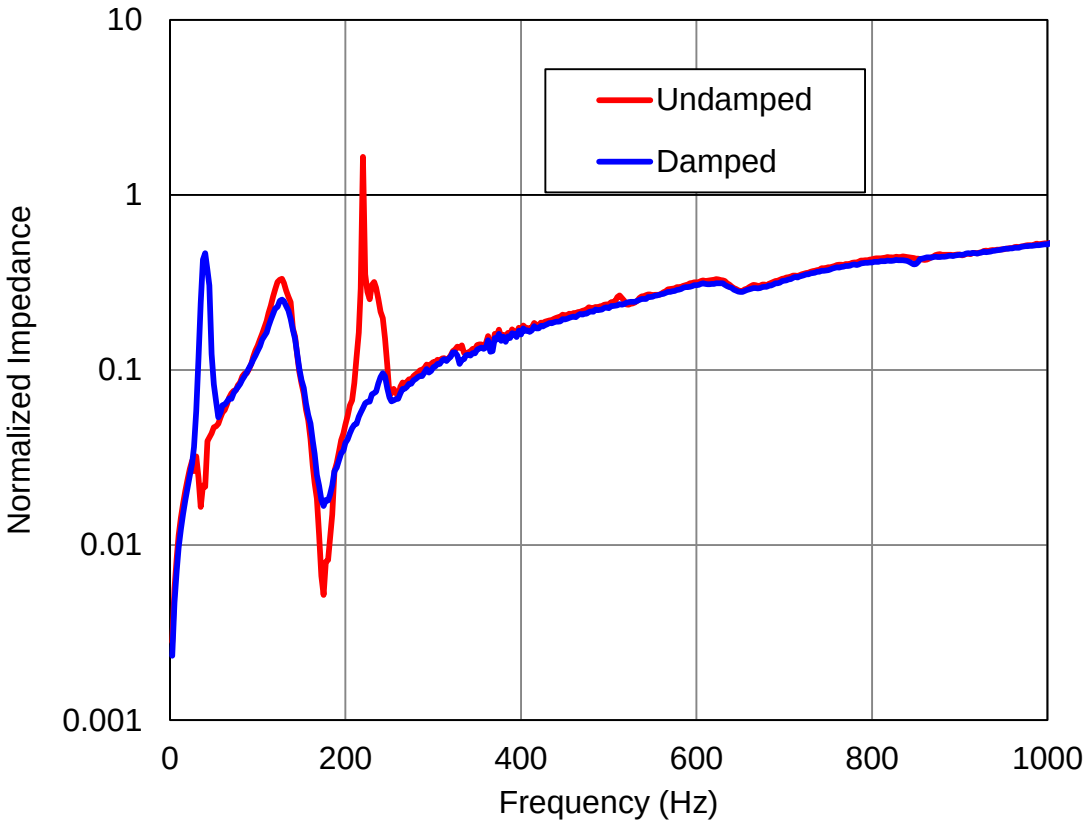

Figure 4.1 Measured downstream impedance for a combustion chamber with and without damping added to a panel.

After a prototype is in place, each panel can be tapped with a hammer. If a tap causes a panel to ring, it is probable that a combustion instability will occur at the ringing frequency.

Adding Absorption into the Combustion Chamber

Fiber absorption can be added to dampen the acoustic modes inside of the combustion chamber. Adding absorption or damping will decrease or increase the impedance at a resonance or anti-resonance respectively.

Adding absorption (fiber in most cases) can be effective in two ways. First, the acoustic losses will be much higher especially above 200 Hz if sound absorption is added to the combustion chamber. However, sound absorption is generally not effective at low frequencies.

For example, a schematic of a hypothetical combustion chamber and exhaust is shown in Figure 4.2 and key dimensions are provided in Table 4.2. The size and topology of the combustion chamber are similar to those examined in Section 3.3.6. Figure 4.3 shows the effect of adding 2 inch (5 cm) fiber on the downstream impedance (Z_D) of the combustion chamber. In the plot, the impedance (Z_D) is normalized by multiplying by $S/\rho c$ where S is the cross-sectional area, ρ is the mass density of the gas, and c is the speed of sound. These results were found using plane wave simulation [34, 28]. It can be seen that the downstream impedance is much lower at the resonances of the combustion chamber which will decrease the likelihood of an instability. Another benefit is that fiber can isolate a panel from the combustion chamber airspace preventing a structural resonance from leading to a combustion instability.

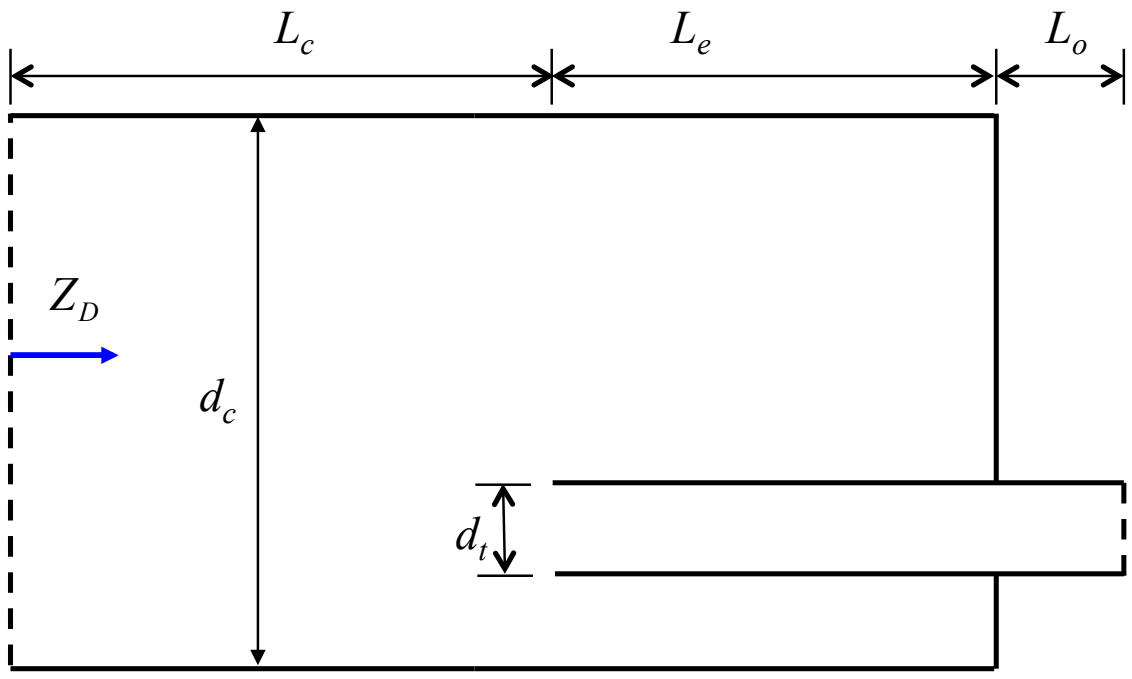

Figure 4.2 Hypothetical combustion chamber with exhaust pipe in lower part.

Table 4.2 Dimensions of hypothetical combustion chamber and exhaust.

Variables	cm	in	Description
L_c	100	39.4	Length of chamber
L_e	50	19.7	Length exhaust pipe in chamber
L_o	100	39.4	Length of outlet
d_c	60	23.6	Diameter of chamber
d_t	10	3.9	Diameter of exhaust

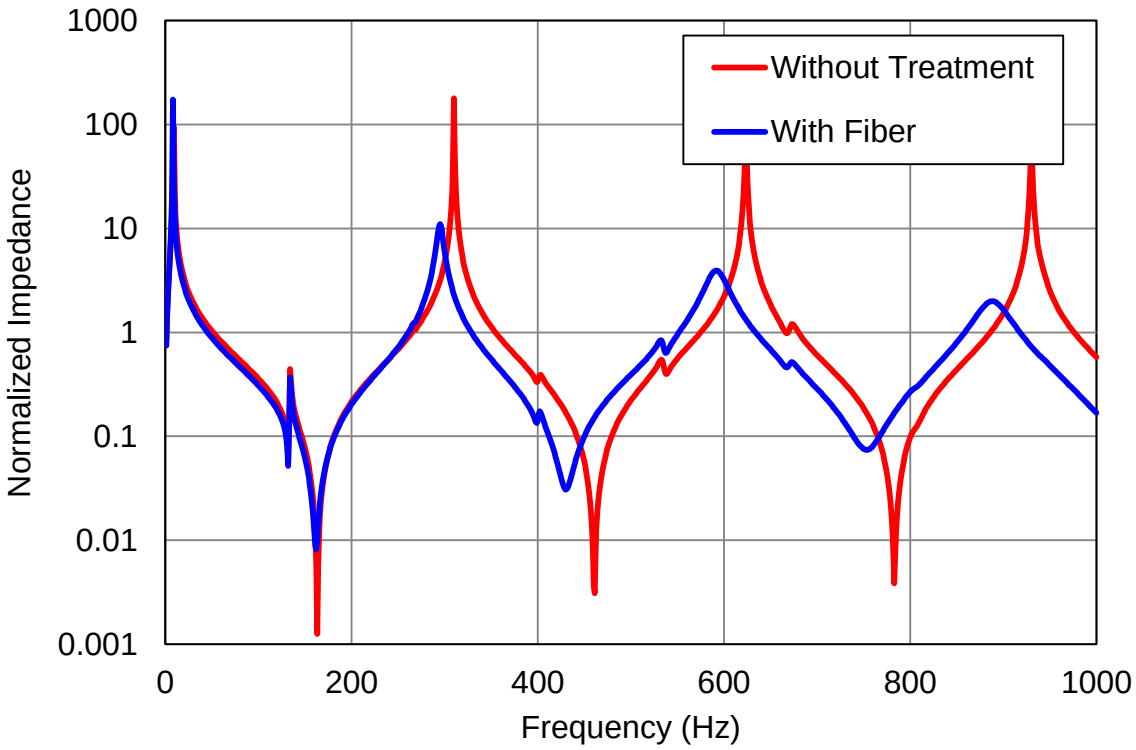

Figure 4.3 Normalized downstream impedance amplitude for the hypothetical combustion chamber

Increase the Upstream Impedance by Adding Damping

From equation (2.10) and (2.11), the magnitude of $Z \times H$ can be expressed as

$$|Z \times H| = \left|\frac{Z_D}{Z_D + Z_u}\right| \tag{4.1}$$

From Equation (4.1), it can be seen that combustion oscillations are more likely if the upstream impedance (Z_U) is (1) small or (2) is out of phase with the downstream impedance (Z_D). In the first case, the upstream impedance will be small if there is an anti-resonance in the inlet system. This can be avoided by adding absorption to the inlet system. Figure 4.4 shows a hypothetical inlet system with dimensions in Table 4.3. If a lined expansion chamber is added (Figure 4.4), the upstream impedance will change as shown in Figure 4.5. Notice that the nadirs of the impedance have all increased.

However, instabilities are also likely to occur if the downstream and upstream impedances are out of phase and equal in magnitude. In that case, the denominator in Equation (4.1) will approach zero. This possibility can be addressed easier after dimensions have been settled on in the next stage.

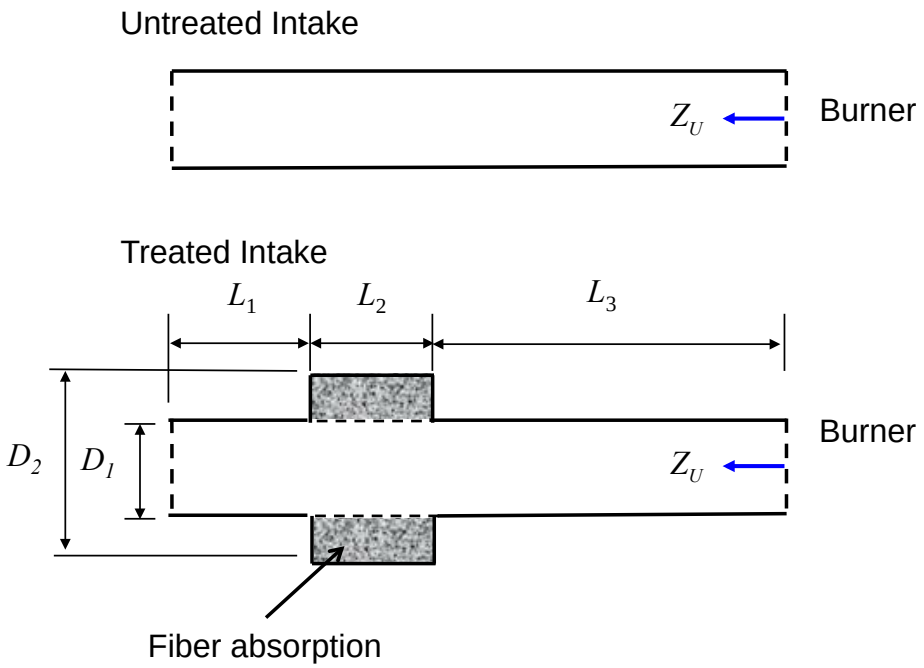

Figure 4.4 Schematic showing a hypothetical intake system with burner on the right. In the low figure, an expansion chamber with fiber lining is shown.

Table 4.3 Dimensions of hypothetical intake system.

Variables	cm	in	Description
L_1	20	7.9	Length from inlet to expansion chamber
L_2	30	11.8	Expansion chamber with fiber
L_3	100	39.4	Length from expansion chamber to burner
D_1	5	2.0	Diameter of the intake
D_2	10	3.9	Diameter of the chamber

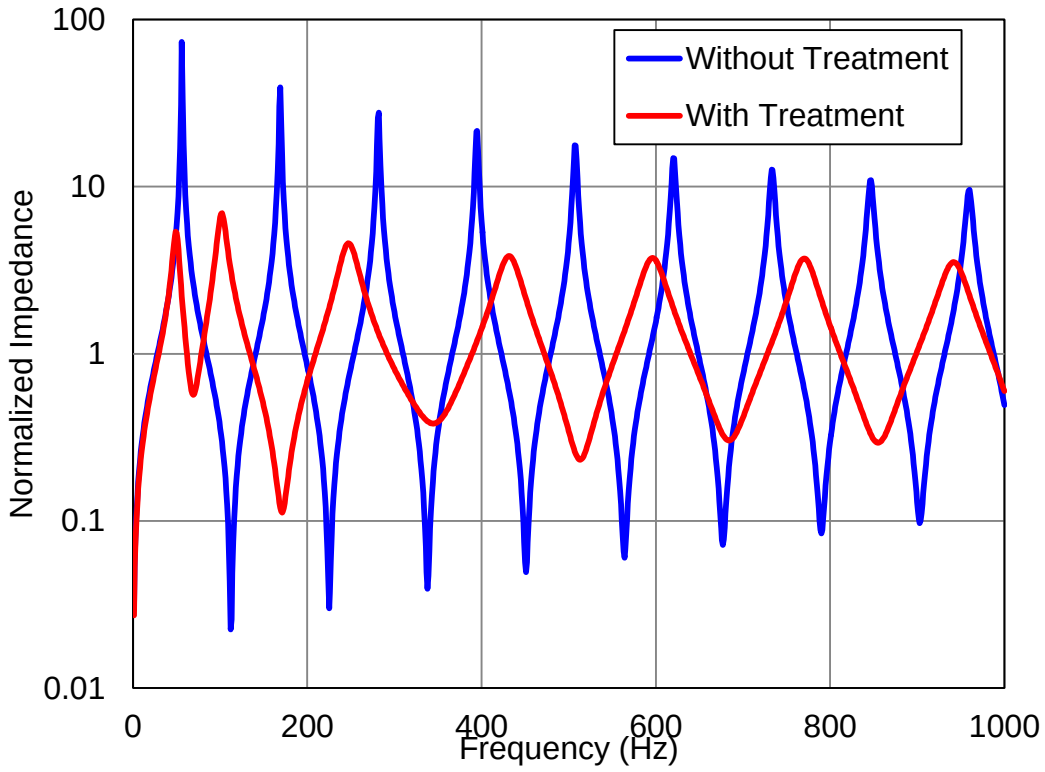

Figure 4.5 Normalized upstream impedance showing the effect of adding a lined expansion chamber.

4.2.3 Detailed Design

During the detailed design stage, the size and arrangement of the combustion chamber and intake system will be determined. With this information, the feedback loop stability model can be applied. The details for the model are presented in CHAPTER 2. Additionally, commercial software [44, 68, 69] is available for determining the upstream and downstream impedance. Commercial software is recommended because there are specialized elements for lined ducts and perforated elements.

Figure 4.6 and Figure 4.7 show results for the combustion chamber and intake system shown in Figure 4.2 and Figure 4.3 respectively. Published results are used for the flame transfer function [16]. If the magnitude of $Z \times H$ exceeds $1/G_f$ and the phases match, then a combustion oscillation may occur. With the model in place, potential instability frequencies can be identified a priori.

Figure 4.6 and Figure 4.7show the magnitude and phase plots, respectively, for the feedback loop stability model. Prior to treatments, the model suggests that combustion oscillations are likely at around 310 Hz. Moreover, the model indicates that an instability is on the threshold of occurring at 220 Hz. Treating the downstream, by adding fiber to the combustion chamber, will decrease the likelihood of an oscillation occurring at 310 Hz. However, it will have little benefit at 220 Hz. Adding the expansion chamber with fiber (Figure 4.4) will further minimize the possibility of a combustion oscillation.

It is best to reduce the possibility of problems before building a prototype as much as possible. However, a positive check does not necessarily mean that the problem will arise on the actual unit. Accordingly, it is not necessary to treat each potential problem at this juncture.

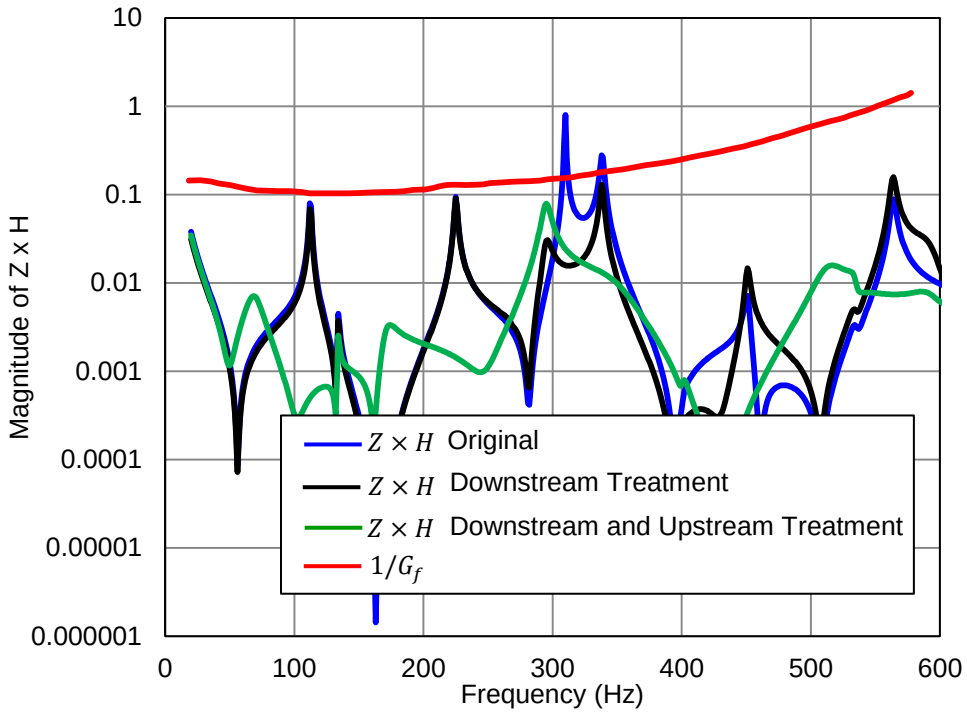

Figure 4.6 loop stability plot showing magnitude of $Z \times H$ and $1/G_f$.

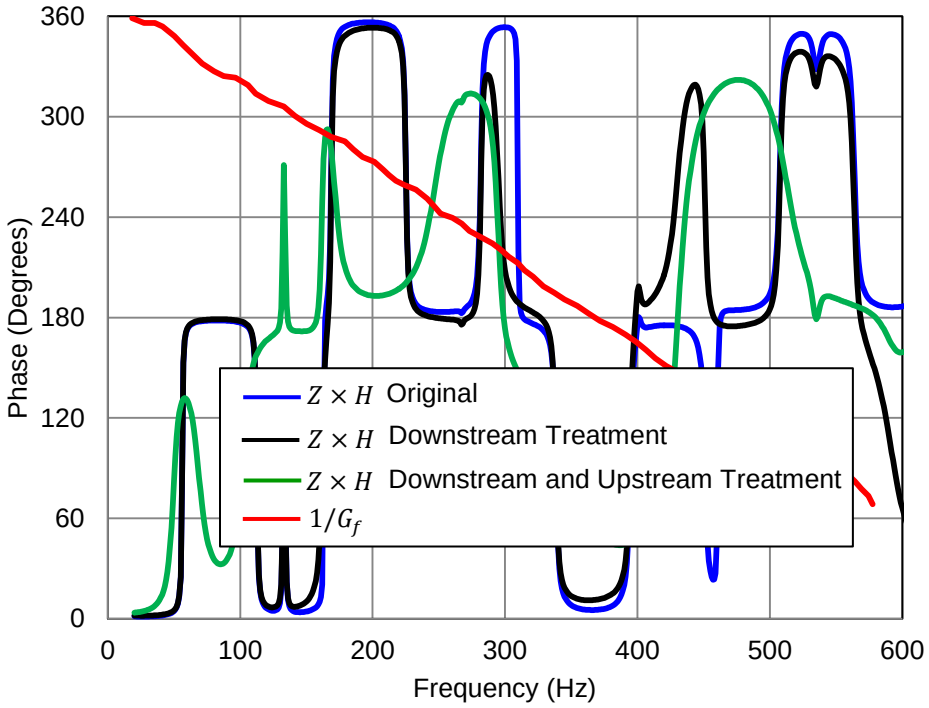

Figure 4.7 loop stability plot showing phase of $Z \times H$ and $1/G_f$.

4.2.4 Prototyping

After a prototype is in place, the boiler, furnace, or water heater should be evaluated at for a number of different intake and vent lengths. Additionally, the equipment should be tested for a number of different air fuel ratios and flow speeds. One way to change the flow rate while not adjusting the acoustics is to place masking tape over the intake or the exit. The tape is too thin and light to impact the acoustics appreciably, but the tape will restrict the flow.

Once testing is completed, the resulting combustion instabilities can be correlated with predictions from the detailed design stage (4.2.3). If instabilities correlate with frequencies from the model, the following different solution options can be considered.

1. There may be opportune locations to add absorption to either the combustion chamber or the intake system.

2. Baade and Tomarchio [16, 64] suggested stretching the flame. “The longer the flame, the longer it takes before the heat release of the flame responds to a change in the mixture flow through the burner ports. This time delay amounts to a phase shift between pressure and heat release.” They noted that this could be accomplished in two ways. The air fuel ratio can be changed or the burner port size can be increased.

3. Putnam [28] noted that drilling a hole in front of the combustion chamber will sometimes prevent oscillations. Indeed, this is one of the tricks that Baade and Tomachio [16, 64] suggested as well. Putnam, quoting the trade literature, recommended drilling a hole (or holes) in the in the combustion chamber just below the flame. Baade [64] showed that adding holes increases the frequency of the downstream resonances. Additionally, it slightly reduces the peak amplitude. This approach is likely to be more advantageous if an instability is on the threshold of occurring.

4. At high frequencies (above 500 Hz), simulation results showed that small changes to the burner geometry could drastically alter the upstream impedance [39]. Accordingly, changing the length from the base of the burner to the burner port surface can solve problems.

It is possible that a combustion oscillation will occur that the aforementioned feedback loop stability model did not predict. In that case, first verify that a structural resonance is not causing the problem. This can be accomplished by tapping panels with an impact hammer as noted earlier.

At low frequencies, equivalence ratio fluctuations can lead to instabilities as indicated in CHAPTER 2. Though this is less common, this problem can sometimes be solved by changing the gas valve or by moving the gas valve further away from the burner. In CHAPTER 2, a similar feedback loop stability model that can be used for diagnosing this particular mechanism is detailed.

4.3 Summary and Conclusions

To my knowledge, this is the first attempt to detail the prevention, diagnosis, and treatment of combustion oscillations throughout the design process. That being the case, it should be regarded as a starting point for further work. Moreover, it should be understood that combustion oscillations are sometimes difficult to solve. In some cases, there are connections between the upstream and downstream portions of the equipment. In that case, Baade's model is not directly applicable. Moreover, there are sometimes multiple paths for the intake air.

Additionally, the presence of an intake fan is difficult to model. It is also possible that a flow instability leading to an aero-acoustic source could be the primary cause in some situations. Accordingly, it is probable that the recommendations presented herein will need to be revised and expanded on in the coming years.

CHAPTER 5 ANALYTICAL AND BEM SOLUTIONS OF BAR SILENCERS

5.1 Introduction

A silencer is a device used in a flow duct to prevent sound from reaching the openings of the duct and radiating as far-field noise [70]. Silencers are necessary devices to attenuate noise in the intake or exhaust system of internal combustion engines, compressors and pumps as well as heating, ventilation and air-conditioning systems (HVAC) [70, 28]. Basically, there are two types: reactive and dissipative. Reactive silencers take advantage of sound reflections due to acoustic impedance mismatch. Mismatches occur at sudden geometry changes (area expansion, contraction and abrupt openings). Dissipative silencers attenuate sound using sound absorbing materials and convert the sound energy into heat. Common reactive acoustic elements include Helmholtz resonators, quarter-wave tube side branches and simple expansion chambers. In dissipative silencers, sound absorbing materials such as foams, fibrous materials, and recently, micro-perforated panels or micro-slit panels are used [51, 71, 72]. Reactive silencers are used to attenuate sound at discrete tones, especially at low-frequencies where dissipative silencers are designed to mitigate high-frequency broadband noise [73].

Dissipative silencers, or absorptive silencers, have the advantages of broadband sound attenuation in many applications such as locomotive or automotive exhaust systems. There are a number of different designs and types of dissipative silencers. One common type is the lined-duct where sound absorbing material is placed around the duct circumference. Another prevailing type is a splitter design where the sound absorbing material is placed centrally and is in the longitudinal direction of the duct. For instance, parallel-baffle silencers are a commonly used splitter design. The sound attenuation of such a silencer is proportional to the perimeter-to-area ratio and length [43]. There have been a number of analytical, numerical and experimental studies on lined-ducts and splitter silencers [74, 75, 76, 77, 78, 79].

In 1983, Nilsson and Söderqvist proposed the idea of bar silencers and claimed that an array of square bars made of sound absorbing materials have certain advantages over the similar splitter configurations [29]. Bar silencers are comprised of an array of rectangular or round bars made of sound absorbing materials packed in a rectangular lattice arrangement within a rigid-walled duct. To protect the material from being blown away by the exhaust gas, each bar is covered by a perforated facing sheet. Bar silencers are used in a noise suppression test cell built by Hedemora Industriakustic for the testing gas turbines [80].

5.2 Metrics for Sound Attenuation

The most commonly used metrics for evaluating the sound attenuation of silencers are insertion loss (*IL*), transmission loss (*TL*) and noise reduction (*NR*) [70, 73, 28, 43]. *IL* is the decrease in sound pressure or sound intensity in dB when an attenuating element is inserted into the path between source and receiver. *TL* is the difference in sound power level in dB between incident and transmitted power. *NR* is the difference in sound pressure level in dB measured upstream and downstream of a sound-attenuating element. The standard procedures for transmission loss or insertion loss measurement have been established [61, 81, 82]. In this work, *TL* is used as the metric. Tao and Seybert [83] presented a good review on the techniques for measuring silencer transmission loss including the two-load method [59] and the two-source method [60].

5.3 Determination of *TL* using numerical simulation

Numerical models have been widely employed to investigate the acoustic performance of silencers. Astley and Cummings [74], Cummings and Astley [84] and Herrin et al. [85] applied the finite element method (FEM) to study lined silencers such as bar silencers. Wu and his co-workers [86, 87, 88, 89] developed a direct-mixed body boundary element method (BEM) to study various reactive and packed silencers. Glav and Åbom [90], and Mimani and Munjal [91] analyzed silencer systems using transfer matrix theory. Selamet et al. [75] used a

pressure and velocity matching technique to compute the transmission loss of a perforated dissipative silencer.

Cummings and Astley [84] proposed a finite element formulation to evaluate the acoustic performance of square bar silencers. They used an isolated single module in their model, assuming the axial attenuation is the same within each cell of such an array and therefore the acoustic performance of the silencer as a whole can be deduced from the attenuation in a single module [84]. They compared the prediction to the measurement with generally reasonable agreement.

The direct-mixed body boundary element method (BEM) proposed by Wu and his co-workers [35, 87, 88] is another candidate numerical method for bar silencers. It is well known that BEM has an advantage over FEM since only the boundary surface must be modeled.

Unlike the traditional BEM, which is limited to a single homogeneous medium, the direct mixed-body BEM can handle multiple bulk-reacting materials along with a baseline medium, i.e. air. All this can be accomplished in a single BEM model without having to resort to the tedious multi-domain approach. In addition, the substructuring technique [88] is ideally suited to bar silencer analysis because the cross-sectional geometry does not change along the length of a bar silencer, and the impedance matrix of a small substructure cut from the middle section can be repeatedly used in the BEM analysis. This allows the BEM to be applied to a bar silencer with little computational cost for additional length.

5.4 Single Cell Module Analysis

Due to the large dimensions, it is not always possible to obtain the transmission loss data experimentally for bar silencers. Alternatively, an analytical solution can be utilized to serve as a validation tool for numerical solutions. Cummings and Astley noted that an analytical solution for square bar silencers is difficult to obtain [84]. Instead, a simplified circular geometry is used to derive the analytical solution for simplicity. The simplified geometry involves a round bar housed inside a rigid cylindrical chamber so that axisymmetric cylindrical coordinates can

be used. Selamet et al. [75] used a similar analytical technique for lined ducts. The sound pressure and particle velocity are explicitly expressed by modal expansion, which can then be used to compute the transmission loss (*TL*) by applying a pressure and velocity matching technique [75, 78]. Although a rigid cylindrical chamber with a cylindrical bar inside is not representative of real-world lattices, the analytical solution can serve as a comparison tool to validate a numerical method.

In addition, it is computationally intensive and time-consuming to model the entire array numerically. To simplify the problem, a small representative cell module is isolated from the lattice for analysis purposes. If a uniform acoustic field across the inlet plane is assumed, the axial attenuation is then the same within each cell and therefore the acoustic performance of the bar silencer can be deduced from the attenuation in a single module [84]. As a result, there should be no appreciable difference between any two cells. This assumption applies to both the analytical and the numerical models.

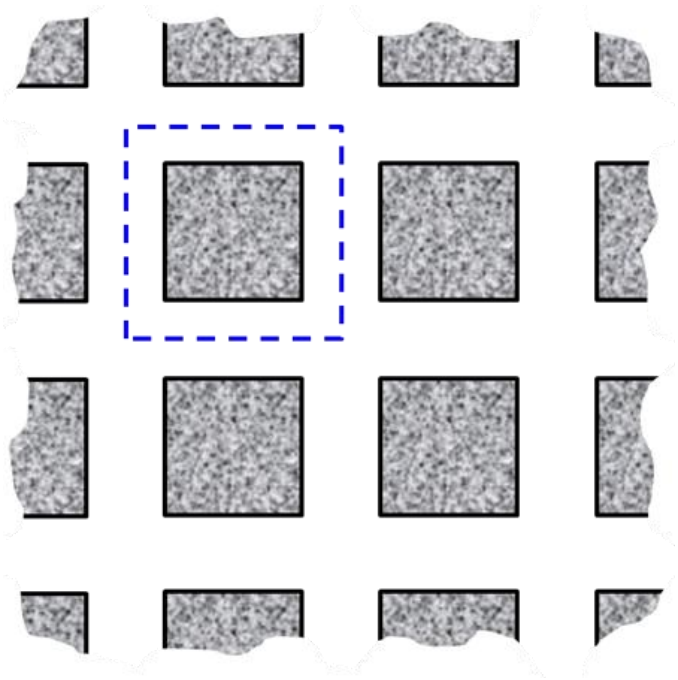

Figure 5.1 An array of square bars; dotted lines enclose a representative cell.

Symmetry is selected so that cell modules can be viewed as a building block for the entire lattice. The rigid-wall boundary condition is then applied to the boundary of the cell module. For the square-bar silencer array shown in Figure 5.1, the smallest building block is a rectangular duct with a single bar inside, as shown in Figure 5.2. The dotted lines in Figure 5.2 represent the rigid wall boundary of the isolated module. For round bars, depending on how the round bars are arranged, the smallest building block could be isolated in different ways, as demonstrated by the dotted lines in Figure 5.3 and Figure 5.4.

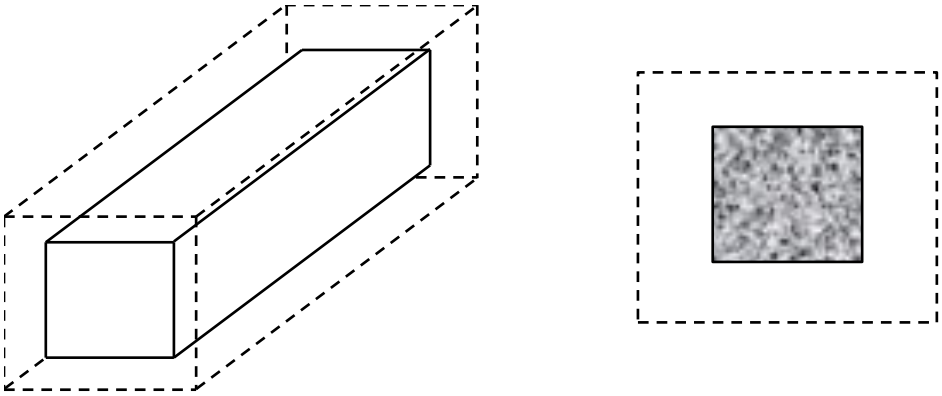

Figure 5.2 An isolated cell module for analysis.

Normally, the sound absorbing material is covered by a perforated facing sheet to protect the material from being blown away by the exhaust gas. Both ends of the bar are covered by a rigid end cap. For modeling purposes, it is assumed that the two end caps are flat and the poles that hold the bar silencers together are ignored. Figure 5.5 shows the side view of an isolated cell module with a round bar inside. The cell module is divided into three different sections along its length: domain A is the inlet duct, domain B is the main duct with an absorbing bar at the center, and domain C is the outlet duct.

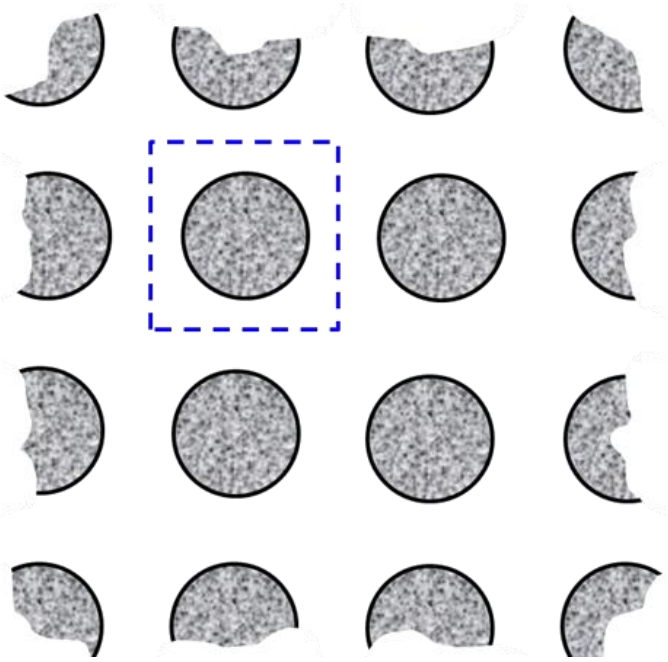

Figure 5.3 One possible arrangement of round bars; dotted lines enclose a representative cell.

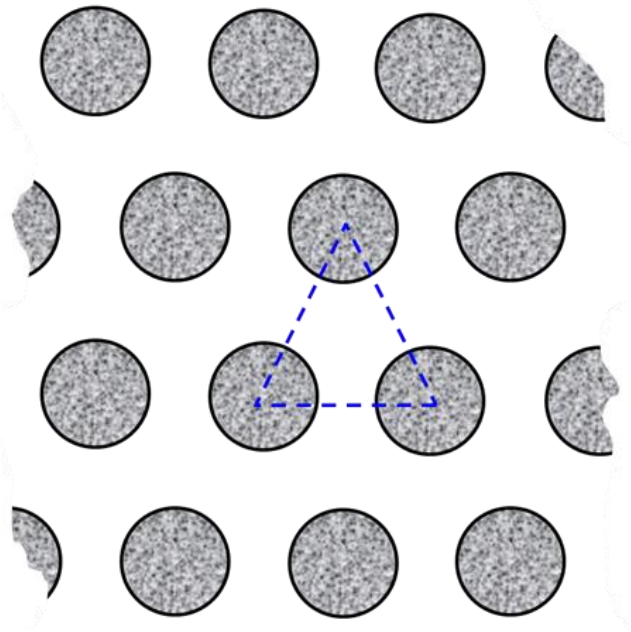

Figure 5.4 Another possible arrangement of round bars; dotted lines enclose a representative cell.

Even for a single cell module, the cross sectional area of the inlet and outlet could still be quite large and the plane wave cut-off frequency will be exceeded in the analysis. The *TL* computation and even the *TL* definition itself above the cut-off frequency are not well established yet. Consequently, two different approaches are used to compute the *TL*, one for the BEM and the other for the analytical solution. In the BEM, the *TL* is still computed from the traditional four-pole parameters as usual. However, the four-pole matrix is defined as the matrix that relates the "averaged sound fields" at the inlet to the "averaged sound fields" at the outlet. Thus, a simple average is taken to average out the sound fields at the inlet and at the outlet, respectively, so that the conventional four-pole matrix can still be defined above the cut-off frequency.

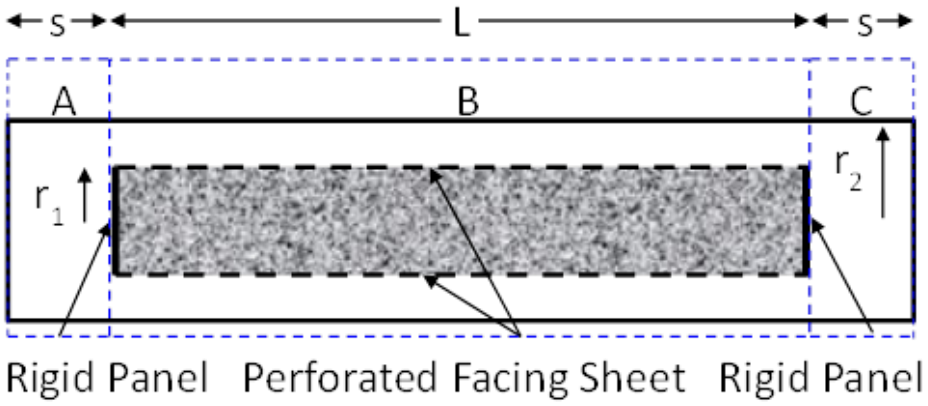

Figure 5.5 Side view of an isolated round bar.

5.5 BEM Solution of A Square Bar Silencer

As mentioned earlier, the analytical solution for a square bar silencer is challenging. In this work, the BEM is compared to an existing test case described by Cummings and Astley [84]. The test case is a 0.4m×0.4m×2m rectangular bar inside a 0.6m×0.6m rigid duct. The bar is made of an anisotropic sound absorbing material with a flow resistivity 19,600 Rayl/m parallel to the direction of the fiber and 31,500 Rayl/m normal to the fiber direction. Unfortunately, the BEM approach used can only deal with isotropic materials, so only the longitudinal flow resistivity 19,600 Rayl/m is used in the model. The bar

is covered by a perforated facing sheet with 33% porosity. In the direct mixed-body BEM, the perforated facing sheet is modeled by a special element type called “IP”, which represents a perforated interface between air and a bulk-reacting material. The two end caps are modeled by another special element type called “ATB”, which represents an air-thin plate-bulk material interface.

Figure 5.6 compares the BEM result to that of Cumming and Astley [84]. The BEM result compares fairly well to the FEM and experimental results even though the BEM only uses the longitudinal flow resistivity in all directions. The BEM calculation is performed using MAP [92], an in-house BEM program developed at University of Kentucky.

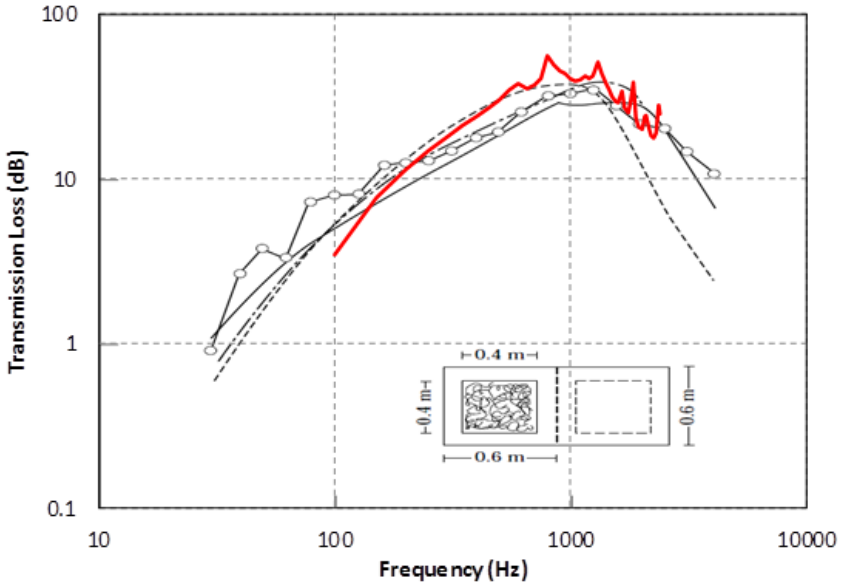

Figure 5.6 Comparison of *TL* results on one Cummings and Astley’s test case; solid read - BEM result; solid black – FEM result; circles – measured data; the other two are FEM results from an equivalent lined duct and an equivalent splitter silencer, respectively.

5.6 Analytical Solution of a Simplified Round Bar Silencer

An analytical solution on a simplified geometry was used to validate the numerical method, which can be used for more complex geometries. It is difficult to develop analytical solutions for the square bar (Figure 5.1) and round bar

configurations (Figure 5.3 or Figure 5.4). Accordingly, the hypothetical and simplified round bar silencer as shown in Figure 5.7 was used for the purpose of deriving an analytical solution as a validation tool for numerical solutions. The simplified geometry in Figure 5.7 cannot be used as a building block for any real-world design, but it will simplify the analysis since axisymmetric cylindrical coordinates can be used.

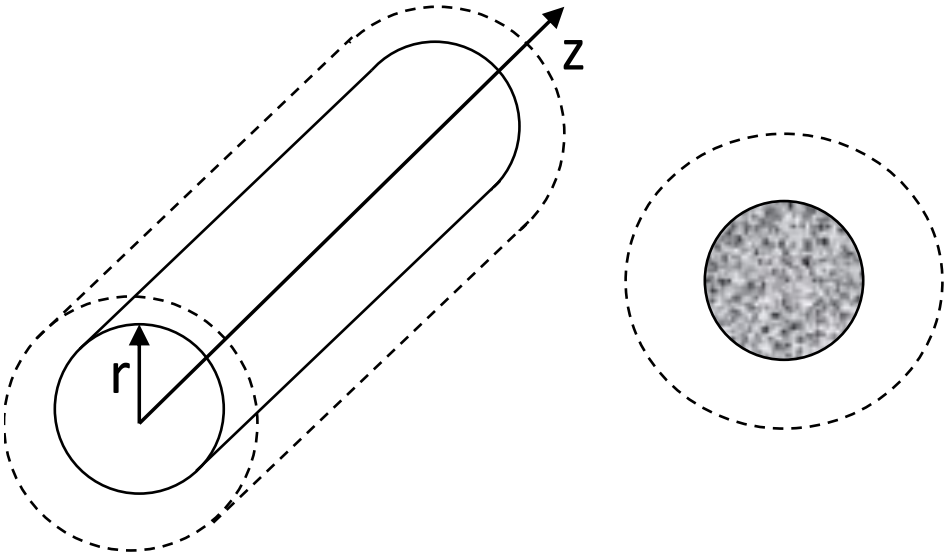

Figure 5.7 A hypothetical round bar silencer.

5.6.1 Helmholtz Equation in Cylindrical Coordinates

The Helmholtz equation in general form can be expressed as

$$\nabla^2 p + k^2 p = 0 \tag{5.1}$$

In the cylindrical coordinate system (r, ϕ, z), the Laplacian operator becomes

$$\nabla^2 = \frac{\partial^2}{\partial r^2} + \frac{1}{r}\frac{\partial}{\partial r} + \frac{1}{r^2}\frac{\partial^2}{\partial \phi^2} + \frac{\partial^2}{\partial z^2} \tag{5.2}$$

If axisymmetry is assumed, then the Laplacian operator is independent of angle (ϕ) and becomes

$$\nabla^2 = \frac{\partial^2}{\partial r^2} + \frac{1}{r}\frac{\partial}{\partial r} + \frac{\partial^2}{\partial z^2} \tag{5.3}$$

In order to obtain the solution to the Helmholtz equation in cylindrical coordinate, the technique of separation of variables can be employed to simplify the problem. Using separation of variables method, the solution can be written as a product of functions of r and z and expressed as

$$p(r,z) = f(r)g(z) \tag{5.4}$$

Substituting the previous expression into Helmholtz equation, one obtains

$$\frac{\partial^2 f}{\partial r^2}\frac{1}{f} + \frac{1}{r}\frac{\partial f}{\partial r}\frac{1}{f} + \frac{\partial^2 g}{\partial z^2}\frac{1}{g} + k^2 = 0 \tag{5.5}$$

Let

$$\frac{\partial^2 f}{\partial r^2}\frac{1}{f} + \frac{1}{r}\frac{\partial f}{\partial r}\frac{1}{f} = -k_r^2 \tag{5.6}$$

and

$$\frac{\partial^2 g}{\partial z^2}\frac{1}{g} = -k_z^2 \tag{5.7}$$

The solution to Equation (5.6) is

$$f(r) = E_1 J_0(k_r r) + E_2 Y_0(k_r r) \tag{5.8}$$

where E_1 and E_2 are amplitude coefficients, J_0 the Bessel function of the first kind of order zero and Y_0 the Bessel function of the second kind of order zero, k_r is the radial wavenumber.

The solution to Equation (5.7) is

$$g(z) = F_1 e^{-ik_z z} + F_2 e^{+ik_z z} \tag{5.9}$$

where F_1 and F_2 are amplitude coefficients, k_z is the longitudinal wavenumber.

Therefore, the general solution to Helmholtz equation in cylindrical coordinates is

$$p(r,z) = \sum_{n=0}^{\infty} (E_{1n} J_0(k_{rn} r) + E_{2n} Y_0(k_{rn} r)) \left(F_{1n} e^{-ik_{zn} z} + F_{2n} e^{+ik_{zn} z}\right) \quad (5.10)$$

where subscript n denotes the mode number.

5.6.2 Modal Expansion

The analytical solution is based on the same approach used for packed silencers in References [75, 78]. The primary difference is that the positions of air and the bulk-reacting material are switched. Instead of packing the bulk-reacting material on the chamber wall, the absorption is positioned at the center. The side view of the round bar silencer is shown in Figure 5.5.

The solution to the Helmholtz equation for each domain is obtained by modal expansion. In domain A (the inlet duct), the sound pressure is

$$p_A(r,z) = \sum_{n=0}^{\infty} \left(A_n^+ e^{-ik_{Azn} z} + A_n^- e^{+ik_{Azn} z}\right) \psi_{An}(r) \quad (5.11)$$

where the subscripts A, z and n denote domain A, axial direction and mode number, respectively. A_n^+ and A_n^- are the modal amplitudes of the right-travelling and reflecting waves respectively. k_{Azn} are the axial wavenumbers. $\psi_{An}(r)$ are the eigenfunctions of the inlet duct defined as

$$\psi_{An}(r) = J_0(k_{Arn} r) \quad (5.12)$$

where k_{Arn} is the radial wavenumber and can be obtained by applying the rigid-wall boundary condition of

$$J_0'(k_{Arn} r) = 0 \quad (5.13)$$

The n^{th} axial wavenumber is

$$k_{Azn} = \begin{cases} \sqrt{k^2 - k_{Arn}^2}, & k \geq k_{Arn} \\ -i\sqrt{k_{Arn}^2 - k^2}, & k < k_{Arn} \end{cases} \tag{5.14}$$

where $k = 2\pi f/c$ is the wavenumber in air, f the frequency and c the speed of sound.

Euler's equation relates the sound pressure to the particle velocity and can be expressed as

$$u_{Az}(r,z) = \frac{i}{\rho\omega}\frac{\partial p}{\partial z} \tag{5.15}$$

Based upon Euler's equation, the axial particle velocity in domain A is

$$u_{Az}(r,z) = \frac{1}{\rho\omega}\sum_{n=0}^{\infty} k_{Azn}\left(A_n^+ e^{-ik_{Azn}z} - A_n^- e^{+ik_{Azn}z}\right)\psi_{An}(r) \tag{5.16}$$

where ρ is the air density and ω is the angular frequency.

In domain B where there are two media, the wavenumbers in the axial direction of both media (the sound absorbing material and air) are assumed to be identical. The axial wavenumbers can be solved by an iterative scheme (Section 5.6.3). The radial wavenumbers in both media are related to the wavenumbers k (for air) and k' (for the sound absorbing material), and the axial wavenumbers k_{Bzn} by

$$k_{Brn}^2 + k_{Bzn}^2 = k^2 \tag{5.17}$$

$$k_{Brn}^{'2} + k_{Bzn}^2 = k^{'2} \tag{5.18}$$

The sound pressure for each medium in domain B is

$$p_B(r,z) = \sum_{n=0}^{\infty}\left(B_n^+ e^{-ik_{Bzn}z} + B_n^- e^{+ik_{Bzn}z}\right)\psi_{Bnp}(r) \tag{5.19}$$

where the subscript B denotes domain B. B_n^+ and B_n^- are modal amplitudes of the right-travelling and reflecting waves, respectively. k_{Bzn} are the axial wavenumbers. $\psi_{Bnp}(r)$ are the eigenfunctions in the radial direction. Since there are two media, the sound pressure can be written in different regions

$$p_B(r,z) = \begin{cases} p_B^f(r,z), & r \le r_1 \\ p_B^a(r,z), & r_1 < r \le r_2 \end{cases} \tag{5.20}$$

with the eigenfunction

$$\psi_{Bnp}(r) = \begin{cases} \psi_{Bnp}^f(r), & r \le r_1 \\ \psi_{Bnp}^a(r), & r_1 < r \le r_2 \end{cases} \tag{5.21}$$

where superscripts f and a denote the sound absorbing material and surrounding airway, respectively.

From the general solution to the Helmholtz equation in cylindrical coordinates, the eigenfunction

$$\psi_{Bnp}(r) = \begin{cases} \psi_{Bnp}^f(r) = C_1 J_0\left(k_{Brn}^{'} r\right) + C_2 Y_0(k_{Brn}^{'} r), & r \le r_1 \\ \psi_{Bnp}^a(r) = C_3 J_0(k_{Brn} r) + C_4 Y_0(k_{Brn} r), & r_1 < r \le r_2 \end{cases} \tag{5.22}$$

can be obtained.

In order to express the eigenfunction, in a more concise form, four boundary conditions are used:

(1) At $r = 0$ the sound pressure must be finite which excludes Y_0 in ψ_{Bnp}^f

$$C_2 = 0 \tag{5.23}$$

(2) At $r = r_2$ the particle velocity is zero due to the rigid wall boundary condition

$$u_{Br}(r_2) = 0 \tag{5.24}$$

(3) At $r = r_1$ the particle velocity is continuous

$$u_{Br}^{f}(r_1) = u_{Br}^{a}(r_1) \tag{5.25}$$

(4)The transfer impedance of the perforated facing sheet is defined at $r = r_1$

$$p_{Bnp}^{a}(r_1) - p_{Bnp}^{f}(r_1) = \rho c \xi u_{Br}^{a}(r_1) \tag{5.26}$$

By assuming $C_1 = 1$ and solving the aforementioned four boundary conditions, the eigenfunction can be written as

$$\psi_{Bnp}(r) = \begin{cases} D\left[J_0(k_{Brn}r) - \dfrac{J_1(k'_{Brn}r_2)}{Y_1(k'_{Brn}r_2)}Y_0(k_{Brn}r)\right], & r_1 \le r \le r_2 \\ J_0(k'_{Brn}r), & r \le r_1 \end{cases} \tag{5.27}$$

with

$$D = \left[J_1(k'_{Brn}r_1) + \frac{i\xi\rho k'_{Brn}}{\rho' k}J_1(k'_{Brn}r_2)\right]\frac{Y_1(k_{Brn}r_2)}{J_0(k_{Brn}r_1)Y_1(k_{Brn}r_2) - J_1(k_{Brn}r_2)Y_0(k_{Brn}r_1)} \tag{5.28}$$

where ρ' is the complex density of the sound absorbing material and can be calculated by an empirical formula. ξ is the normalized transfer impedance of the perforated facing sheet. A simple empirical formula [93] for transfer impedance of a perforate is used and is expressed as

$$\xi = (6.0 \times 10^{-3} + i4.8 \times 10^{-5} f)/\sigma \tag{5.29}$$

where f is frequency and σ is the porosity.

The characteristic impedance Z' and complex wavenumber k' of the fibrous material, from which the complex density ρ' and speed of sound c' can be derived, can be determined by the empirical model proposed by Delany and Bazley [94] and are expressed as

$$Z' = Z_0(1 + 0.0571X^{-0.754} - j0.087X^{-0.732}) \tag{5.30}$$

$$k' = k_0(1 + 0.0978X^{-0.7} - j0.0189X^{-0.595}) \tag{5.31}$$

where X denotes a dimensionless parameter in terms of density of air ρ, frequency f and the flow resistivity of the material R.

$$X = \frac{\rho f}{R} \tag{5.32}$$

Z_0 is the characteristic impedance of air and k_0 the wavenumber in the air.

The axial particle velocity for each medium in domain B is

$$u_{Bz}(r,z) = \frac{1}{\rho\omega}\sum_{n=0}^{\infty} k_{Bzn}\left(B_n^+ e^{-ik_{Bzn}z} - B_n^- e^{+ik_{Bzn}z}\right)\psi_{Bnu}(r) \tag{5.33}$$

where the radial modal eigenfunctions of the velocity are

$$\psi_{Bnu}(r) = \begin{cases} D\left[J_0(k_{Brn}r) - \dfrac{J_1(k'_{Brn}r_2)}{Y_1(k'_{Brn}r_2)}Y_0(k_{Brn}r)\right], & r_1 \le r \le r_2 \\ \dfrac{\rho}{\rho'}J_0(k'_{Brn}r), & r \le r_1 \end{cases} \tag{5.34}$$

Moreover, the characteristic equation, which will be used to calculate the longitudinal wavenumber (k_{Bzn}) in Section 5.6.3, is

$$\begin{aligned} &\frac{\rho' k_{Brn}}{\rho k'_{Brn}}\left(\frac{J_0(k'_{Brn}r_1)}{J_1(k'_{Brn}r_1)} + \frac{i\xi\rho k'_{Brn}J_1(k'_{Brn}r_1)}{\rho' k_0}\right) \\ &= \frac{J_0(k_{Brn}r_1)Y_1(k_{Brn}r_2) - Y_0(k_{Brn}r_1)J_1(k_{Brn}r_2)}{J_1(k_{Brn}r_1)Y_1(k_{Brn}r_2) - Y_1(k_{Brn}r_1)J_1(k_{Brn}r_2)} \end{aligned} \tag{5.35}$$

The sound pressure in domain C is

$$p_C(r,z) = \sum_{n=0}^{\infty}\left(C_n^+ e^{-ik_{Czn}(z-L)} + C_n^- e^{+ik_{Czn}(z-L)}\right)\psi_{Cn}(r) \tag{5.36}$$

where the subscript C indicates domain C, C_n^+ and C_n^- are modal amplitudes of the right-travelling and reflecting waves respectively. k_{Czn} are the axial wavenumbers. $\psi_{Cn}(r)$ are the eigenfunctions of domain C and can be written as

$$\psi_{Cn}(r) = J_0(k_{Crn}r) \tag{5.37}$$

The axial particle velocity in domain C is

$$u_{Cz}(r,z) = \frac{1}{\rho\omega}\sum_{n=0}^{\infty} k_{Czn}\left(C_n^+ e^{-ik_{Czn}(z-L)} - C_n^- e^{+ik_{Czn}(z-L)}\right)\psi_{Cn}(r) \tag{5.38}$$

5.6.3 Iterative Scheme for Solving k_{Bzn}

Rearranging the characteristic equation (5.35), the axial wavenumber (k_{Bzn}) in domain B can be obtained by iteratively solving the equation

$$F(\xi, R, f, k_{Bzn}) = F_1 - F_2 = 0 \tag{5.39}$$

where

$$F_1 = \rho' k_{Brn}\left(J_1(k_{Brn}r_1)Y_1(k_{Brn}r_2) - Y_1(k_{Brn}r_1)J_1(k_{Brn}r_2)\right) \left(k_0 J_0(k'_{Brn}r_1) + \frac{i\rho\xi k'_{Brn}J_1(k'_{Brn}r_1)}{\rho'}\right) \tag{5.40}$$

$$F_2 = \rho k'_{Brn}k_0 J_1(k_{Brn}r_1)\left(J_0(k_{Brn}r_1)Y_1(k_{Brn}r_2) - Y_0(k_{Brn}r_1)J_1(k_{Brn}r_2)\right) \tag{5.41}$$

Since the derivative of $F\left(\xi, R, f, k_{Bzn}\right)$ is not readily obtained, the secant method [95], replacing the derivative evaluation in Newton's method with a finite difference approximation based on the two most recent iterates, is better suited. The solutions of the root of Equation (5.39) provided an initial guess for $k_{Bzn,0}$ and the loop

$$k_{Bzn,i+1} = k_{Bzn,i} - \frac{F\left(\xi, R, f, k_{Bzn,i}\right)}{s_i} \tag{5.42}$$

is used, where $i = 1,2,\ldots,N$. s_i is the secant defined as

$$s_i = \frac{F\left(\xi, R, f, k_{Bzn,i}\right) - F\left(\xi, R, f, k_{Bzn,i-1}\right)}{k_{Bzn,i} - k_{Bzn,i-1}} \tag{5.43}$$

The loop will be terminated as the difference between the most recent iterates approaches a designated small number.

Selamet et al. [75] pointed out that the selection of a suitable initial estimate for the desired axial wavenumber $k_{Bzn,0}$ is critical in this approach. Following Selamet et al. [75], the axial wavenumber k_{Bzn} is calculated using the secant method.

5.6.4 Pressure and Velocity Continuity Conditions

The pressure and velocity are continuous in the annular part (air pathway) at the interface between domains A and B, and at the interface between domains B and C as well. At the two rigid end caps, sound pressure will not be continuous but the particle velocity will be zero. These interface conditions are summarized as follows:

$$\begin{cases} u_A = 0, & r \le r_1 \;\; z = 0 \\ P_A = P_B, & r_1 \le r \le r_2 \;\; z = 0 \end{cases} \tag{5.44}$$

$$u_B = \begin{cases} 0, & r \le r_1 \;\; z = 0 \\ u_A, & r_1 \le r \le r_2 \;\; z = 0 \end{cases} \tag{5.45}$$

$$\begin{cases} u_C = 0, & r \le r_1 \;\; z = L \\ P_B = P_C, & r_1 \le r \le r_2 \;\; z = L \end{cases} \tag{5.46}$$

$$u_B = \begin{cases} 0, & r \le r_1 \;\; z = L \\ u_C, & r_1 \le r \le r_2 \;\; z = L \end{cases} \tag{5.47}$$

Expressing the above interface conditions in the modal expansion leads to

$$\begin{cases} \sum_{n=0}^{\infty} k_{Azn}(A_n^+ - A_n^-)\psi_{An}(r) = 0, & r \le r_1 \;\; z = 0 \\ \sum_{n=0}^{\infty}(A_n^+ + A_n^-)\psi_{An}(r) = \sum_{n=0}^{\infty}(B_n^+ + B_n^-)\psi_{Bnp}^a(r), & r_1 \le r \le r_2 \;\; z = 0 \end{cases} \tag{5.48}$$

$$\sum_{n=0}^{\infty} k_{Bzn}(B_n^+ - B_n^-)\psi_{Bnu}(r) = \begin{cases} 0, & r \le r_1 \;\; z = 0 \\ \sum_{n=0}^{\infty} k_{Azn}(A_n^+ - A_n^-)\psi_{An}(r), & r_1 \le r \le r_2 \;\; z = 0 \end{cases} \tag{5.49}$$

$$\begin{cases} \sum_{n=0}^{\infty} k_{Czn}(C_n^+ - C_n^-)\psi_{Cn}(r) = 0, \qquad r \le r_1 \;\; z = L \\ \sum_{n=0}^{\infty}(B_n^+ e^{-ik_{Bzn}L} + B_n^- e^{+ik_{Bzn}L})\psi_{Bnp}^a(r) = \sum_{n=0}^{\infty}(C_n^+ + C_n^-)\psi_{Cn}(r), \qquad r_1 \le r \le r_2 \;\; z = L \end{cases} \tag{5.50}$$

$$\sum_{n=0}^{\infty} k_{Bzn}\left(B_n^+ e^{-ik_{Bzn}L} - B_n^- e^{+ik_{Bzn}L}\right)\psi_{Bnu}(r) = \begin{cases} 0, \qquad r \le r_1 \;\; z = L \\ \sum_{n=0}^{\infty} k_{Czn}(C_n^+ - C_n^-)\psi_{Cn}(r), \qquad r_1 \le r \le r_2 \;\; z = L \end{cases} \tag{5.51}$$

5.6.5 Transmission Loss

Below the plane wave cut-off frequency, only plane wave modes propagate through the silencer. The conventional definition of the *TL* is the difference between the incident and transmitted sound power embedded in the plane wave mode. However, once the frequency exceeds the plane wave cut-off frequency, the higher order modes [96] start propagating as well so that the power conveyed by these higher order modes must be taken into account when evaluating *TL*. The *TL* above the plane wave cut-off frequency is defined as the difference between the summation of the incident and transmitted modal sound powers.

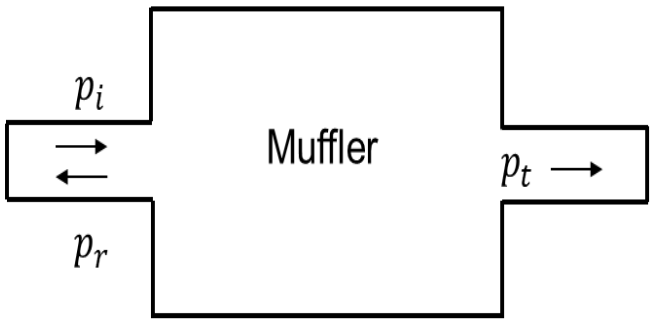

Figure 5.8 Schematic showing a silencer.

Usually, the inlet and outlet ducts of an arbitrary silencer system are cylindrical tubes as shown in Figure 5.8. Hence, only radial modes are assumed to be

excited. Applying modal expansion series theory (Equation (5.11)), the sound wave field in the inlet and outlet tubes can be expressed conveniently.

The incident sound wave can be expressed as

$$p_i(r,z) = \sum_{n=0}^{\infty} p_{in}^{+} e^{-jk_{izn}z} \psi_{in}(r) \tag{5.52}$$

where subscript i represents the incident wave, n the mode number and z the axial direction. p_{in}^{+} is the modal amplitude, k_{izn} the wavenumber and $\psi_{in}(r)$ the eigenfunction which equals to

$$\psi_{in}(r) = J_0(k_{irn} r) \tag{5.53}$$

where k_{irn} is the radial wavenumber and J_0 the Bessel function of the first kind, order zero.

The particle velocity of the incident wave can be written as

$$u_i(r,z) = \frac{1}{\rho\omega} \sum_{n=0}^{\infty} p_{in}^{+} e^{-jk_{izn}z} \psi_{in}(r) \tag{5.54}$$

where ρ denotes the density of air and ω the angular frequency.

The intensity of the incident wave then can be calculated

$$I_i = \frac{1}{2} Re(p_i u_i^{*}) \tag{5.55}$$

where $*$ denotes the conjugant and $Re(\cdot)$ denotes the real part of a complex number.

With the intensity available, the sound power can be determined by integrating the intensity over the cross-sectional area of the inlet

$$W_i = \int_{S_i} I_i \, dS \tag{5.56}$$

where S_i is the cross-sectional area of the inlet.

Since the eigenfunctions are orthogonal, Equation (5.56) can be simplified as

$$W_i = \frac{S_i}{2\rho c}\sum_{n=0}^{N} Re(\frac{k_{izn}}{k})|p_{in}^{+}|^2\psi_{in}^2(r_i) \tag{5.57}$$

where c is the speed of sound in air, k the wavenumber and r_i the radius of the inlet.

In a similar way, the sound power of the transmitted wave can be written as

$$W_o = \frac{S_o}{2\rho c}\sum_{n=0}^{N} Re(\frac{k_{ozn}}{k})|p_{on}^{+}|^2\psi_{on}^2(r_o) \tag{5.58}$$

where S_o is the cross-sectional area of the outlet, k_{ozn} the wavenumber, p_{on}^{+} the modal amplitude, $\psi_{on}(r_o)$ the eigenfunction and r_o the radius of the outlet.

It should be noted that in order to evaluate the *TL*, a unit planar incident wave can be assumed and therefore Equation (5.58) can be reduce as

$$W_i = \frac{S_i}{2\rho c} \tag{5.59}$$

However, in the outlet pipe, when the N^{th} higher order mode starts propagating in the inlet, the wavenumber $k_{izn} > 0, n = 0, 1, \dots, N$. Based upon the definition of transmission loss, the transmission loss is the difference between the incident and transmitted sound power.

$$TL = 10\log_{10}\frac{W_i}{W_o} \tag{5.60}$$

5.6.6 Prediction of Transmission Loss

To solve the system of equations, the modal expansion, which is an infinite series, must be truncated to an appropriate finite series (a total of N modes). In addition, the incident wave is assumed planar and A_0^{+} is set to a unity. The higher-order incident waves $A_n^{+}\ (n > 0)$ are assumed zero. An anechoic termination is imposed at the outlet, which eliminates all C_n^{-}. Therefore, a total of

$4N$ coefficients (A_n^- , B_n^+ , B_n^- and C_n^+) need to be solved, which requires $4N$ equations based on the interface conditions. Discretizing the cross-sectional area into N equal subareas ($r_j = (N-j)r_2/N, j = 1,2,\dots,N$) and performing integration of the sound pressure and particle velocity over the N discretized subareas at the two interface locations, $4N$ equations can be established as

$$-\sum_{n=0}^{N-1} A_n^- \int_{r_j}^{r_2} \psi_{An} dr + \sum_{n=0}^{N-1} (B_n^+ + B_n^-) \int_{r_j}^{r_2} \psi_{Bnp}^a(r) dr = r_2 - r_j, r_j \geq r_1 \tag{5.61}$$

$$\sum_{n=0}^{N-1} k_{Azn} A_n^- \int_{r_j}^{r_2} \psi_{An}(r) dr + \sum_{n=0}^{N-1} k_{Bzn} (B_n^+ - B_n^-) \int_{r_j}^{r_2} \psi_{Bnu}^a(r) dr = k_{Az0}(r_2 - r_j), r_j \geq r_1 \tag{5.62}$$

$$\sum_{n=0}^{N-1} (B_n^+ e^{-ik_{Bzn}L} + B_n^- e^{+ik_{Bzn}L}) \int_{r_j}^{r_2} \psi_{Bnp}^a(r) dr - \sum_{n=0}^{N-1} C_n^+ \int_{r_j}^{r_2} \psi_{Cn}(r) dr = 0, r_j \geq r_1 \tag{5.63}$$

$$\sum_{n=0}^{N-1} k_{Bzn} \left(B_n^+ e^{-ik_{Bzn}L} - B_n^- e^{+ik_{Bzn}L}\right) \int_{r_j}^{r_2} \psi_{Bnu}^a(r) dr - \sum_{n=0}^{N-1} k_{Czn} C_n^+ \int_{r_j}^{r_2} \psi_{Cn}(r) dr = 0, r_j \geq r_1 \tag{5.64}$$

$$\sum_{n=0}^{N-1} k_{Azn} A_n^- \int_{r_j}^{r_2} \psi_{An}(r) dr + \sum_{n=0}^{N-1} k_{Bzn} (B_n^+ - B_n^-) \int_{r_1}^{r_2} \psi_{Bnp}^a(r) dr = k_{Az0}\left(r_2 - r_j\right), r_j \leq r_1 \tag{5.65}$$

$$\begin{aligned} &\sum_{n=0}^{N-1} k_{Azn} A_n^- \int_{r_1}^{r_2} \psi_{An}(r) dr \\ &+ \sum_{n=0}^{N-1} k_{Bzn} (B_n^+ - B_n^-) \left(\int_{r_j}^{r_1} \psi_{Bnu}^f(r) dr + \int_{r_1}^{r_2} \psi_{Bnu}^a(r) dr \right) = k_{Az0}(r_2 - r_1), r_j \leq r_1 \end{aligned} \tag{5.66}$$

$$\sum_{n=0}^{N-1} (B_n^+ e^{-ik_{Bzn}L} + B_n^- e^{+ik_{Bzn}L}) \int_{r_1}^{r_2} \psi_{Bnp}^a(r) dr - \sum_{n=0}^{N-1} k_{Czn} C_n^+ \int_{r_j}^{r_2} \psi_{Cn}(r) dr = 0, r_j \leq r_1 \tag{5.67}$$

$$\begin{aligned} &\sum_{n=0}^{N-1} k_{Bzn} (B_n^+ e^{-ik_{Bzn}L} - B_n^- e^{+ik_{Bzn}L}) \left(\int_{r_j}^{r_1} \psi_{Bnu}^f(r) dr + \int_{r_1}^{r_2} \psi_{Bnu}^a(r) dr \right) \\ &- \sum_{n=0}^{N-1} k_{Czn} C_n^+ \int_{r_1}^{r_2} \psi_{Cn}(r) dr = 0, r_j \leq r_1 \end{aligned} \tag{5.68}$$

By solving the above $4N$ equations, the $4N$ unknowns (A_n^-, B_n^+, B_n^- and C_n^+) are determined and finally the transmission loss can be evaluated by Equation (5.60)

5.7 BEM solution of a Simplified Round Bar Silencer with Conical Adapters

Another approach to estimate the *TL* above the cut-off frequency is to reduce the non-planar wave phenomenon to a planar wave problem. This idea originates from the *TL* measurement when a geometry mismatch between the test object and the test rig occurs. To measure the *TL* of a silencer whose inlet and/or outlet tube are larger than the impedance tube, adapters, normally conical adapters, have to be designed and built up for the connection as shown in Figure 5.9.

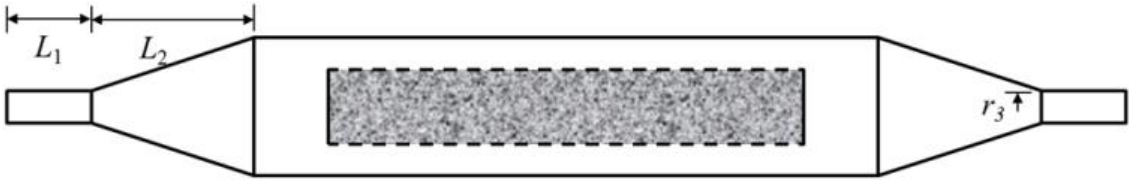

Figure 5.9 A round bar silencer with a pair of conical adapters.

Since the *TL* of a pair of conical adapters is fairly low at higher frequencies, it is practical to estimate the *TL* of the silencer using the *TL* of the entire system in the high frequency range.

5.8 Test Case and Results

With reference to Figure 5.5, the dimensions of the test case are r_1=0.254m, r_2=0.342m, L=6m, and s=0.2m. s is not used in the analytical solution but is needed for the BEM model. The flow resistivity of the sound absorbing material is 16000 Rayl/m and the porosity of the perforate facing sheet is 10%. The cut-off frequency of the duct is 611 Hz. In the analytical solution, the modal expansion series is truncated at N=9. In the BEM, a uniform velocity distribution is applied at the inlet and at the outlet to obtain the impedance matrix, which is then converted into the four-pole matrix [56].

The dimensions of the adapters are $r_3 = 0.1$m, $L_1 = 0.2$m and $L_2 = 0.5$m. Figure 5.10 shows the *TL* comparison between the analytical solutions and the BEM solutions. The analytical solution and the BEM without adapter compare well below the cut-off frequency. The BEM model with adapters results in higher *TL* in the plane wave range. Above the plane wave cut-off frequency, all three models behave similarly. The analytical solution predicts higher *TL* at the higher frequencies. The BEM model with adapters produces a smoother curve than the one without adapters. In general, these three methods provide acceptable agreement with each other and suggest that the simulation approach proposed is suitable for determining *TL* above the plane wave cut-off frequency.

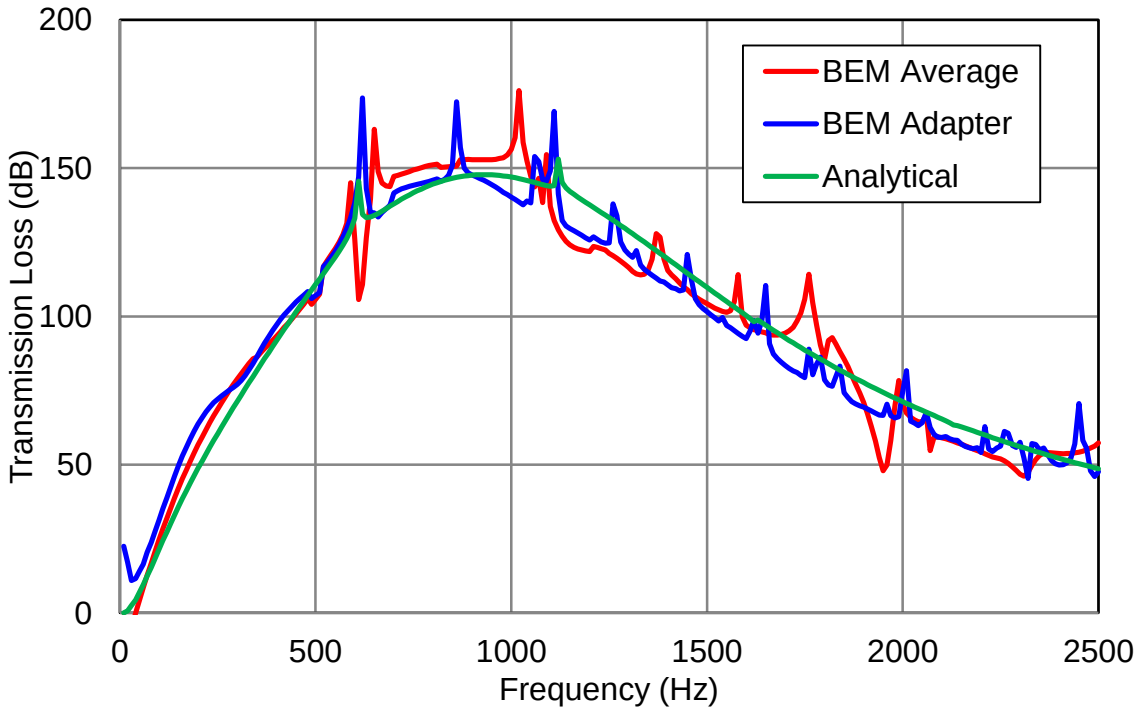

Figure 5.10 *TL* comparison of a bar silencer above plane wave range.

5.9 Parametric Studies

A parametric study is conducted to assess the effects of different parameters, such as flow resistivity, perforate porosity, length of bar and cross-sectional area ratio. The analytical approach is used in the examples which follow. The default

case is the test case used in Section 5.8. While investigating a specific parameter, the others are fixed according to the default case.

5.9.1 Effect of Flow Resistivity

Analytical *TL* results for the bar silencer with different flow resistivities are presented in Figure 5.11. The flow resistivities are 2000, 4000, 8000, 16000 and 20000 Rayls/m. As shown in the plot, *TL* improves as the flow resistivity increases at higher frequencies (above 800Hz) but reduces the attenuation at lower frequencies (below 800Hz).

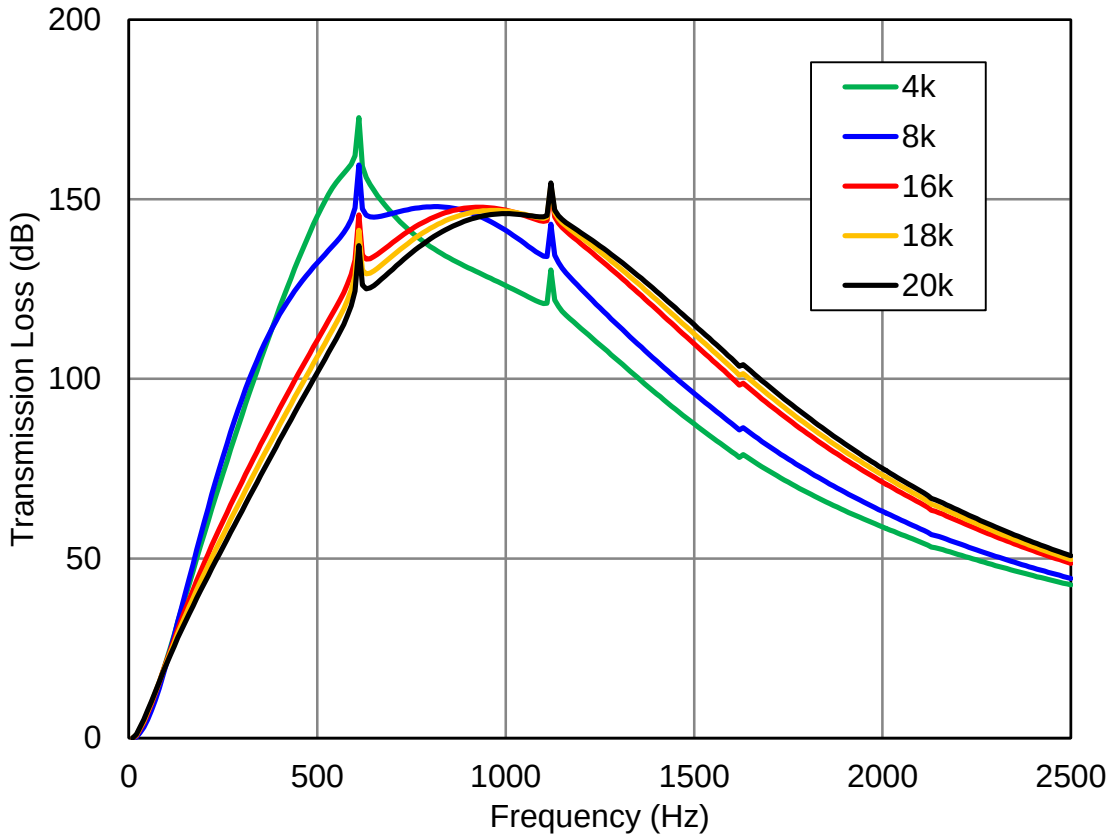

Figure 5.11 TL results for bar silencer with different flow resistivities.

5.9.2 Effect of Perforate Porosity

Perforate porosities of 1%, 5%, 10%, 20% and 30% are considered. The porosity impacts the result significantly as shown in Figure 5.12. With 1% opening area, the facing sheet is nearly sealed which reduces the sound absorption

functionality of the enclosed fibrous material. A larger porosity greatly improves the acoustic performance of the bar silencer. Above 500 Hz, both 20% and 30% are almost acoustically transparent, and their *TL*'s are similar.

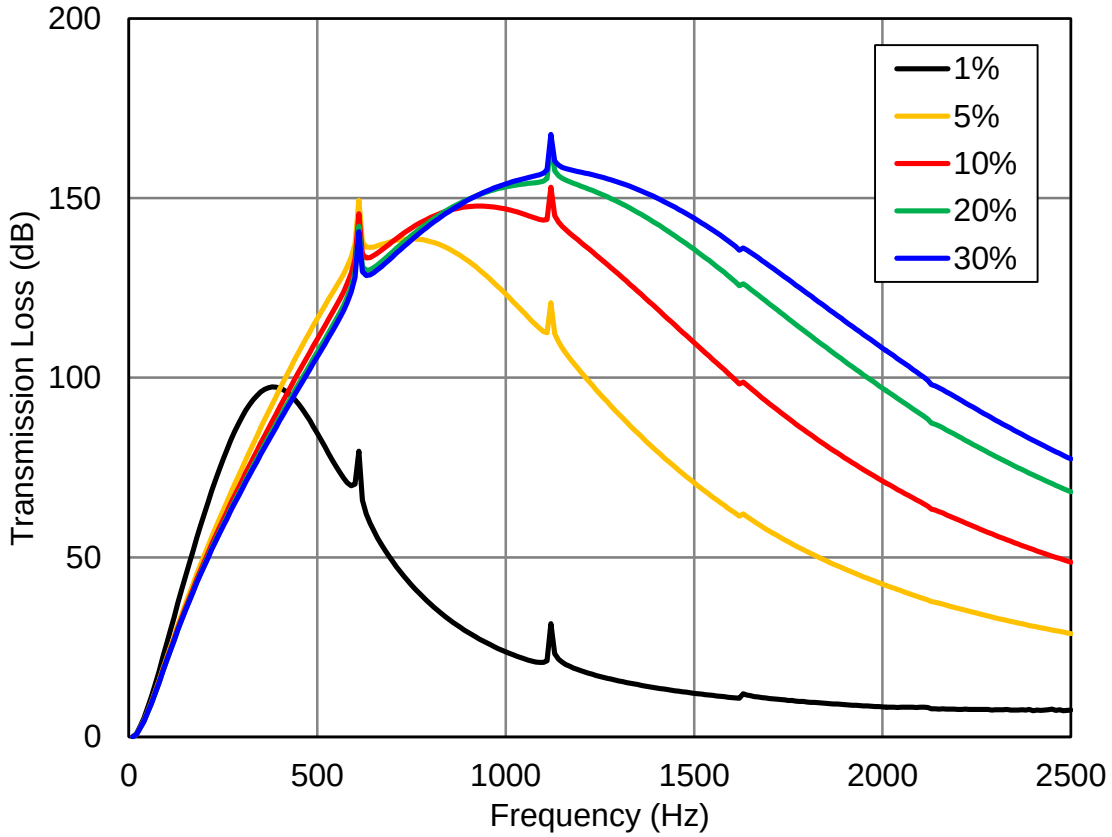

Figure 5.12 *TL* results for bar silencer with different porosity.

5.9.3 Effect of Length of Bars

The amount of sound absorbing material plays a critical role in *TL* at higher frequencies. It is of interest to investigate the effect of length of bar on *TL* (*L* =4,5,6,7,8m).

As shown in Figure 5.13, longer bars produce better *TL* as expected, especially in the frequency range of 500 – 1500Hz. However, as shown Figure 5.14, the acoustic attenuation has a linear relation to the length of bars, i.e. attenuation of a unit length of bars is constant.

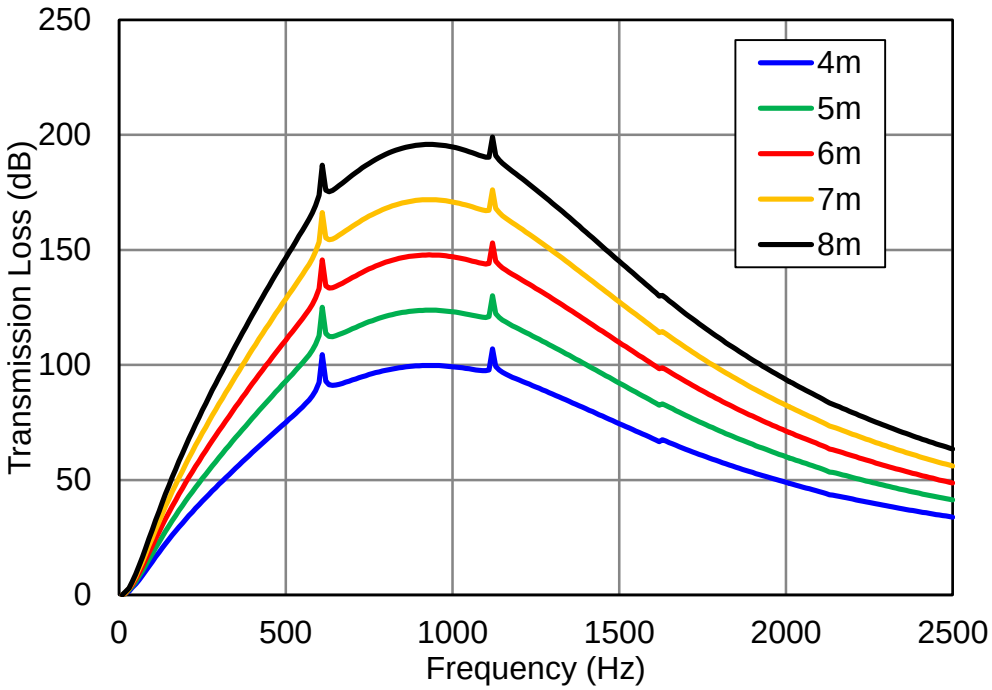

Figure 5.13 *TL* results for bar silencer with different length of bars.

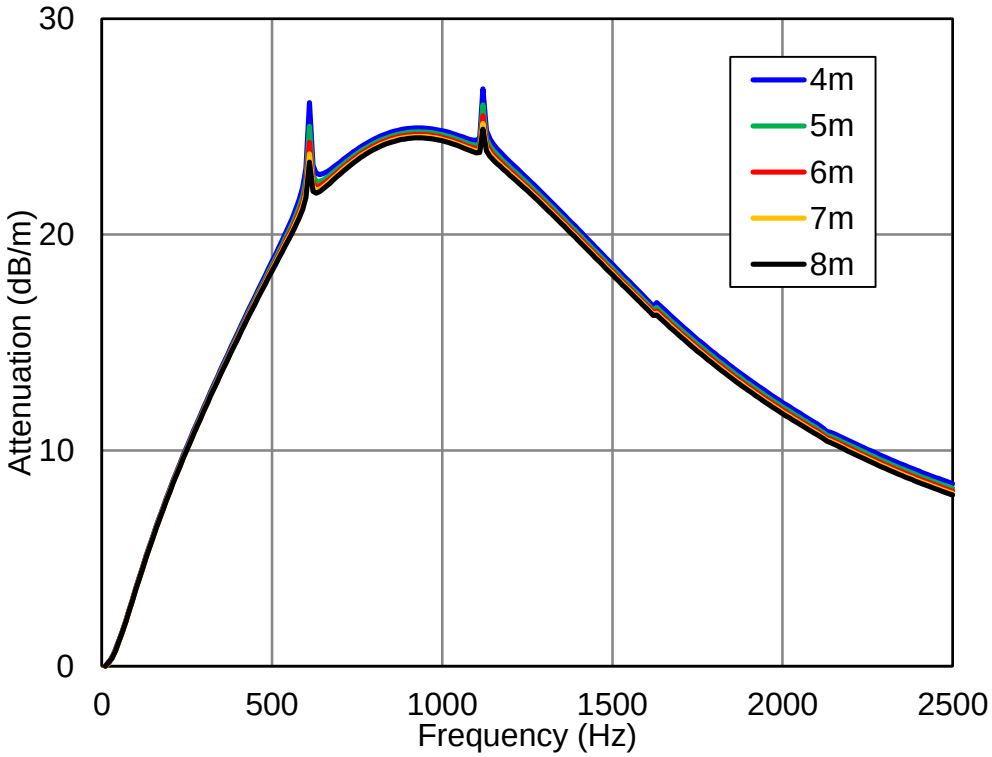

Figure 5.14 *TL* normalized with respect to the length of bars.

5.9.4 Effect of Cross-Sectional Area Ratio

The last parameter under investigation is percentage of fibrous material in the sense of cross-sectional area ratio as shown in Figure 5.7. The ratio can be expressed as

$$\beta = \frac{S_1}{S_2} \tag{5.69}$$

where S_1 and S_2 are the cross-sectional area of the single bar and the entire cell module respectively.

r_1 is fixed while r_2 varied (r_2 =16,15,13.5,13,12.5 in) to obtain different cross-sectional area ratios (β =39%,44%,55%,59%,64%).

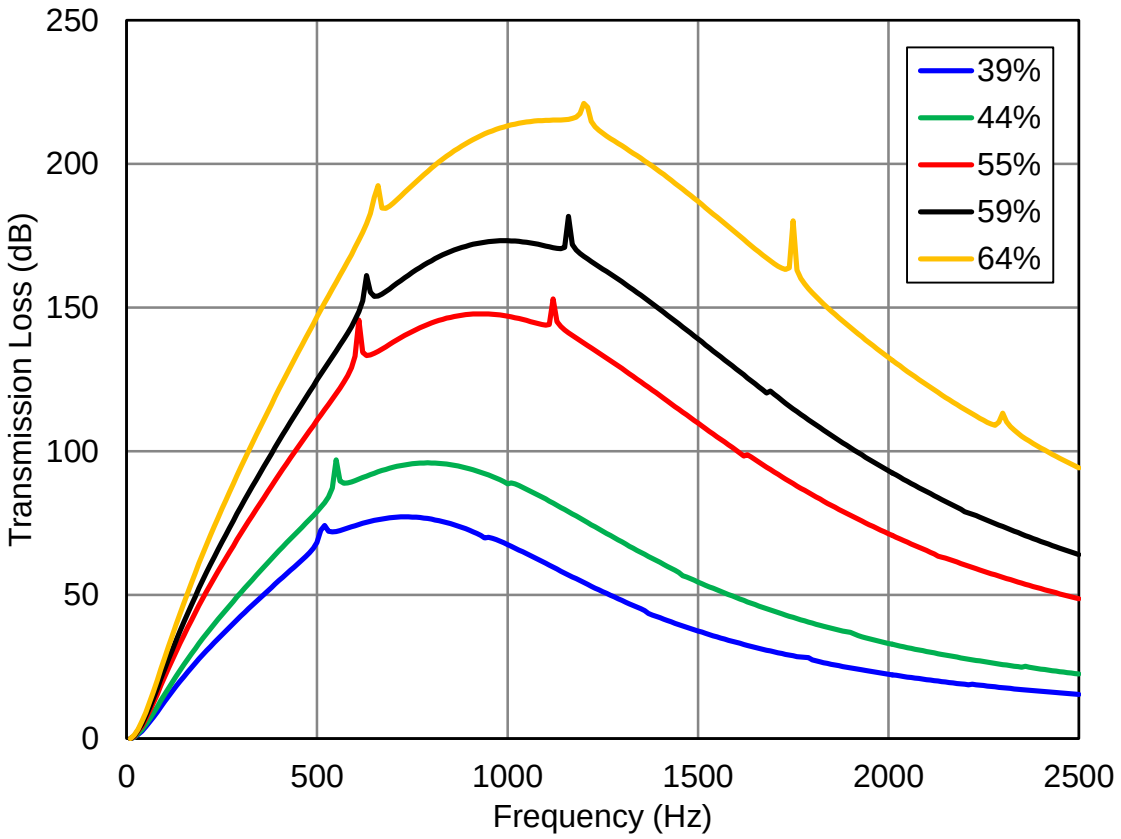

Figure 5.15 *TL* results for bar silencer with different cross-sectional area ratios.

Similar to the effect of varying the length of bars, a larger cross-sectional area ratio provides greater sound attenuation especially above 500Hz.

5.10 Summary

Bar silencers have broadband sound attenuation as a result of sound absorbing materials embedded. A single cell module is used for the sound attenuation analyses of bar silencers using the direct mixed-body BEM and analytical solutions. It is demonstrated that the direct-mixed body boundary element method is feasible to model bar silencers. An analytical solution based on the modal expansion theory and pressure and velocity matching technique is used to serve as a comparison tool.

Due to the large dimension of bar silencers, higher order modes start propagating beyond the plane wave cut-off frequency. The sound waves in the inlet and outlet pipes are no longer planar. Two approaches using BEM are developed to consider the non-planar wave propagation: 1) averaging the sound pressure and particle velocity at the inlet and outlet pipes; 2) adding a pair of conical adapters to increase the cut-off frequency of the inlet and outlet pipes. The analytical solution calculates the incident and transmitted powers including all the propagating modes.

In addition, a parametric study including the effects of flow resistivity, perforate porosity, length of bars and cross-sectional area ratio is conducted.

CHAPTER 6 USING THE RECIPROCAL WORK IDENTITY TO EVALUATE THE TRANSMISSION LOSS OF SILENCERS

6.1 Introduction

Silencers, both reactive and dissipative types, are devices to attenuate exhaust noise in various environments. The reactive silencers take advantage of impedance mismatch due to geometry changes, for instance, area contraction and expansion. The dissipative silencers, on the other hand, use sound absorbing materials to dissipate the sound energy. In practice, most silencers are a combination of the two types since the reactive type is to abate sound consisting of discrete tones, especially in the low frequency range, while the dissipative type is best suited to addressing high frequency broadband noise [73].

The use of a silencer is prompted by the need to reduce the radiated noise of source but, in most applications, the final selection is based on trade-offs between the predicted acoustical performance, back pressure, mechanical strength, volume/weight ratio, and cost [43]. To evaluate the acoustical performance of silencers, basic criteria are required to provide quantitative description. The most frequently used performance metrics are in terms of insertion loss (*IL*), transmission loss (*TL*) and noise reduction (*NR*) [28]. The transmission loss is a good performance measure of silencers since it represents the inherent capability of sound attenuation of silencers if we assume no reflection from the source and the termination. The *TL* is defined as the difference in dB between the incident sound power at the upstream L_{wi} and the transmitted sound power at the downstream L_{wt} [28]:

$$TL = L_{wi} - L_{wt} \tag{6.1}$$

Several analytical approaches have been used to determine the attenuation of silencers. Certainly, the most ubiquitous technique is the transfer matrix approach detailed by Munjal in his classic text [28]. Other approaches have been developed that are ideal for analyzing complex systems of interconnecting ducts. For instance, Glav and Åbom [90] proposed a general formalism for analyzing

acoustic 2-port network systems using a scattering matrix approach. Kar and Munjal [97] posed an alternative matrix approach.

Numerical simulation is also commonly used to evaluate the performance of silencers. Commonly used approaches include acoustic finite [98, 99, 100, 101, 102] and boundary [56, 57, 58, 103, 104] element methods. Numerical simulation is especially useful when the plane wave cut-off frequency is exceeded in the silencer.

If the plane wave analysis is used, transmission loss is normally calculated directly from the four-pole parameters [28] . If numerical simulation is used, the four-pole parameters can be determined by selecting appropriate boundary conditions [56, 105, 106, 107]. Alternatively, the four-pole parameters can be determined from an impedance matrix [56] .

Other approaches have abandoned an explicit determination of the four-pole parameters. For example, Munjal [28] utilized a two-port approach to calculate the transmission loss from the sound pressure at the source and termination, and particle velocity at the source. Alternatively, wave decomposition can be used to determine the incident and transmitted power. Both the two-port and three-point approaches assume an anechoic termination.

In this study, an alternative approach for determining transmission loss is developed based on the reciprocal work identity and the wave decomposition theory. No plane wave assumption has to be made in the inlet/outlet ducts and no explicit anechoic termination impedance has to be applied at the outlet. Just imagine how hard it would be to construct the true anechoic termination impedance beyond the cut-off frequency when the conventional characteristic impedance $Z = \rho c$ does not hold anymore. Below the cut-off frequency, there is no difference between the proposed method and the conventional four-pole method. A fairly complex silencer example is used to demonstrate the proposed method and verify the equivalency between the proposed method and the conventional four-pole method below the plane wave cut-off frequency. At

frequencies above the cut-off, the feasibility is demonstrated using a simple expansion chamber silencer.

6.2 Review of Current Techniques

6.2.1 Conventional Four-Pole Method

One of the most common methods to evaluate the *TL* is the conventional four-pole method. Below the cut-off frequency of the inlet/outlet ducts, the inherent property of a silencer shown in Figure 6.1 can be described by using the four-pole parameters A, B, C and D [56]:

$$\begin{Bmatrix} p_1 \\ u_1 \end{Bmatrix} = \begin{bmatrix} A & B \\ C & D \end{bmatrix} \begin{Bmatrix} p_2 \\ -u_2 \end{Bmatrix} \tag{6.2}$$

where p_1 and p_2 are the sound pressures, u_1 and u_2 the normal particle velocities at the inlet and the outlet, respectively. Due to the inward normal direction used in most boundary element method (BEM) software, a negative sign is added to u_2 in Equation (6.2). By imposing two different sets of boundary conditions, the four-pole parameters A, B, C and D can be obtained from

$$\begin{aligned} A &= \left.\frac{p_1}{p_2}\right|_{u_2=0,u_1=1} & B &= \left.\frac{p_1}{-u_2}\right|_{p_2=0,u_1=1} \\ C &= \left.\frac{u_1}{p_2}\right|_{u_2=0,u_1=1} & D &= \left.\frac{u_1}{-u_2}\right|_{p_2=0,u_1=1} \end{aligned} \tag{6.3a,b,c,d}$$

Two separate BEM runs have to be carried out in order to obtain all these four-pole parameters at each frequency.

Once the four-pole parameters A, B, C and D are available, the transmission loss of the silencer can be evaluate by

$$TL = 20\log_{10}\left(\frac{1}{2}\left|A + \frac{B}{\rho c} + \rho c C + D\right|\right) + 10\log_{10}\frac{S_i}{S_o} \tag{6.4}$$

where S_i and S_o denote the cross-sectional area of the inlet and outlet respectively, ρ the density of air and c is the speed of sound.

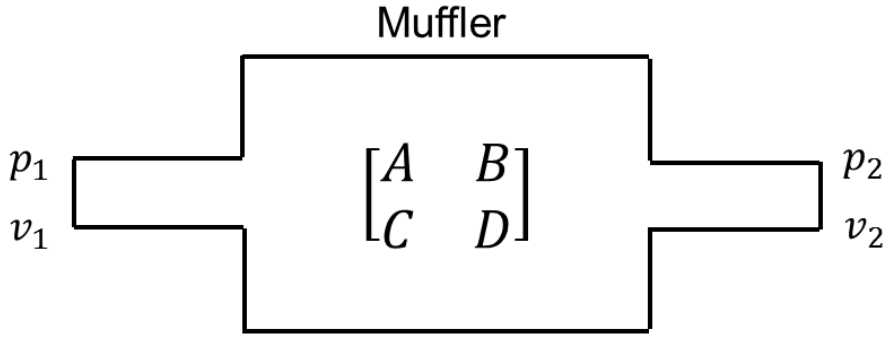

Figure 6.1 Schematic showing a silencer with four-pole parameters.

Wu et al. [56] pointed out that since two sets of boundary conditions are distinct, two BEM runs do not share the same BEM coefficient matrix. Hence, the matrix decomposition routine needs to be called twice at each frequency, which makes the conventional four-pole method an impractical choice for computing the transmission loss.

6.2.2 Improved Four-Pole Method

Instead of computing the four-pole parameters directly, an improved method was proposed by Wu et al. [56]. The method also requires two BEM runs but in a more efficient way. Rearrange the four-pole matrix in Equation (6.2) to get the impedance matrix:

$$\begin{Bmatrix} p_1 \\ p_2 \end{Bmatrix} = \begin{bmatrix} Z_{11} & Z_{12} \\ Z_{21} & Z_{22} \end{bmatrix} \begin{Bmatrix} u_1 \\ -u_2 \end{Bmatrix} \tag{6.5}$$

where

$$\begin{aligned} Z_{11} &= p_1|_{u_1=1,u_2=0} \quad Z_{12} = p_1|_{u_1=0,u_2=-1} \\ Z_{21} &= p_2|_{u_1=1,u_2=0} \quad Z_{22} = p_2|_{u_1=0,u_2=-1} \end{aligned} \tag{6.6a,b,c,d}$$

Like the conventional four-pole method, two separate BEM runs are still required to compute the impedance matrix. Nonetheless, two BEM runs share the same coefficient matrix because the two sets of boundary conditions are both velocity

boundary conditions. Therefore, the second BEM run only requires a trivial back-substitution procedure. The impedance matrix can be easily converted into the four-pole parameters by

$$A = \frac{Z_{11}}{Z_{21}}, \quad B = Z_{12} - \frac{Z_{11}Z_{22}}{Z_{21}}, \quad C = \frac{1}{Z_{21}}, \quad D = -\frac{Z_{22}}{Z_{21}} \qquad \text{(6.7a,b,c,d)}$$

Eventually, the *TL* now can be calculated by Equation (6.4).

6.2.3 Three-Point Method

The three-point method [86, 108] is based on the same simple plane wave decomposition as in the two-microphone method. Compared to the four-pole method, the three-point method requires only one single BEM run. To do so, $u_1 = 1$ is applied at the inlet and an anechoic termination impedance is applied at the outlet.

With reference to Figure 6.2, let x_1 and x_2 be the coordinates of two field points in the inlet duct. The corresponding sound pressures p_1 and p_2 can be written as

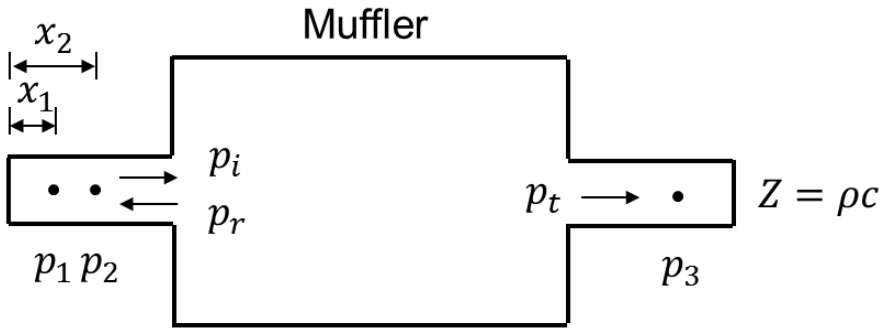

Figure 6.2 Schematic showing the three-point method.

$$p_1 = p_i e^{-jkz_1} + p_r e^{+jkz_1}$$
$$p_2 = p_i e^{-jkz_2} + p_r e^{+jkz_2} \qquad \text{(6.8a,b)}$$

where p_i and p_r denote the incident and reflected wave respectively, k denotes the wavenumber in the medium air.

The incident wave p_i can be extracted by solving Equation (6.8a,b) simultaneously,

$$p_i = \frac{p_1 e^{+jkz_2} - p_2 e^{+jkz_1}}{j2\sin\big(k(z_2 - z_1)\big)} \tag{6.9}$$

provided that $\sin\big(k(z_2 - z_1)\big) \neq 0$. The transmitted sound pressure can be found anywhere in the outlet tube. The *TL* then can be determined by

$$TL = 20\log_{10}\frac{|p_i|}{|p_t|} + 10\log_{10}\frac{S_i}{S_o} \tag{6.10}$$

6.2.4 Two-Port Method

The two-port method is documented in the book by Munjal [28]. Like the three-point method, the two-port method requires only one BEM run at each frequency with $u_1 = 1$ at the inlet and the anechoic termination impedance at the outlet. Without using any field points inside the silencer, the method relies only on solutions at the inlet and the outlet. Below the plane wave cut-off frequency, the anechoic termination implies

$$p_2 = -\rho c u_2 \tag{6.11}$$

Substitute the above condition into the four-pole matrix in Equation (6.2) and rearrange. The four-pole relationship becomes

$$A + \frac{B}{\rho c} = -\frac{p_1}{\rho c u_2} \tag{6.12}$$

$$\rho c C + D = -\frac{u_1}{u_2} \tag{6.13}$$

Finally, the *TL* in Equation (6.4) can be rewritten as

$$TL = 20\log_{10}\left(\frac{1}{2}\left|\frac{p_1 + \rho c u_1}{\rho c u_2}\right|\right) + 10\log_{10}\frac{S_i}{S_o} \tag{6.14}$$

It is noted that neither the three-point method nor the two-port method can produce the four-pole matrix as a by-product.

6.3 Reciprocal Work Identity Method

6.3.1 Reciprocal Work Identity

In a homogeneous medium, the sound propagation is governed by the Helmholtz equation

$$\nabla^2 p + k^2 p = 0 \tag{6.15}$$

where p is the sound pressure. For an arbitrary silencer system shown in Figure 6.1, we may apply different sets of boundary conditions on its boundary. For each different set of boundary conditions, the sound field is expected to be different. Let p_A and p_B represent two different sound fields corresponding to the two boundary condition sets A and B, respectively. Both sound fields, p_A and p_B satisfy the Helmholtz equation,

$$\nabla^2 p_A + k^2 p_A = 0 \tag{6.16}$$

$$\nabla^2 p_B + k^2 p_B = 0 \tag{6.17}$$

The Green's second identity is then applied to relate these two sound fields,

$$\int_{\Omega} (p_A \nabla^2 p_B - p_B \nabla^2 p_A)\, dV = \int_{\partial\Omega} \left(p_A \frac{\partial p_B}{\partial n} - p_B \frac{\partial p_A}{\partial n} \right) dS \tag{6.18}$$

where n denotes the normal direction, Ω the physical domain and $\partial\Omega$ the boundary of the physical domain.

Substituting Equations (6.16) and (6.17) into Equation (6.18), we obtain

$$\int_{\partial\Omega} \left(p_A \frac{\partial p_B}{\partial n} - p_B \frac{\partial p_A}{\partial n} \right) dS = 0 \tag{6.19}$$

In linear acoustics, the momentum equation relates the normal derivative of sound pressure to the normal particle velocity by

$$\frac{\partial p}{\partial n} = -j\rho\omega u \tag{6.20}$$

where ω the angular frequency and u the particle velocity in the normal direction. Equation (6.19) becomes

$$\int_{\partial\Omega} (p_A u_B - p_B u_A)\, dS = 0 \tag{6.21}$$

where u_A and u_B are the particle velocities in the normal direction. Equation (6.21) is the so-called the reciprocal work identity.

All boundary surfaces except the inlet and the outlet are either rigid or covered by a sound absorbing lining. In the simplest case, assume all chamber surfaces are rigid, and hence, all normal velocity terms are zero except at the inlet and outlet. It is easy to see that the boundary integral in Equation (6.21) reduces to the inlet and outlet surfaces only. On the other hand, if the chamber wall has a lining that can be represented by a local impedance Z,

$$p = -Zu_n \tag{6.22}$$

Equation (6.21) will also reduce to the inlet and outlet surfaces only, due to the "reciprocal" relationship in Equation (6.21). Even if the silencer has some complex internal components, such as extended inlet/outlet tubes, thin baffles, flow plugs, perforated tubes, and bulk-reacting materials, we can always divide the silencer interior into different homogeneous sub-domains, and apply Equation (6.21) individually to each sub-domain. All the sub-domain boundary integrals are then added together. The integrals along any interface between two neighboring sub-domains will cancel out due to the opposite normal directions, and in the end, the integral will always reduce to the inlet and outlet surfaces only. In any event, Equation (6.21) becomes

$$\int_{S_i+S_o} (p_A u_B - p_B u_A)\, dS = 0 \tag{6.23}$$

where S_i is the inlet surface, and S_o is the outlet surface. In the frequency range where the plane wave theory still applies, sound pressure and particle velocity are both uniform over any cross-sectional area and Equation (6.23) becomes

$$(p_{Ai}u_{Bi} - p_{Bi}u_{Ai})S_i + (p_{Ao}u_{Bo} - p_{Bo}u_{Ao})S_o = 0 \tag{6.24}$$

where the subscripts A, B denote the two different sound fields, and i, o denote the inlet and outlet, respectively. At frequencies above the cutoff, integration over the inlet and outlet cross-sectional areas is required.

6.3.2 Transmission Loss Computation

Using the reciprocal work identity, let A represent the sound field with an anechoic termination so that the *TL* is defined. However, we will not explicitly apply the anechoic condition in the BEM model. Instead, in the inlet and outlet ducts, an analytical wave decomposition expression up to an order as high as required by a particular frequency will be used to represent sound field A. Doing so will eliminate the need to find an appropriate impedance boundary condition at the anechoic termination. It should be noted that $Z = \rho c$ can no longer represent an anechoic termination at high frequencies.

For sound field B, the BEM simulation is performed multiple times with different boundary condition sets. The boundary conditions are neither tied to an anechoic termination nor to the four-pole matrix. After all, the four-pole matrix is no longer defined at high frequencies. In the following, we will demonstrate the idea by still staying below the plane wave cut-off frequency of the inlet/outlet ducts. The idea can be easily extended to high frequencies later (see Section 6.5). At low frequencies, the plane wave theory still holds, and there are two plane waves in the inlet duct for sound field A. If we set $x = 0$ at the inlet location, then the sound pressure there is

$$p_{Ai} = p_{Ai}^{+} + p_{Ai}^{-} \tag{6.25}$$

where p_{Ai}^{+} and p_{Ai}^{-} represent the complex amplitudes of the incident and reflected waves, respectively. The corresponding particle velocity is

$$u_{Ai} = \frac{1}{\rho c}(p_{Ai}^{+} - p_{Ai}^{-}) \tag{6.26}$$

In the outlet duct with an anechoic termination, there is no reflection. If we also set $x = 0$ locally at the outlet location, then

$$p_{Ao} = p_{Ao}^{+} \tag{6.27}$$

where p_{Ao}^{+} is the complex amplitude of the transmitted wave. The corresponding particle velocity is

$$u_{Ao} = \frac{1}{\rho c} p_{Ao}^{+} \tag{6.28}$$

To find the *TL*, we will need to know how much power is transmitted for a given incident power. Basically there are two unknowns, p_{Ai}^{-} and p_{Ao}^{+}, for a given incident wave p_{Ai}^{+}. Normally a reflection coefficient R and a transmitted coefficient T both normalized to the incident wave are preferred. Therefore, we will need two equations to solve for the two unknowns. This is when the BEM will come into play. The BEM with any two random boundary condition sets for sound field B can provide two such equations. For example, we could apply $u = 1$ at the inlet and $u = 0$ at the outlet for the first set, and $u = 0$ at the inlet and $u = -1$ at the outlet for the second set, just as in the improved four-pole method. Both sets are meant for sound field B, but only one set at a time. Then the subscript B is replaced by the numeric subscripts, 1 and 2. In other words, 1 represents B_1, and 2 represents B_2. Apply the reciprocal work identity, Equation (6.24), twice, one between A and B_1, and the other between A and B_2, the following two simultaneous equations are obtained:

$$(p_{Ai}u_{1i} - p_{1i}u_{Ai})S_i + (p_{Ao}u_{1o} - p_{1o}u_{Ao})S_o = 0 \tag{6.29}$$

$$(p_{Ai}u_{2i} - p_{2i}u_{Ai})S_i + (p_{Ao}u_{2o} - p_{2o}u_{Ao})S_o = 0 \tag{6.30}$$

Substituting Equations (6.25) - (6.28) as well as $u_{1i} = 1,\ u_{1o} = 0, u_{2i} = 0,$ and $u_{2o} = -1$, into Equations (6.29) and (6.30) to get

$$\begin{bmatrix} (\rho c + p_{1i})S_i & -p_{1o}S_o \\ p_{2i}S_i & -(\rho c + p_{2o})S_o \end{bmatrix} \begin{Bmatrix} R \\ T \end{Bmatrix} = \begin{Bmatrix} (p_{1i} - \rho c)S_i \\ p_{2i}S_i \end{Bmatrix} \tag{6.31}$$

where R and T are defined by

$$R = \frac{p_{Ai}^{-}}{p_{Ai}^{+}} \tag{6.32}$$

$$T = \frac{p_{Ao}^{+}}{p_{Ai}^{+}} \tag{6.33}$$

Finally, the *TL* can be determined by

$$TL = -20\log_{10}|T| + 10\log_{10}\frac{S_i}{S_o} \tag{6.34}$$

It can be proved that Equations (6.4) and (6.34) are mathematically equivalent (Section 6.4). There is no difference between the new method and the improved four-pole method below the plane wave cut-off frequency. Both methods apply the same sets of boundary conditions in the BEM. It is just how the *TL* is evaluated. However, the new method has a potential advantage at high frequencies when the plane wave theory does not hold anymore.

6.3.3 Test Case

A fairly complex silencer model shown in Figure 6.3 is used to test the new *TL* method using the reciprocal work identity. The BEM computation is done in MAP [92].

The porosity of the perforated tube in the third chamber is 20%. Equation (5.29) is employed to calculate the transfer impedance of perforates. The chamber is lined with polyester (flow resistivity R =16,000 MKS rayl/m) of 0.05m thickness.

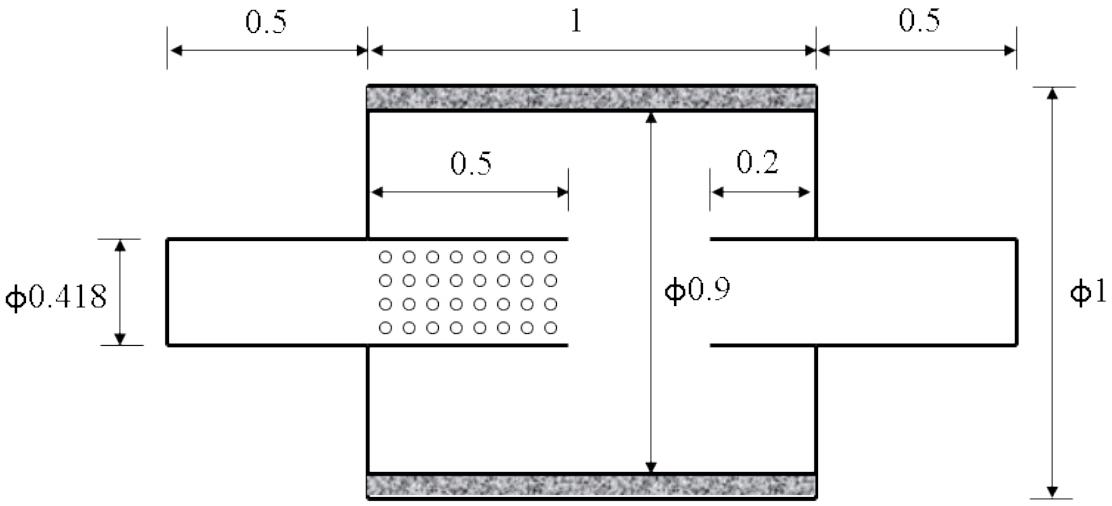

Figure 6.3 Configuration and dimension of the test silencer (SI Unit).

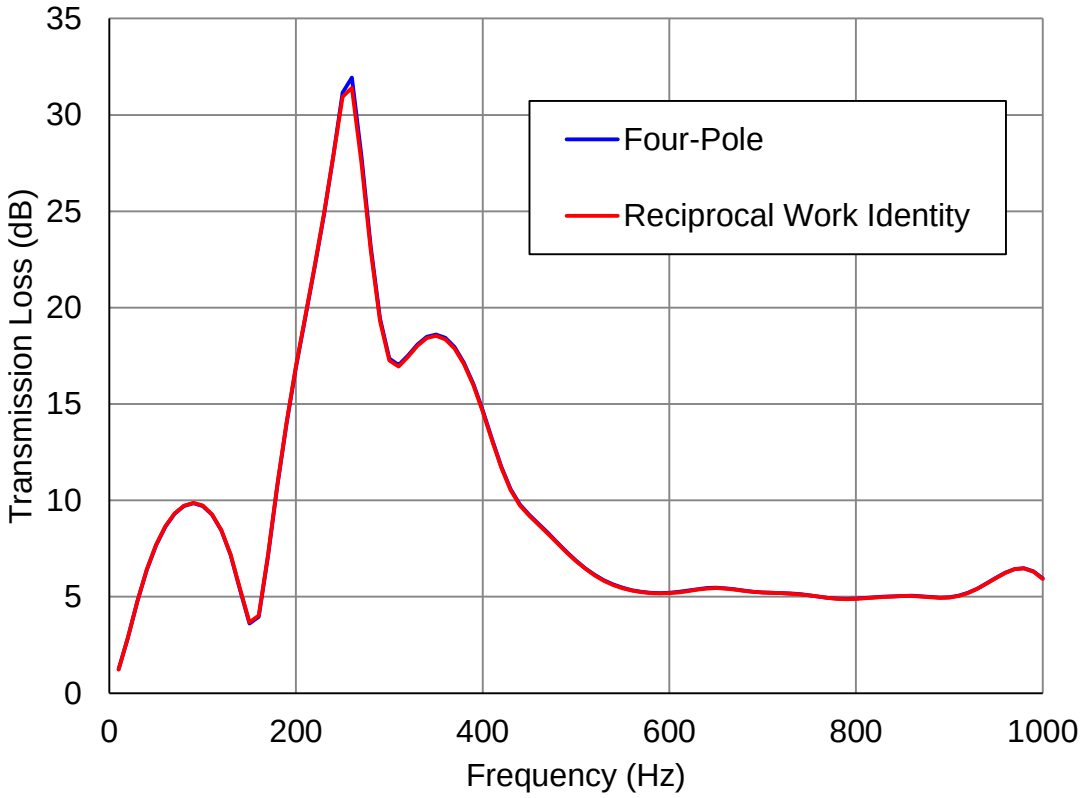

Figure 6.4 *TL* comparison between methods of four-pole and reciprocal work identity.

The BEM simulation results are shown in Figure 6.4. It is seen that the *TL* prediction from the new reciprocal work identity method matches very well with the one from the four-pole method below 1000 Hz, the plane wave cut-off frequency of the inlet/outlet ducts. The new reciprocal work identity method has not been fully extended to high frequencies yet. The purpose of this test case is to simply confirm that the new method does produce the same *TL* as the conventional four-pole method below the plane wave cut-off frequency.

6.4 Equivalency to the Four-Pole Method

In the conventional four-pole method, if the boundary condition ($u_1 = 1, u_2 = 0$) is imposed, Equation (6.2) can be rewritten as

$$\begin{Bmatrix} p_{1i} \\ 1 \end{Bmatrix} = \begin{bmatrix} A & B \\ C & D \end{bmatrix} \begin{Bmatrix} p_{1o} \\ 0 \end{Bmatrix} \tag{6.35}$$

where subscript 1 denotes the first boundary condition, i and o denote the inlet and outlet.

If the second condition ($u_1 = 0, u_2 = -1$) is imposed, Equation (6.2) can be rewritten as

$$\begin{Bmatrix} p_{2i} \\ 0 \end{Bmatrix} = \begin{bmatrix} A & B \\ C & D \end{bmatrix} \begin{Bmatrix} p_{2o} \\ 1 \end{Bmatrix} \tag{6.36}$$

where subscript 2 denotes the second boundary condition.

Combining Equations (6.35) and (6.36), we have

$$\begin{bmatrix} A & B \\ C & D \end{bmatrix} = \frac{1}{p_{1o}} \begin{bmatrix} p_{1i} & p_{2i}p_{1o} - p_{1i}p_{2o} \\ 1 & -p_{2o} \end{bmatrix} \tag{6.37}$$

Hence, the *TL* can be calculated by substituting the four-pole parameters into Equation (6.4)

$$TL = 20 \log_{10} \left| \frac{2\rho c p_{1o}}{(\rho c + p_{1i})(\rho c + p_{2o}) - p_{2i}p_{1o}} \right| + 10 \log_{10} \frac{S_i}{S_o} \tag{6.38}$$

Due to the acoustic reciprocity theory, the determinant of the four-pole matrix is unity ($AD - BC = 1$), we can derive the relation from Equation (6.37)

$$p_{1o} = -p_{2i} \tag{6.39}$$

In the method of reciprocal identity, the transmission coefficient can be obtained by solving Equation (6.31)

$$T = \frac{2\rho c p_{2i}}{p_{1o}p_{2i} - (\rho c + p_{1i})(\rho c + p_{2o})} \tag{6.40}$$

Therefore, the TL can be determined by

$$TL = 20\log_{10}\left|\frac{2\rho c p_{2i}}{p_{1o}p_{2i} - (\rho c + p_{1i})(\rho c + p_{2o})}\right| + 10\log_{10}\frac{S_i}{S_o} \tag{6.41}$$

Using relation in Equation (6.40), it can be proved that Equation (6.38) is identical to Equation (6.42).

6.5 *TL* beyond the Plane Wave Cut-Off Frequency

6.5.1 Theory

In this section, the reciprocal work identity method is used to evaluate the *TL* at high frequencies. For demonstration purposes, we will focus on axisymmetric modes only. At frequencies above the plane wave cut-off frequency, the radial modes will appear, and the general axisymmetric representation of sound pressure in the inlet and outlet ducts is

$$p(r) = \sum_{n=0}^{\infty}\left(p_n^{+}e^{-jk_{zn}z} + p_n^{-}e^{+jk_{zn}z}\right)J_0(k_{rn}r) \tag{6.42}$$

where subscripts z and r denote the axial and radial directions, respectively, J_0 is the Bessel function of the first kind of order zero, and the superscripts $+$ and $-$ represent the incident and reflected waves, respectively. Although the series expansion goes to infinity in Equation (6.42), there will only be a finite number of propagating modes in each frequency range. For demonstration purposes, we

will just focus on the occurrence of one higher-order mode beyond the plane wave cut-off frequency. In other words, below the second plane wave cut-off frequency, there are only two propagating modes, $n = 0,1$.

Recall that the sound field with an anechoic termination for the *TL* definition is labeled "sound field A" in the reciprocal work identity. Therefore, the sound pressure at the inlet location (where we set $z = 0$) is

$$p_{Ai}(r) = p_{Ai0}^{+} + p_{Ai0}^{-} + J_0(k_r r)p_{Ai1}^{-} \tag{6.43}$$

where the subscript i represents the waves in the inlet duct, and 0 and 1 are two propagating modes, $n = 0$ and $n = 1$, respectively. The corresponding particle velocity is

$$u_{Ai}(r) = \frac{1}{\rho\omega}[k(p_{Ai0}^{+} - p_{Ai0}^{-}) - k_{x1}J_0(k_r r)p_{Ai1}^{-}] \tag{6.44}$$

In the outlet duct, there is no reflection due to the anechoic termination. Therefore, the sound pressure at the outlet location (where we also set $z = 0$ locally) is

$$p_{Ao}(r) = p_{Ao0}^{+} + J_0(k_r r)p_{Ao1}^{+} \tag{6.45}$$

where the subscript o represents the waves in the outlet duct. The corresponding particle velocity there is

$$u_{Ao}(r) = \frac{1}{\rho\omega}[kp_{Ao0}^{+} + k_{x1}J_0(k_r r)p_{Ao1}^{+}] \tag{6.46}$$

There are five wave amplitudes in Equations (6.43) - (6.46), p_{Ai0}^{+}, p_{Ai0}^{-}, , p_{Ai1}^{-}, p_{Ao0}^{+} and p_{Ao1}^{+}. If we assume a unit incident plane wave ($p_{Ai0}^{+} = 1$), the remaining four amplitudes can be solved in the reciprocal work identity by imposing four different boundary condition sets in the BEM model (sound fields B_1 to B_4).

If four sound field B_j $(j = 1, 2, 3, 4)$ are chosen, the sound pressure p_{Bij}, p_{Boj} and the normal particle velocities v_{Bij}, v_{Boj} can be obtained from BEM analysis(i, o

represent the inlet and outlet respectively). The 4 x 4 system of equations can be derived from the reciprocal work identity, Equation (6.23), as

$$Ax = b \tag{6.47}$$

where $A = [a_{jk}]\,(j,k = 1,2,3,4)$ is the system matrix, $x = [p_{Ai0}^{-},\ p_{Ai1}^{-},\ p_{Ao0}^{+},\ p_{Ao1}^{+}]^T$ is vector of the unknown wave amplitudes and $b = [b_j]^T\ (j = 1,2,3,4)$ is the right hand side vector.

The expressions for a_{jk} are

$$a_{j1} = \int_{S_i} \left(v_{Bij} + \frac{p_{Bij}}{\rho c}\right)\, dS \tag{6.48}$$

$$a_{j2} = \int_{S_i} \left(v_{Bij} + \frac{k_{x1}}{\rho\omega} p_{Bij}\right) J_0(k_{r1} r)\, dS \tag{6.49}$$

$$a_{j3} = \int_{S_o} \left(v_{Boj} - \frac{p_{Boj}}{\rho c}\right)\, dS \tag{6.50}$$

$$a_{j4} = \int_{S_o} \left(v_{Boj} - \frac{k_{x1}}{\rho\omega} p_{Boj}\right) J_o(k_{r1} r)\, dS \tag{6.51}$$

The expression for b_j is

$$b_j = -\int_{S_i} \left(v_{Bij} - \frac{p_{Bij}}{\rho c}\right)\, dS \tag{6.52}$$

With all the magnitude available, the *TL* can be evaluated by (5.60).

It should be pointed out that the *TL* can be extended to take into account additional higher order modes beyond the first one since the transmitted power is simply the summation of the modal power. If N modes are considered including the plane wave mode, then $2N$ boundary conditions will be required to solve the system of equations since there are $2N$ unknown wave amplitudes.

6.5.2 Test Case

To validate the *TL* beyond the cut-off frequency as discussed above, a simple expansion chamber, shown in Figure 6.5 (SI Unit), is used as a test case since its analytical solution is widely available in the literature [75, 104].

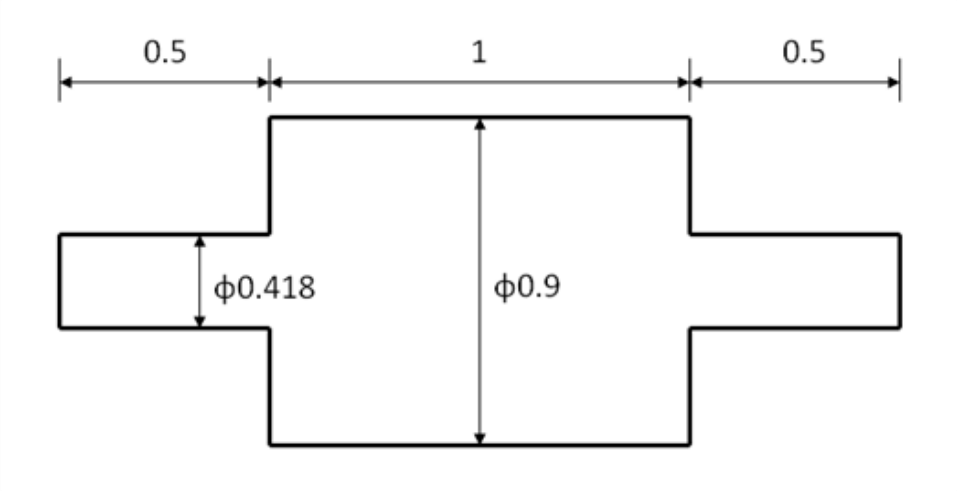

Figure 6.5 A simple expansion chamber.

Following Selamet [75], the analytical solution based on pressure and velocity matching technique is developed. In addition, four different boundary conditions, listed in Table 6.1, were imposed to obtain the *TL* via boundary element method in MAP [92].

Table 6.1 Four boundary conditions (SI Unit) in BEM

BC	Inlet	Outlet
1	$v = 1$	$v = 0$
2	$v = 0$	$v = 1$
3	$v = 1$	$Z = 2 + i$
4	$Z = 2 + i$	$v = 1$

The *TL* comparison is shown in Figure 6.6. The plane wave cut-off frequency for the inlet/outlet pipe is 1000Hz and the first higher order mode cut-off frequency is

1832Hz. *TL* from BEM agrees with the analytical solution well in the frequency range.

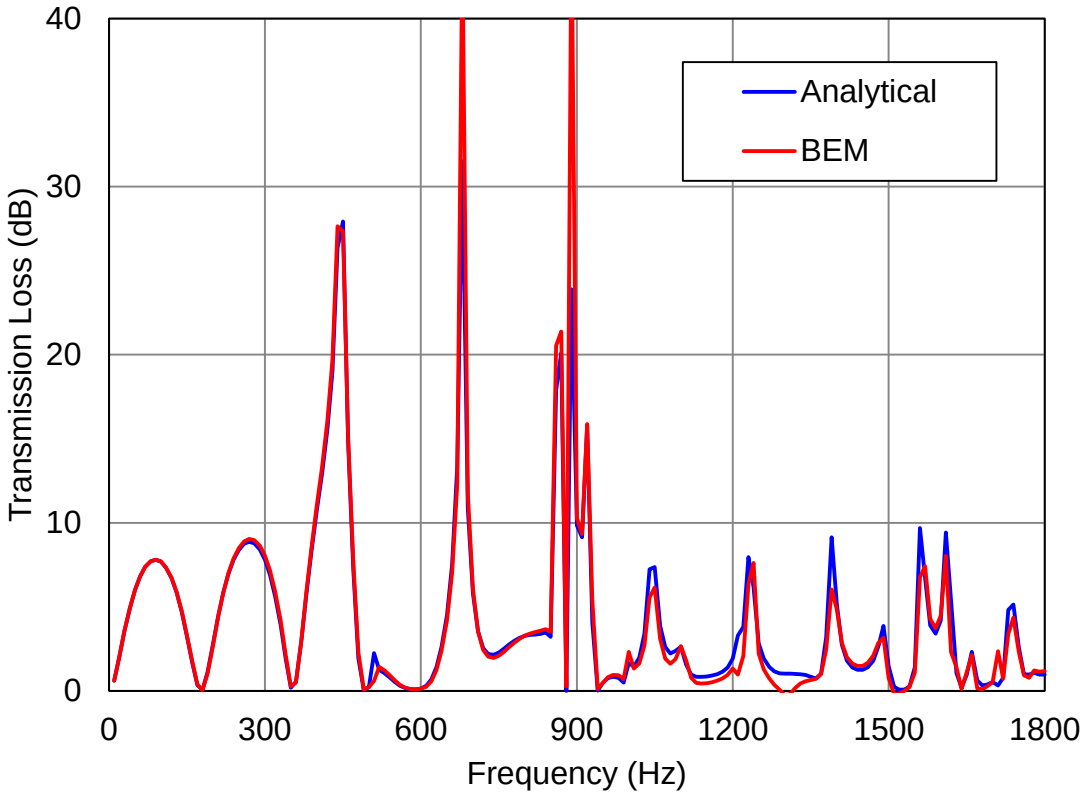

Figure 6.6 *TL* comparison between analytical and BEM solutions.

6.6 Summary

A new computational method based on the reciprocal work identity is proposed to evaluate the *TL* of silencers at all frequencies. At frequencies below the plane wave cut-off frequency of the inlet/outlet ducts, the new method is equivalent to the improved four-pole method in terms of accuracy and computational efficiency. Since the new method does not assume plane waves in the inlet and outlet ducts, and does not explicitly apply the anechoic termination impedance condition, it can be extended to the *TL* computation beyond the plane wave cut-off frequency. In this study, we have demonstrated the method below the cut-off frequency using a fairly complex silencer model. In addition, the proposed method is used to evaluate the *TL* including the first higher order mode for a simple expansion

chamber. It shows this approach can be used to calculate the *TL* including additional higher order modes.

CHAPTER 7 CONCLUSIONS AND RECOMMENDATIONS

Airborne noise from power generation equipment is diagnosed and treated in this dissertation. First of all, a feedback loop model is used to diagnose the occurrence of combustion oscillations. The model has been validated and enhanced. Secondly, a numerical model for evaluating the acoustic performance of bar silencers is developed and validated. To support that effort, a reciprocal work identity method is proposed to assess the transmission loss at frequencies above the plane wave cut-off frequency.

7.1 Diagnosing Combustion-Driven Oscillations

Combustion-driven oscillations are a common problem with power generation equipment that normally occurs under very specific operating conditions. Sound is generated by the flame and is reflected from the combustion chamber into the mixture supply or even further upstream to the gas valve. The reflected sound waves disturb the mixture flow or equivalence ratio and therefore lead to a fluctuating heat release which causes the fluctuations of the flame. The resulting oscillations are clearly abnormal and objectionable. They also deteriorate combustion efficiency, increase pollutant emission, and damage or destroy the equipment.

A feedback loop stability model for mixture flow fluctuations is reviewed and summarized. Three components must be determined prior to the diagnosis: 1) Z, the driving point impedance of the combustion chamber; 2) H, the transfer function relating the perturbation of the mixture flow to the acoustic pressure in the combustion chamber; and 3) G_f, the flame transfer function. Oscillations are more likely to occur at frequencies where the magnitude of $Z \times H$ exceeds $1/G_f$ and the phase of $Z \times H$ equals to $1/G_f$.

The model was adjusted to include equivalence ratio fluctuations. In this case, H is replaced by two components: 1) H_1, the transfer function relating the fluctuating velocity at the gas valve to the fluctuating pressure at the burner; and

2) H_2 relates the equivalence ratio at the gas valve to the fluctuating velocity at the gas valve.

The two feedback loop stability models were then applied to two commercial boilers which exhibited combustion-driven oscillations. In each case, the model successfully identified the likely causes and also possible solutions. Accordingly, the feedback loop stability model is a useful tool for approach combustion instability problems.

As noted earlier, the upstream and downstream acoustic impedances are important inputs for both models. In this work, principles for determining the acoustic impedance by simulation and measurement are summarized. Prior literature had paid little attention to realistically simulating the acoustics for HVAC equipment like boilers, furnaces, and water heaters. An approach for including the effect of structural-acoustic coupling was developed and validated. Secondly, acoustic FEM was used to determine the acoustic impedance above the plane wave cut-off frequency. Thirdly, experimental determination of hard to model boiler components was also demonstrated. Finally, a method of characterizing the transfer impedance of burners was proposed. The transfer impedance was measured and effective parameters (porosity and hole diameter) were estimated. Due to the perforation characteristic of burners, the transfer impedance is used.

A design approach is proposed to formalize a process for preventing, diagnosing and treating combustion. Potential solutions to solve combustion-driven oscillations are developed.

In summary, the main contributions from this work are as follows.

- A low-order feedback loop model was developed to identify equivalence ratio fluctuations.
- An acoustic finite element model was integrated into the low-order model for determining acoustic impedances. This allows the model to be extended to higher frequencies for certain elements.

- The transfer matrix of the blower was measured. The approach documented permits the modeling of components that are difficult to model using plane wave theory or acoustic finite element analysis.
- The acoustic transfer impedance of burners was measured. This was the first study where this quantity was measured for burners.
- A method was proposed and validated for measuring the burner transfer impedance and fitting the measured data to Maa's theory [51, 52]. The method permits the calculation of an effective hole diameter and porosity. The advantage of this approach is that the fitted transfer impedance results are smoother and more accurate at low frequencies.
- The flexible plate vibration is incorporated into the plane wave model.
- A design approach for preventing and solving combustion oscillation problems was proposed.

The following recommendations for future work are recommended.

- A more in depth study on burners should be conducted experimentally determined how changing the geometry of burners will impact the onset of combustion instabilities.
- The proposed design process should be substantiated and enhanced by a number of case studies.
- Acoustic methods for determining the flame transfer function should be further enhanced and developed.
- Empirical models for the flame transfer function should be developed and validated for different burner types and fuels.
- Combustion driven oscillations likely occur in cases of flue gas recirculation and for flow instabilities. More research into these areas is required.

7.2 Simulation of Bar Silencers

In contrast to combustion-driven oscillations, turbulent combustion noise has a broadband spectrum. In the gas turbine industry, bar silencers are often used to attenuate the broadband noise.

A bar silencer is comprised of an array of rectangular or round bars made of sound absorbing materials packed in a rectangular lattice arrangement. Each bar is covered by a perforated facing sheet to protect the material from being blown away by the exhaust gas. The dimensions of bar silencers are typically large.

The direct-mixed body BEM is employed to simulate the acoustic performance of bar silencers. Assuming a uniform acoustic field across the inlet plane, the acoustic performance can be deduced from the attenuation in a single module since the axial attenuation within each cell is the same. Due to the difficulty of obtaining measurement data, an analytical solution for a simplified circular geometry is developed to serve as a validation tool for the model. It is based on the pressure and velocity matching technique. A method is proposed to calculate the incident and transmitted power beyond the plane wave cut-off frequency which included the higher order mode effects above the cutoff. In addition, a parametric study focusing on the effects of flow resistivity, perforate porosity, length of bars, and cross-sectional area ratio is performed.

To numerically investigate the transmission loss beyond the plane wave cut-off frequency, a novel approach is developed and validated based on the reciprocal work identity. Imposing no anechoic termination boundary condition, it can indirectly calculate the incident and transmitted sound waves via the reciprocal work identity. For simplicity, the procedure is illustrated using a simple expansion chamber.

The main contributions of the work on bar silencers are as follows.

- The direct mixed-body boundary element method was applied to simulate the acoustic performance of bar silencers.
- An analytical model based on the pressure and velocity matching technique was developed and used as a validation tool for the BEM model.
- A parametric study is conducted to investigate the influence of varying different bar silencer parameters.
- The higher order propagation modes are included the transmission loss calculation.

- A new numerical approach which is based on the reciprocal work identity is developed to determine the transmission loss.
- The feasibility of the reciprocal work identity method is demonstrated using a fairly complex silencer.
- Extension of *TL* computation above the plane wave cut-off frequency is demonstrated using a simple expansion chamber.

The following recommendations for future work are recommended.

- Analytical models should be developed for more realistic geometries (i.e., square bars). The work presented in this research was for a simplified round bar.
- The BEM model should be validated experimentally for a large silencer arrangement.
- The BEM should be used to investigate the effects of different configurations and cross-sectional areas of bars.
- The mean flow effect should be included in the model.
- The reciprocal work identity should be applied to determining the transmission loss for a bar silencer configuration.

APPENDIX A PLANE WAVE ASSUMPTION IN BURNERS

It was also assumed that plane waves propagate in the burners as well. In order to validate the assumption, a FEM analysis was conducted as follows.

As shown in Figure A.1, burner is placed in a simplified combustion chamber. Eight unit constant monopoles are evenly distributed around the burner circumference at the mid-length of the burner. An anechoic termination is imposed at the bottom of burner. The temperature in the burner and combustion chamber is assumed 20 and 811 Celsius degrees respectively. The density of air and speed of sound were correspondingly assigned.

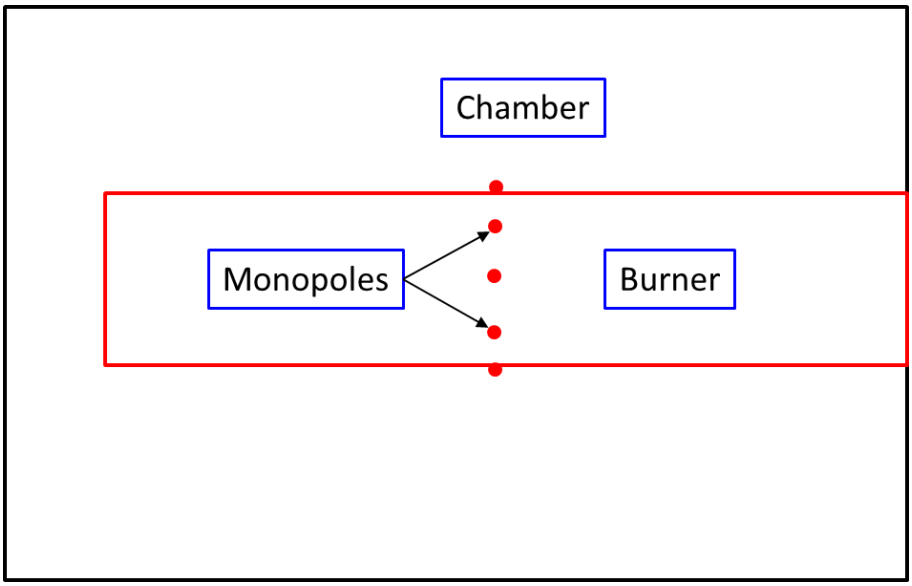

Figure A.1 Schematic showing a burner in a combustion chamber.

The results show that planar wave propagation exists at all frequencies. Figure A.2 and Figure A.3 demonstrate plane wave propagation at 10Hz and 1500Hz respectively. It concludes that the transfer matrix theory is applicable in the burner region.

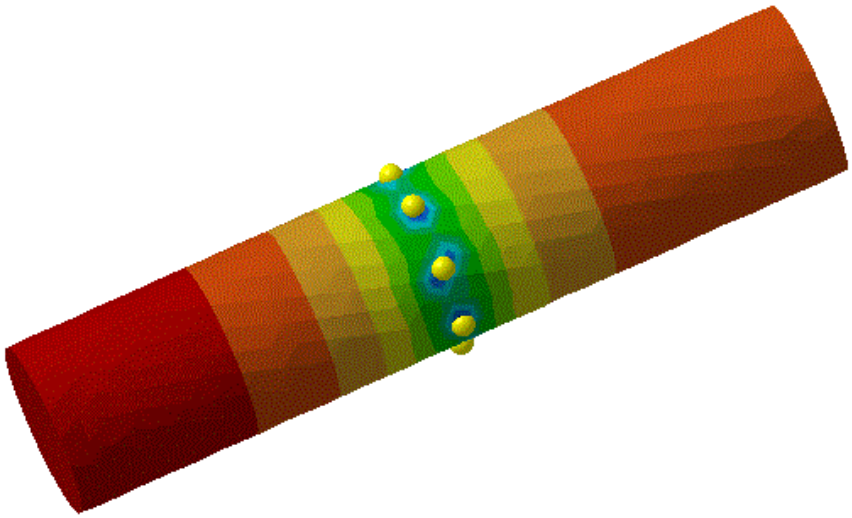

Figure A.2 Plane wave propagation at 10Hz.

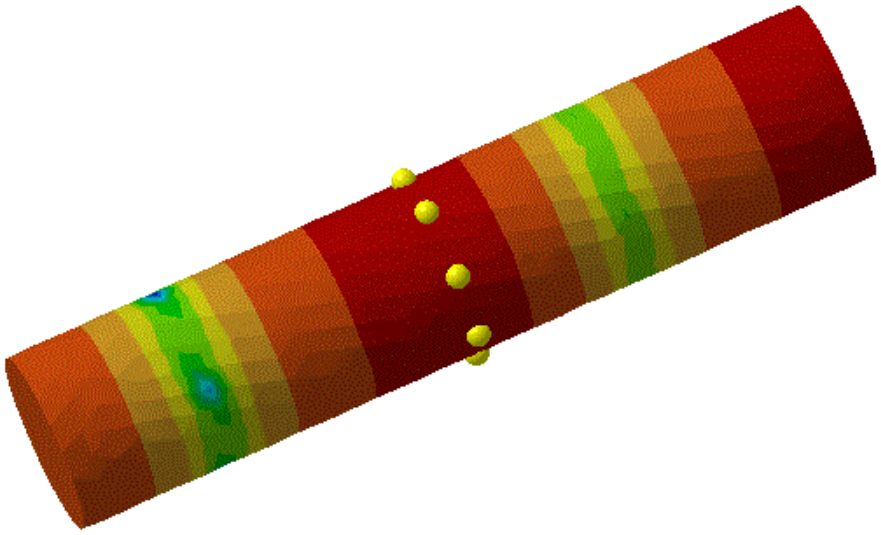

Figure A.3 Plane wave propagation at 1500Hz.

REFERENCES

[1] "Chapter 32 Boilers," in *2012 ASHRAE Handbook - HVAC Systems and Equipment*, Atlanta, GA, American Society of Heating, Refrigerating and Air-Conditioning Engineers, 2012.

[2] H. Willis, Distributed Power Generation: Planning and Evaluation, New York: Marcel Dekker, 2000.

[3] T. C. Lieuwen and V. Yang, Combustion Instabilities in Gas Turbine Engines, Operational Experience, Fundamental Mechanisms, and Modeling, Reston, VA: Amerian Institute of Aeronautics and Astronautics, 2005.

[4] M. P. Boyce, Gas Turbine Engineering Handbook, 2nd ed., Boston: Gulf Professional Publishing, 2001.

[5] V. K. Khanna, "A Study of the Dynamics of Laminar and Turbulent Fully and Partially Premixed Flames," PhD Dissertation, Virginia Polytechnic Institute and State University, 2001.

[6] P. K. Baade, "Design Criteria and Models for Preventing Combustion Oscillations," *ASHRAE Transaction,* vol. 84, no. 1, pp. 449-465, 1978.

[7] T. Lieuwen, H. Torres, C. Johnson and B. T. Zinn, "A mechanism of Combustion Instability in Lean Premixed Gas Turbines Combustors," *Journal of Engineering for Gas Turbines and Power,* vol. 123, no. 1, pp. 182-189, 2001.

[8] A. A. Putnam, Combustion-Driven Oscillations in Industry, New York:

Elsevier, 1971.

[9] M. I. Ali, T. Wu and K. Saito, "Combination Effect of Reburn, Post-Flame Air, and Acoustic Excitation on NOx Reduction," *Fuel,* 2013 (to appear).

[10] M. E. Elsari, "The Use of Passive Devices for the Suppression of Combustion Oscillations In Gas-Fired Appliances," PhD Dissertation, University of Hull, 2002.

[11] A. A. Putnam, "Combustion Noise in Industrial Burners," *Noise Control Engineering Journal,* vol. 7, no. 1, pp. 24-34, 1976.

[12] R. A. Putnam, W. Krebs and S. S. Sattinger, "Chapter 77, Furnace and Burner Noise Control," in *Handbook of Noise and Vibration Control, M. J., Crocker eds.*, Hoboken, New Jersey, John Wiley, 2007, pp. 956-965.

[13] D. Fritsche, "Origin and Control of Thermoacoustic Instabilities in Lean Premixed Gas Turbine Combustion," PhD Dissertation, Swiss Federal Institute of Technology, 2005.

[14] M. Elsari and A. Cummings, "Combustion Oscillations in Gas Fired Appliances: Eigen-Frequencies and Stability Regimes," *Applied Acoustics,* vol. 64, pp. 565-580, 2003.

[15] P. K. Baade, "How to Solve Abnormal Combustion Noise Problems," *Sound and Vibration,* pp. 22-27, July 2004.

[16] P. K. Baade and M. J. Tomarchio, "Tricks and Tools for Solving Abnormal Combustion Noise Problems," *Sound and Vibration,* pp. 12-17, July 2008.

[17] V. W. Goldschmidt, R. G. Leonard, J. F. Riley, G. Wolfbrand and P. K. Baade, "Transfer Function of Gas Flames: Methods of Measurement and Representative Data," *ASHRAE Transactions,* vol. 84, no. 1, pp. 466-476,

1978.

[18] V. N. Kornilov, "Experimental Research of Acoustically Perturbed Bunsen Flames," PhD Dissertation, Eindhoven University of Technology, 2006.

[19] T. Lieuwen, "Modeling Premixed Combustion-Acoustic Wave Interactions: A Review," *Journal of Propulsion and Power,* vol. 19, no. 5, pp. 765-781, 2003.

[20] T. Sattelmayer, "Influence of the Combustor Aerodynamics on Combustion Instabilities from Equivalence Ratio Fluctuations," in *Proceedings of ASME TURBOEXPO*, Munich, Germany, May 8-11, Paper No. 2000-GT-082, 2000.

[21] T. Sattelmayer, "Influence of the Combustor Aerodynamics on Combustion Instabilities From Equivalence Ratio Fluctuations," *Journal of Engineering for Gas Turbines and Power,* vol. 125, no. 1, pp. 11-19, 2003.

[22] M. P. Auer, C. Hirsch and T. Sattelmayer, "Influence of the Interaction of Equivalence Ratio and Mass Flow Fluctuations on Flame Dynamics," in *Proceedings of ASME Turbo Expo Power for Land, Sea and Air*, Reno-Tahoe, Nevada, USA, June 6-9, Paper No. GT2005-68373, 2005.

[23] D. E. Scarborough, "An Experimental and Theoretical Investigation of a Fuel System Tuner for the Suppression of Combustion Driven Oscillations," PhD Dissertation, Georgia Institute of Technology, 2012.

[24] R. Coleman and P. J. Remington, "Chapter 18: Active Control of Noise and Vibration," in *Noise and Vibration Control Eningeering, Principles and Applications 2nd Ed I.L. Ver and L.L.Beranek eds.*, Hoboken, New Jersey, John Wiley, 2005, pp. 721-865.

[25] M. A. Heckl, "Active Control of the Noise From a Rijke Tube," *Journal of*

Sound and Vibration, vol. 124, no. 1, pp. 117-133, 1988.

[26] A. P. Dowling and A. S. Morgans, "Feedback Control of Combustion Oscillations," *Annual Review of Fluid Mechanics,* vol. 37, pp. 151-182, 2005.

[27] N. Docquier and S. Candel, "Combustion Control and Sensors: A Review," *Progress in Energy and Combustion Science,* vol. 28, no. 2, pp. 107-150, 2002.

[28] M. L. Munjal, Acoustics of Ducts and Mufflers with Applications to Exhaust and Ventilation System Design, New York: Wiley-Interscience, 1987.

[29] N. A. Nilsson and S. Soderqvist, "The Bar Silencer - Improving Attenuation by Constricted Two-Dimensional Wave Propagation," in *Proceedings of Inter-Noise*, 1983.

[30] B. Higgins, "On the Sound Produced by a Current of Hydrogen Gas Passing through a Tube," *Journal of Natural Philosophy and Chemical Arts,* vol. 1, p. 129, 1802.

[31] J. Rayleigh, The Theory of Sound, New York: Dover, 1945.

[32] V. N. Kornilov, K. Schreel and L. de Goey, "Parametric Study of the Transfer Function of Perturbed Bunsen Flames," in *International Congress of Sound and Vibration*, Lisbon, July 11-14, 2005.

[33] D. W. Herrin, L. Zhou and T. Li, "Validation of a Low-Order Acoustic Model of Boilers and Its Application for Diagnosing Combustion Driven Oscillations," ASHRAE Report 1517-TRP, American Society of Heating, Refrigerating and Air-Conditioning Engineers, 2012.

[34] L. Zhou, D. W. Herrin and T. Li, "Measurement and Simulation of Acoustic

Load Impedance for Boilers (RP-1517)," *ASHRAE Tranctions (under review),* 2013.

[35] T. W. Wu, C. Cheng and Z. Tao, "Boundary Element Analysis of Packed Silencer with Protective Cloth and Embedded Thin Surfaces," *Journal of Sound and Vibration,* vol. 261, no. 1, pp. 1-15, 2003.

[36] J. Liu, X. Hua and D. W. Herrin, "Estimation of Effective Parameters for Microperforated Panel Absorbers and Applications," *Applied Acoustics (under review),* 2013.

[37] F. Fahy, Foundations of Engineering Acoustics, London: Elsevier Academic, 2001.

[38] L. J. Eriksson, "Higher Order Mode Effects in Circular Ducts and Expansion Chambers," *Journal of Acoustical Society of America,* vol. 68, no. 2, pp. 545-550, 1980.

[39] L. Zhou, D. W. Herrin and T. Li, "Assessing the Causes of Combustion Driven Oscillations in Boilers using a Feedback Loop Stability Model (RP-1517)," *ASHRAE Transactions (under review),* 2013.

[40] ASTM E1050-98, *Standard Test Method for Impedance and Absorption of Acoustical Materials Using a Tube, Two Microphones, and a Digital Frequency Analysis System,* Philadelphia: American Society of Testing and Materials, 1998.

[41] I. Spectronics, *ACUPRO Measurement System,* 2012.

[42] A. F. Seybert, *ACUPRO Manual: Measurement of Acoustical Properties of Materials and Systems,* 2007.

[43] M. L. Munjal, A. G. Galaitsis and I. L. Ver, "Chapter 9: Passive Silencers,"

in *Noise and Vibration Control Engineering, Principles and Applications I.L. Ver and L.L. Beranek ed.*, Hoboken, New Jersey, John Wiley, 2005, pp. 279-344.

[44] M. Abom, R. Glav, S. Nygard and T. Elnady, *SIDLAB Acoustics User's Manual, Release 2.6,* 2011.

[45] I. MathWorks, *MATLAB User's Guide,* 2012.

[46] M. L. Munjal, "Chapter K: Muffler Acoustics," in *Formulas of Acoustics, 2nd Ed., F.P. Mechel ed.*, Berlin, Springer-Verlag, 2008, pp. 689-740.

[47] F. Karal, "The Analogous Acoustical Impedance for Discontinuities and Constrictions of Circular Cross Section," *Journal of Acoustical Society of America,* vol. 25, no. 2, pp. 327-334, 1953.

[48] F. P. Mechel, P. A. Mertens and W. M. Schilz, "Interaction Between Air Flow and Airborne Sound in a Duct," Aerospace Medical Research Laboratories, Wright-Patterson Air Force Base, AMRL-TR-65-53, 1965.

[49] K. N. Rao and M. L. Munjal, "Experimental Analysis of Impedance of Perforates with Grazing Flow," *Journal of Sound and Vibration,* vol. 108, no. 2, pp. 283-295, 1986.

[50] ASTM C522-03, *Standard Test Method for Air Flow Resistance of Acoustical Materials,* Philadelphia: American Society of Testing and Materials, 2003.

[51] D. Y. Maa, "Microperforated Panel Wideband Absorbers," *Noise Control Engineering Journal,* vol. 29, pp. 77-84, 1997.

[52] D. Y. Maa, "Theory and Design of Microperforated Panel Sound Absorbing Construction," *Scientia Sinica,* vol. 18, pp. 55-71, 1975.

[53] S. Allam, Y. Guo and M. Abom, "Acoustical Study of Micro-Perforated Plates for Vehicle Applications," in *SAE Noise and Vibration Conference*, St. Charles, IL, May 19-21, Paper No. 2009-01-2037, 2009.

[54] W. Soedel, Vibratons of Shells and Plates, 3rd Ed., CRC Press, 2004.

[55] D. J. Ewins, Modal Testing: Theory, Practice and Application, Baldock, Hertfordshire, UK: Research Studies Press, 2000.

[56] T. W. Wu, P. Zhang and C. Cheng, "Boundary Element Analysis of Mufflers with an Improved Method for Deriving the Four-Pole Parameters," *Journal of Sound and Vibration,* vol. 217, pp. 767-779, 1998.

[57] D. W. Herrin, Z. Tao, E. L. Scalf, S. A. Allen and A. F. Seybert, "Using Numerical Acoustics to Predict the Attenuation of HVAC Plenums," *ASHRAE Transactions,* vol. 113, no. 1, 2007.

[58] D. W. Herrin, Z. Tao, A. E. Carter, J. Liu and A. F. Seybert, "Using Numerical Methods to Analyze Multicomponent HVAC Systems," *ASHRAE Transactions,* vol. 113, no. 1, 2007.

[59] T. Y. Lung and A. G. Doige, "A Time-Averaging Transient Testing Method for Acoustic Properties of Piping Systems and Mufflers," *Journal of Acoustical Society of America,* vol. 73, pp. 867-876, 1983.

[60] M. L. Munjal and A. G. Doige, "Theory of A Two Source-Location Method for Direct Experimental Evaluation of the Four-Pole Parameters of An Aeroacoustic Element," *Journal of Sound and Vibration,* vol. 141, no. 2, pp. 323-333, 1990.

[61] ASTM E2611-09, *Measurement of Normal Incidence Sound Transmission of Acousitcal Material Based on the Transfer Matrix Method,* West

Conshohocken, PA: ASTM International, 2009.

[62] H. Levine and J. Schwinger, "On the Radiation of Sound from an unflanged Circular Pipe," *Physical Review,* vol. 73, no. 4, pp. 383-406, 1948.

[63] A. D. Pierce, Acoustics: An Introduction to Its Physical Principles and Applications, McGraw-Hill, 1981.

[64] P. K. Baade and M. J. Tomarchio, "Decomnstration of Tricks and Tools for Solving Self Excited Combustion Oscillation Problems," in *Noise-Con*, Dearborn, MI, 2008.

[65] I. 11688-1:1998, *Acoustics - Recommended Practice for the Design of Low-Noise Machinery and Equipment - Part 1: Planning,* 1998.

[66] M. Bockhoff, "Chapter 66 - Design of Low Noise Machinery," in *Handbook of Noise and Vibration Control, ed. M. Crocker*, New Jersey, Wiley, 2007, pp. 794-804.

[67] D. J. Kato and R. A. Knepper, "A Modal Analysis Approach to Combustion Driven Oscillations," in *The Fourth International Modal Analysis Conference*, Los Angeles, CA, 1986.

[68] M. L. Munjal, *FRITAmuff User's Manual,* Bangalore, India: Facility for Research in Technical Acoustics, IISc, 2008.

[69] E. Dokumaci, *ADEM User's Manual,* 2012.

[70] H. Boden and R. Glav, "Chapter 85: Exhaust and Intake Noise and Acoustical Design of Mufflers and Silencers," in *Handbook of Noise and Vibration Control, M.J. Crocker eds.*, Hoboken, New Jersey, John Wiley, 2007, pp. 1034-1053.

[71] D. Y. Maa, "Potential of Microperforated Panel Absorber," *Journal of the Acoustical Society of America,* vol. 104, pp. 2861-2866, 1998.

[72] D. Y. Maa, "Theory of Microslit Absorbers," *Acta Acustica,* vol. 25, no. 6, pp. 481-485, 2000.

[73] H. P. Wallin, U. Carlsson, M. Abom, H. Boden and R. Glav, Sound and Vibration, Stockholm: KTH Royal Institute of Technology, 2011.

[74] R. J. Astley and A. Cummings, "A Finite Element Scheme for Attenuation in Ducts Lined with Porous Material: Comparison with Experiment," *Journal of Sound and Vibration,* vol. 116, no. 2, pp. 239-263, 1987.

[75] A. Selamet, M. B. Xu and I. J. Lee, "Analytical Approach for Sound Atenuation in Perforated Disspative Silencers," *Journal of Acoustical Society of America,* vol. 115, no. 5, pp. 2091-2099, 2004.

[76] F. P. Mechel, "Theory of Baffle-Type Silencers," *Acustica,* vol. 70, pp. 93-111, 1990.

[77] F. P. Mechel, "Numerical Results to the Theory of Baffle-Type Silencers," *Acustica,* vol. 72, pp. 7-20, 1990.

[78] M. B. Xu, A. Selamet, I. J. Lee and N. T. Huff, "Sound Attenuation in Dissaptive Expansion Chambers," *Journal of Sound and Vibration,* vol. 272, pp. 1125-1133, 2004.

[79] B. Venkatesham and M. L. Munjal, "Acoustic Performance of an Industrial Muffler," in *Inter-Noise*, Lisbon, June 13-16, 2010.

[80] H. Industriakustic, "Test cell improves environment for gas turbine overhauls," *Offshore,* vol. 61, no. 3, p. 102, 2001.

[81] ISO 7235:2003(E), *Acoustics - Laboratory Measurement Procedures for Ducted Silencers and Air-Terminal Units - Insertion Loss, Flow Noise and Total Pressure Loss,* Geneva, Switzerland: International Organization for Standardization, 2003.

[82] ISO 11691:1995(E), *Acoustics - Measurement of Insertion Loss of Ducted Silencers Without FLow - Laboratory Survey Method,* Geneva, Switzerland: International Organization for Standardization, 1995.

[83] Z. Tao and A. F. Seybert, "A Review of Current Techniques for Measuring Muffler Transmission Loss," in *SAE Noise and Vibration Conference*, Grand Traverse, MI, May 5, Paper No. 2003-01-1653, 2003.

[84] A. Cummings and R. J. Astley, "Finite Element Computation of Attenuation in Bar-Silencers and Comparison with Measured Data," *Journal of Sound and Vibration,* vol. 196, no. 3, pp. 351-369, 1996.

[85] D. W. Herrin, S. Ramalingam, Z. Cui and J. Liu, "Predicting Insertion Loss of Large Duct Systems Above the Plane Wave Cutoff Frequency," *Applied Acoustics,* vol. 73, no. 1, pp. 37-42, 2012.

[86] T. W. Wu and G. C. Wan, "Muffler Performance Studies Using a Direct Mixed-Body Boundary Element Method and a Three-Point Method for Evaluating Transmission Loss," *Journal of Vibration and Acoustics,* vol. 118, pp. 479-484, 1996.

[87] T. W. Wu, C. Cheng and P. Zhang, "A Direct Mixed-Body Boundary Element Method for Packed Silencers," *Journal of Acoustical Society of America,* vol. 111, no. 6, pp. 2566-2572, 2002.

[88] G. Lou, T. W. Wu and C. Cheng, "Boundary Element Analysis of Packed Silencers with a Substructuring Technique," *Engineering Analysis with*

Boundary Element, vol. 27, pp. 643-653, 2003.

[89] C. Jiang, T. W. Wu and C. Cheng, "A Single-Domain Boundary Element Method for Packed Silencers with Multiple Bulk-Reacting Sound Absorbing Materials," *Engineering Analysis with Boundary Elements,* vol. 34, pp. 971-976, 2010.

[90] R. Glav and M. Abom, "A General Formalism for Analyzing Acoustic 2-Port Networks," *Journal of Sound and Vibration,* vol. 202, no. 5, pp. 739-747, 1997.

[91] A. Mimani and M. L. Munjal, "Acoustical Analysis of a General Network of Multi-Port Elements - An Impedance Matrix Approach," *International Journal of Acoustics and Vibration,* vol. 17, no. 1, pp. 23-46, 2012.

[92] T. W. Wu, *MAP User's Manual,* Lexington, KY: University of Kentucky, 2012.

[93] J. W. Sullivan and M. J. Crocker, "Analysis of Concentric-Tube Resonators Having Unpartioned Cavities," *Journal of Acoustical Society of America,* vol. 64, pp. 207-215, 1978.

[94] M. E. Delany and E. N. Bazley, "Acoustical Properties of Fibrous Absorbent Materials," *Applied Acoustics,* vol. 3, pp. 105-116, 1970.

[95] C. B. Moler, Numerical Computing with MATLAB, Society for Industrial and Applied Mathematics, 2004.

[96] P. M. Morse and K. U. Ingard, Theoretical Acoustics, New York: McGraw-Hill, 1968.

[97] T. Kar and M. L. Munjal, "Generalized analysis of a muffler with any number of interacting ducts," *Journal of Sound and Vibration,* vol. 285, pp. 585-596,

2005.

[98] A. Craggs, "A Finite Element Method for Damped Acoustic Systems: An Application to Evaluate the Performance of Reactive Mufflers," *Journal of Sound and Vibration,* vol. 48, no. 3, pp. 377-392, 1976.

[99] A. Craggs, "A Finite Element Method for Modeling Dissipative Mufflers with a Locally Reactive Lining," *Journal of Sound and Vibration,* vol. 84, no. 3, pp. 285-296, 1977.

[100] K. S. Peat, "Evaluation of Four-Pole Parameters for Ducts with FLow by the Finite Element Method," *Journal of Sound and Vibration,* vol. 84, no. 3, pp. 389-395, 1982.

[101] A. Sahasrabudhe, S. A. Ramu and M. L. Munjal, "Matrix Condensation and Transfer Matrix Techniques in the 3D Analysis of Expansion Chamber Mufflers," *Journal of Sound and Vibration,* vol. 147, no. 3, pp. 371-394, 1991.

[102] K. F. de Lima, R. Barbieri and N. Barbieri, "Application of the Galerkin-FEM and the Improved Four-Pole parameter Method to Predict Acoustic Performance of Expansion Chambers," *Journal of Sound and Vibration,* vol. 276, pp. 1101-1107, 2004.

[103] C. N. Wang, C. C. Tse and Y. N. Chen, "Analysis of Three Dimensional Muffler with Boundary Element Method," *Applied Acoustics,* vol. 40, no. 2, pp. 91-106, 1993.

[104] A. Selamet and P. M. Radavich, "The Effect of Length on the Acoustic Attenuation Performance of Concentric Expansion Chambers: an Analytical, Computational, and Experimental Investigation," *Journal of Sound and Vibration,* vol. 201, no. 4, pp. 407-426, 1997.

[105] J. Kim and W. Soedel, "General Formulation of Four-Pole Parameters for Three Dimensional Cavitities Utilizing Modal Expansion with Special Attention to the Annular Cylinder," *Journal of Sound and Vibration,* vol. 129, pp. 237-254, 1989.

[106] J. Kim and W. Soedel, "Analysis of Gas Pulsation in Multiply Connected Three Dimensional Acoustic Cavity with Special Attenuation to Natural Mode or Wave Cancellation," *Journal of Sound and Vibration,* vol. 131, pp. 103-114, 1989.

[107] J. Kim and W. Soedel, "Development of general procedure to formulate four pole parameters by modal expansion and its application to three dimensional cavities," *ASME Transactions, Jouranl of Vibration and Acoustics,* vol. 112, pp. 452-459, 1990.

[108] G. C. Wan, "Prediction and Measurement of the Acoustic Performance of Mufflers," in *Proceedings of Inter-Noise*, 1995.

VITA

Limin Zhou was born in Jiangsu, China. He studied in Department of Mechanical Engineering at Southeast University, Nanjing, China and received his degree of Bachelor of Science in June 2005. That fall he was recommended to enroll in the graduate school of Southeast University and then received his degree of Master of Science in March 2008.

In August 2008, he was admitted to the graduate school at the University of Kentucky and involved in the research of acoustics, noise and vibration control engineering. He has been assigned teaching assistant for couple of undergraduate courses in the past three and half years. He was awarded the Young Scientists Conference Attendance Grants by the International Institute of Noise Control and Engineering (I-INCE) at the 41st International Congress and Exposition on Noise Control Engineering (INTER-NOISE 2012). In the same year, he also received the Leo Beranek Student Medal for Excellence in the Study of Noise and Control from the Institute of Noise and Control Engineering (INCE). During his graduate tenure, he has published 5 journal article (4 in press) and 7 conference papers (2 in press). Additionally, he has 1 journal article under review and 2 journal articles to be submitted.

Limin Zhou